



SCUOLA
NORMALE
SUPERIORE

Some Perspectives on Climate Change through Energy Balance Models

A Thesis Submitted in Partial Fulfilment of the Requirements for the
Degree of Doctor of Philosophy in

Sustainable Development and Climate Change

Doctoral Programme of National Interest



PhD SDC

**SUSTAINABLE DEVELOPMENT
AND CLIMATE CHANGE**

In the Curriculum
EARTH SYSTEM AND ENVIRONMENT

by

Gianmarco Del Sarto

Supervisor: Prof. Franco Flandoli

January, 2025

Abstract

This dissertation explores various aspects of an elementary class of climate models called Energy Balance Models (EBMs), in which Earth's temperature evolution is governed by the balance between the radiation absorbed and emitted by the planet. Although EBMs occupy the lowest level in the hierarchy of climate models, they are appreciated for their capacity to provide qualitative insights. Our research, which we summarise below, follows this direction.

The first line of our research focuses on understanding and providing rigorous results for a class of 1D-EBMs with a spatially heterogeneous radiation term, including an additive parameter modelling the effect of greenhouse gases (GHGs) in the atmosphere. In particular, we study the long-term behaviour of the model. To analyse the steady-state solutions of the parabolic partial differential equation governing the model, we interpret them as solutions of the Euler-Lagrange equation arising from an associated variational problem. We provide sufficient conditions for the existence of at least three steady-state solutions, corresponding to two local minima and one saddle point of the variational functional. In other words, we identify hypotheses that lead to the coexistence of "cold," "warm," and unstable "intermediate" climates. We then examine the relationship between the value function—representing the minimum of the variational functional across all temperature profiles—and the global mean temperature, both as functions of GHG concentration. In particular, we show how the value function plot provides information about the bifurcation diagram of the model, and vice versa. Furthermore, we prove that the global mean temperature, as a function of GHG concentration, is non-decreasing.

The second line of research investigates climate change issues using the same class of 1D-EBMs. To this end, we incorporate local instability effects and additive white noise into the model. The former parametrises the super-greenhouse effect, a feedback mechanism occurring in the tropics that can lead to a decrease in outgoing radiation. The latter, inspired by Hasselmann's work, accounts for fast weather fluctuations not captured by the slow dynamics of EBMs, enriching the dynamics of Earth's temperature with statistical information. Focusing on the long-term behaviour, we study the invariant measure of the model. In particular, we use its variance as

a proxy indicator for the frequency of extreme weather events and demonstrate, through numerical simulations, an increase in variance corresponding to higher GHG concentrations.

We conclude the dissertation by presenting the main ideas of ongoing research on a fast-slow system, where the fast component describes solar radiation, while the slow component is a zero-dimensional EBM. In this model, the variance of the resulting stochastic EBM increases with temperature, without invoking local instabilities. Additionally, we show how this model shares many similarities with the stochastic EBM proposed by Hasselmann, which we summarise mathematically in terms of the deterministic limit, fluctuations around the deterministic limit, and large deviations from it.

Contents

Introduction	5
0.0.1 Low dimensional energy balance models	5
0.1 Deterministic model - Main Results	10
0.1.1 Potential functional and its minimiser	10
0.1.2 Value Function and uniqueness for the functional minimiser	13
0.1.3 Value function graph and bifurcation diagram	15
0.2 A new 1D-EBM for climate change and extreme events	16
0.2.1 Motivation	16
0.2.2 Model details and properties	20
0.2.3 Increase in extreme weather events frequency	21
0.3 A non-autonomous framework for weather, macroweather, and climate	25
0.4 A fast-slow energy balance model	27
0.4.1 Link with Hasselmann's proposal	30
0.4.2 Averaging principle: deterministic limit	32
0.4.3 Gaussian fluctuations	32
0.4.4 Large deviations principle	33
1 A class of space heterogeneous one-dimensional energy balance models	35
1.1 Model formulation	36
1.2 Functional definition	41
1.3 Gibbs invariant measure and functional minimum point	42
1.4 Variational problem - existence	48
1.5 Variational problem - uniqueness	52
1.6 Value function - semiconcavity, concavity and non-increasing derivative	57
1.7 Mountain Pass Theorem and existence of at least three steady-state solutions	60
1.8 Numerical methods	67

2	A stochastic one-dimensional energy balance model for climate change	69
2.1	The non-autonomous scheme with three timescales	70
2.1.1	The weather timescale	71
2.1.2	Macroweather timescale for T	71
2.1.3	The averaging approximation	72
2.1.4	Hasselmann's proposal	72
2.1.5	Macroweather and climate	74
2.2	A new 1D-EBM with tropics bistability	76
2.2.1	The macroweather timescale and the global mean temperature increase due to CO_2 concentration	76
2.2.2	Model formulation	79
2.2.3	Deterministic properties of the model	81
2.2.4	Stochastic properties of the model	83
2.2.5	Variance and extreme weather events increase	85
2.3	Supplement information	89
2.3.1	Numerical methods	89
2.3.2	Spectral properties of the operator \tilde{A}	91
3	Energy balance models from Hasselmann's perspective	93
	Conclusions	104
	Bibliography	115

Introduction

This dissertation explores several mathematical aspects of energy balance models (EBMs), a fundamental class of climate models. Specifically, we investigate how the long-term behaviour of climate dynamics is influenced by variations in atmospheric carbon dioxide concentration, a key driver of the greenhouse effect. This analysis, which draws on tools from the calculus of variations, stochastic analysis, and numerical methods for (stochastic) equations, provides insights into the global temperature distribution and the frequency of extreme weather events. A primary objective of our work is to understand why climate change leads to an increased occurrence of extreme weather events. In this introduction, we outline the motivation behind our research and present an overview of our results. The detailed arguments are presented in Chapters 1-2-3. The former two chapters are based on [24] and [25], respectively. The last chapter is, instead, an ongoing research project, which contains the details of the results presented in Section 0.4 of this Introduction.

0.0.1 Low dimensional energy balance models

Energy balance models are a fundamental tool used to understand the Earth's climate system and its energy dynamics. It represents the energy budget within the Earth's atmosphere, land, oceans, and ice by quantifying the balance between incoming solar radiation and outgoing solar radiation. Although highly simplified compared to general circulation models, EBMs are appreciated for their interpretability, mathematical tractability, and ability to capture the essential dynamics of the Earth system [12, 77, 67, 40, 28, 14]. Two important feedback mechanisms are typically present in such models: the ice-albedo feedback and the Stefan-Boltzmann law. The positive ice-albedo feedback occurs when the melting of ice and snow reduces the surface reflectivity (albedo), causing the planet to absorb more solar radiation. According to the Stefan-Boltzmann law, a warmer body emits more radiation, thereby providing a negative feedback which stabilises the planet's temperature. Depending on the precise configuration, these mechanisms may endow EBMs with bistability, suggesting the existence of two stable climates commonly referred to as the snowball climate and the warm

climate. The snowball climate, supported by paleoclimatic evidence from the Cryogenian period around 650 million years ago, is characterised by the absence of vegetation and ice caps extending over the entire planet's surface. In contrast, the warm climate exhibits relatively low albedo, ice caps limited to the polar regions, and the presence of oceans and vegetation. Additionally, EBMs typically allow for a third possible climate, albeit unstable. Transitions between stable climates in an EBM, as well as in general multistable models, can occur in various ways. But two important mechanisms are the following. The first consists of changes in factors influencing the climate system, such as variations in greenhouse gas (GHG) concentrations like carbon dioxide (CO_2), altering the balance of incoming and outgoing radiation and amplifying the greenhouse effect. Mathematically, this mechanism can be described by assuming that the model depends on one additional parameter, and changes in the parameter lead the model to undergo a bifurcation [4]; the second consists in noise-induced transitions resulting from unresolved processes in climate models or the representation of short-timescale weather as stochastic forcing acting on slow variables, as observed in stochastic reduced models [49, 62]. These two types of transitions correspond to mechanisms recognised to induce *climate tipping*, that is rapid non-linear changes in the climate system with potentially irreversible and catastrophic consequences [57, 76, 56, 61, 42].

A zero-dimensional (0D) EBM is the simplest version of EBM describing the evolution in time for the annual averaged global mean temperature T , without any space dependence [7, 68, 72, 42]. This model is given by an ordinary differential equation (ODE) of the form:

$$\begin{aligned} C_T \frac{dT}{dt} &= \bar{Q}_0 \beta(T) + q - \sigma_0 \varepsilon_0 T^4, \quad t > 0, \\ T|_{t=0} &= T_0. \end{aligned} \tag{1}$$

In this equation, $C_T > 0$ represents the heat capacity, $\bar{Q}_0 > 0$ is the globally averaged solar radiation and the co-albedo β is modelled by a continuous function (over-bars typically denote globally averaged quantities). The term $\bar{R}_e(T) = \sigma_0 \varepsilon_0 T^4$ on the right-hand side of Eq. (1) accounts for the outgoing solar radiation, following the Stefan-Boltzmann law (where σ_0 denotes the Stefan-Boltzmann constant and ε_0 is the globally averaged emissivity). We will adopt the notation $\bar{R}_e(T; q) = \sigma_0 \varepsilon_0 T^4 - q$, thus incorporating the effect of carbon dioxide into OLR. Further, $q > 0$ is a positive parameter modelling the effect of the CO_2 on the energy budget [6, 80]. In the next paragraph, we clarify its additive structure.

Let C represent the global CO_2 concentration in parts per million (ppm), and consider, for explanatory purposes, a dependence of outgoing radiation on both temperature T and CO_2 concentration C . To avoid notation misunderstanding, denote the outgoing radiation as $\hat{R}_e = \hat{R}_e(T, C)$, emphasizing

its dependence on these two variables. Linearizing \hat{R}_e with respect to temperature around a reference temperature T_0 , we obtain:

$$\hat{R}_e(T, C) \approx A(C) + B(T - T_0),$$

where $A(C)$ encapsulates the dependence on CO₂ concentration. From [65], radiative transfer models suggest that the variation of outgoing radiation with respect to changes in CO₂ can be expressed as:

$$A(C) = A_1 - A_2 \cdot \ln\left(\frac{C}{C_0}\right),$$

where C_0 is a reference CO₂ concentration, and $A_1, A_2 > 0$ are constants derived from the models. Substituting this into the linearised expression, we have:

$$\hat{R}_e \approx A_1 + B(T - T_0) - q, \quad q = A_2 \cdot \ln\left(\frac{C}{C_0}\right).$$

This shows that the radiative forcing of CO₂ manifests as an additive term, q , in the energy budget equation.

The fixed points of the model are the solutions of the equation:

$$\frac{dT}{dt} = 0,$$

corresponding to points in Figure 1 where the absorbed radiation $\bar{R}_a(T) = \bar{Q}_0\beta(T)$ and the emitted radiation $\bar{R}_e(T; q)$ intersect. Figure 1a furthermore illustrates that this model is generally characterised by bistability, with two stable fixed points T_S and T_W . These points correspond to the snowball and warm climate states mentioned earlier and are separated by an unstable intermediate fixed point T_M . Furthermore, as highlighted by Figure 1b, the stable points correspond to minimum points of a primitive function \bar{F} for the negative radiation budget \bar{R} . In other words, \bar{F} is any regular function such that:

$$\bar{F}'(T) = \bar{R}_e(T; q) - \bar{R}_a(T) = -\bar{R}(T; q).$$

To better capture the variability of global mean surface temperature, it has been proposed to add a stochastic forcing, such as white noise, to the radiation balance. This is interpreted as the effect of the fast components of the climate system, i.e. the weather, over slow components [44, 69, 49, 32]. For this reason, we are interested in considering the stochastic differential equation (SDE) given by:

$$dT = \bar{R}(T; q)dt + \varepsilon dW_t, \tag{2}$$

where $\varepsilon > 0$ is the noise intensity and $(W_t)_{t \geq 0}$ is a Brownian motion [5]. This SDE is of gradient type and possesses a unique Gibbs invariant measure $\bar{\nu}$ [55]. An invariant measure is a probability distribution $\bar{\nu}$ in the state space

of Eq. (2) (i.e. the real numbers in this case) with the property that if a solution T is distributed according to $\bar{\nu}$ at some time t then it remains so for all later times. It is given by:

$$\bar{\nu}(dT) = \frac{1}{Z} \exp\left(-\frac{2}{\varepsilon^2} \bar{F}(T; q)\right) dT, \quad (3)$$

where Z is a normalization constant and dT denotes the standard volume element on \mathbb{R} (we note the technical detail that to give meaning to Eq. (2) and Eq. (3), the radiation budget \bar{R} should be extended to negative values for the Kelvin temperature T in a way such that $\bar{F} \rightarrow +\infty$ as $T \rightarrow -\infty$). The key observation from the explicit formula (3) is that $\bar{\nu}$ is concentrated around the minimum points of the function \bar{F} . Indeed, if T_0 is a strict minimum point and $T_1 \neq T_0$ is a point close to T_0 s.t. $\bar{F}(T_1; q) > \bar{F}(T_0; q)$, then the mass given by the measure ν in a small neighbourhood of T_1 is exponentially lower than the mass around T_0 ; more specifically, the ratio between the two masses is given by $\exp\left(-\frac{2}{\varepsilon^2} (\bar{F}(T_1; q) - \bar{F}(T_0; q))\right)$.

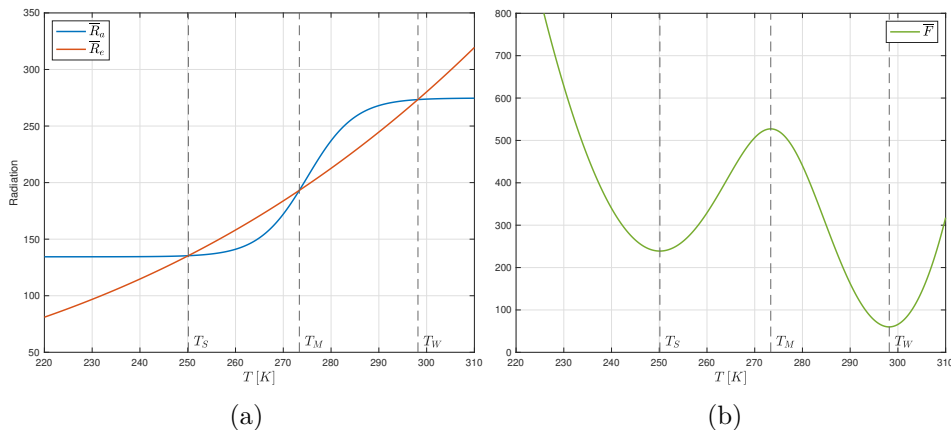


Figure 1: (a) Absorbed radiation \bar{R}_a and emitted radiation \bar{R}_e for a 0D-EBM. The graphs intersect in the three fixed points of the model $T_S < T_M < T_W$; T_S and T_W are stable, T_M is unstable. (b) Double-well potential \bar{F} associated to 0D-EBM. The function \bar{F} satisfies $\bar{F}' = \bar{R}_e - \bar{R}_a$. The minimum points T_S and T_W of \bar{F} correspond to stable fixed points.

A one-dimensional (1D) EBM is given by a parabolic partial differential equation where the space variable is one-dimensional [12, 77, 72]. Denoting the temperature averaged in the zonal direction by $u = u(t, x)$, it extends the 0D-EBM by introducing the sine of the latitude $x = \sin(\phi)$, where $\phi \in [-\frac{\pi}{2}, \frac{\pi}{2}]$ denotes the latitude and $t \geq 0$ represents time. We assume that the non-linear radiation balance of the planet, denoted by $R(x, u; q)$, depends on the sine of the latitude and on an additive parameter q . This parameter models the effect of carbon dioxide concentration on the radiation

budget [6]. Atmospheric and ocean transport of heat between latitudes is modelled in a very simplified way by a diffusion term. Assuming spatially homogeneous diffusion in this introductory section and thus ignoring the dependence of κ on latitude and temperature, we obtain a non-degenerate reaction-diffusion equation:

$$\begin{aligned} \partial_t u &= \kappa \Delta u + R(x, u; q), \quad t > 0, \quad x \in (-1, 1), \\ u_x(t, -1) &= u_x(t, 1) = 0, \quad t \geq 0 \\ u(0, x) &= u_0(x), \quad x \in [-1, 1] \end{aligned} \tag{4}$$

where $\Delta = \partial_{xx}$ denotes the Laplace operator in dimension one, the Neumann boundary conditions impose no-heat flux at the poles and u_0 is an initial condition. The non-linear radiation balance of the radiation absorbed and emitted by the planet $R(x, u; q)$ is given by

$$R(x, u; q) = Q_0(x)\beta(u) + q - \varepsilon_0\sigma_0u^4,$$

where $Q_0(x)$ is a positive smooth function describing the the space-dependent solar radiation at point x , $\beta \in (0, 1)$ is a smooth increasing function parametrising the co-albedo, and $q > 0$ is an additive parameter modelling the effect of CO₂ concentration on the energy balance. Lastly, the emitted radiation is again given by the map $u \mapsto \varepsilon_0\sigma_0u^4$, where ε_0, σ_0 are constants denoting respectively the Earth's emissivity and the Stefan-Boltzmann constant.

The steady-state solutions of this model, representing the asymptotic solutions for the time-evolving dynamics, correspond to the non-negative solutions $u = u(x)$ of the elliptic problem:

$$\begin{aligned} 0 &= \kappa u'' + R(x, u; q), \quad x \in (-1, 1), \\ u'(-1) &= u'(1) = 0, \end{aligned} \tag{5}$$

where $u = u(x)$ depends only on the space variable. This elliptic problem forms a necessary condition for $u = u(x)$ to be our extremal (in particular a local minimiser) for the potential functional

$$F_q(u) = \int_{-1}^1 \mathcal{R}(x, u; q) dx + \frac{\kappa}{2} \|u'\|_2^2 \tag{6}$$

where $\partial_u \mathcal{R}(x, u; q) = -R(x, u; q)$ and $\|u'\|_2^2 = \int_{-1}^1 (u')^2 dx$ is the square of the norm of u' in $L^2(-1, 1)$. The calculus of variations is a widely employed technique for studying the existence of a solution to the previous problem [67, 71, 70, 11]. However, proving the existence of a local (but not global) minimum point is generally challenging, and this technique focuses on studying the existence of the global minimum point. The functional F_q in Eq. (6) has another interpretation though which renders it more important than being merely a characterisation of solutions to the elliptic problem. Indeed,

consider the stochastic partial differential equation (SPDE) on the Hilbert space $H = L^2(-1, 1)$ given by:

$$du = (\kappa \Delta u + R(x, u; q)) dt + \varepsilon dW_t, \quad (7)$$

obtained by adding a space-time white noise $(W_t)_{t \geq 0}$ modelled by a cylindrical Brownian motion on $H = L^2(-1, 1)$ to Eq. (5). R has a cut-off at negative temperature as in Section 0.1.1 and $\varepsilon > 0$ is the noise intensity. We refer to [22] for more details about SPDEs. It can be shown that Eq. (7) has a unique invariant Gibbs measure ν [20], given (broadly speaking) by an expression as in Eq. (3), with F_q replacing \bar{F} (see Section 0.1.1 and 1.1). Therefore, as in the zero-dimensional case, ν concentrates on minimum points of the functional F_q . These minimisers satisfy the elliptic problem (5), which therefore describes temperature profiles around which the solutions of the stochastic problem (7) tend to cluster.

0.1 Deterministic model - Main Results

0.1.1 Potential functional and its minimiser

In this section, we: (i) provide an intuitive motivation for why the invariant measure for the stochastic EBM in Eq. (7) concentrates on minimum points of the functional F_q , (ii) prove the existence of global minimum points for F_q using the direct method, (iii) present sufficient conditions on the viscosity κ and the space-averaged potential $\bar{\mathcal{R}}(u) = \frac{1}{2} \int_{-1}^1 \mathcal{R}(x, u) dx$, with $\partial_u \mathcal{R} = -R = R_e - R_a$, to ensure that the 1D-EBM has at least three steady-state solutions.

Firstly, consider the stochastic EBM (7). Assume that for a negative value of u , where the model has no physical meaning, the Stefan-Boltzmann law is extended as:

$$R_e(u; q) = \begin{cases} \varepsilon_0 \sigma_0 u^4 - q, & \text{if } u \geq 0 \\ -q, & \text{if } u < 0, \end{cases} \quad (8)$$

and β is smoothly extended to $\tilde{\beta}$ by setting it to zero outside the physically relevant range, as described in the Section 1.2. Then, Eq. (7) possesses a unique Gibbs invariant probability measure given by:

$$\begin{aligned} \nu(du) &= \frac{1}{Z} \exp \left(-\frac{2}{\varepsilon^2} \int_{-1}^1 \varepsilon_0 \sigma_0 \frac{(u^5)_+}{5} - Q_0(x) B(u) - qu dx \right) \mu(du), \\ \mu &\sim \mathcal{N}(0, -\frac{\varepsilon^2}{2\kappa} \Delta^{-1}), \end{aligned} \quad (9)$$

where $(u)_+ = \max\{u, 0\}$ is the positive part, $\mathcal{N}(0, -\frac{\varepsilon^2}{2\kappa} \Delta^{-1})$ denotes a symmetric Gaussian measure with covariance operator $\mathcal{Q} = -\frac{\varepsilon^2}{2\kappa} \Delta^{-1}$ over the

Hilbert space $H = L^2(-1, 1)$, B is a primitive of the co-albedo β , and Z is the normalization constant. See ([20]) for a rigorous derivation of the invariant measure for a reaction-diffusion model with a polynomial homogeneous reaction term. We move to explain in what sense ν is concentrated around minimum points of F_q . In fact, for $u \in H$ the Gaussian measure μ is formally given by:

$$\mu(du) = \frac{1}{Z_1} \exp\left(-\frac{1}{2}\langle \mathcal{Q}^{-1}u, u \rangle\right) du,$$

where $\mathcal{Q}^{-1} = -\frac{2\kappa}{\varepsilon^2}\Delta$. Here, Z_1 is a normalization constant, $\langle \cdot, \cdot \rangle$ denotes the scalar product in H , and du is a formal notation for the Lebesgue measure on H . If we perform an integration by parts, we get

$$\mu(du) = \frac{1}{Z_1} \exp\left(\frac{\kappa}{\varepsilon^2}\langle u'', u \rangle\right) du = \frac{1}{Z_1} \exp\left(-\frac{\kappa}{\varepsilon^2}\|u'\|_2^2\right) du.$$

Plugging the previous identity into Eq. (1.3), we obtain:

$$\begin{aligned} \nu(du) &\propto \exp\left(-\frac{2}{\varepsilon^2}\left(\int_{-1}^1 \varepsilon_0 \sigma_0 \frac{(u^5)_+}{5} - Q_0(x)B(u) - qu \, dx + \frac{\kappa}{2}\|u'\|_2^2\right)\right) du \\ &\propto \exp\left(-\frac{2}{\varepsilon^2}F_q(u)\right) du. \end{aligned}$$

From this heuristic formula, we see that points u such that $F_q(u)$ is not a global minimum have exponentially smaller density than the minimum points. Indeed, if u_1 is a global minimum point and $u \neq u_1$, then the mass given by ν in a small neighbourhood around u is exponentially smaller than the mass given to a neighbourhood of the same size around u_1 ; in particular, the ratio between the two masses is given by $\exp\left(-\frac{2}{\varepsilon^2}(F_q(u) - F_q(u_1))\right)$. The previous derivation is formal because the Lebesgue measure cannot be defined on an infinite dimensional Hilbert space. For a more rigorous explanation, see Section 1.3.

Next, we discuss the properties of the functional

$$F_q: H^{1,2}(-1, 1) \cap \{u \geq 0\} \rightarrow \mathbb{R}$$

given by:

$$F_q(u) = \int_{-1}^1 \frac{(u)_+^5}{5} \varepsilon_0 \sigma_0 - Q_0(x)B(u) - qu \, dx + \frac{1}{2} \int_{-1}^1 \kappa(x)(u'(x))^2 \, dx,$$

where $H^1 = H^{1,2}(-1, 1)$ denotes the Sobolev space of order 1 and exponent 2, i.e. the function space where a function u and its derivative u' (in weak-sense) are both square integrable over $[-1, 1]$. See ([11]) for more details about Sobolev spaces. The functional F_q , depending on the parameter q , is

known in the literature as potential functional or Lyapunov function ([71, 72]). The study of the functional F_q gives useful information thanks to its links with the invariant measure for the stochastic 1D-EBM, as we have seen, and the stable steady-state solutions for the deterministic 1D-EBM which emerge as necessary conditions for the stationarity of F_q . Going deeper with the former point, the first variation of F_q in the point u in direction h is given by:

$$\begin{aligned} \delta F_q(u, h) &= \frac{d}{ds} F_q(u + sh)|_{s=0} \\ &= \int_{-1}^1 \left(u^4 \varepsilon_0 \sigma_0 - Q_0(x) \beta(u) - q \right) h \, dx + \int_{-1}^1 \kappa(x) u'(x) h'(x) \, dx \\ &= \int_{-1}^1 \left[u^4 \varepsilon_0 \sigma_0 - Q_0(x) \beta(u) - q - (\kappa(x) u'(x))' \right] h \, dx \end{aligned}$$

where in the last identity we have used the integration by parts. Since h is arbitrary, u is a stationary point for the functional F_q if and only if it is a steady-state solution for the EBM. In particular, local extremum points for F_q correspond to steady-state solutions of the EBM. Any local minimiser of F_q represents a locally attractive solution of the deterministic 1D-EBM. In view of our interpretation of F_q in terms of the invariant measure, however, global minimisers play a special role since if present and unique they are exponentially more likely than any other state (including minimisers that are just local). The following result establishes the existence of a global minimum point for F_q .

Theorem 1. *If $q > 0$, then there exists a global regular non-negative minimiser for F_q . In other words, if we consider the variational problem*

$$\inf \left\{ F_q(u) \mid u \in H^1, u \geq 0 \right\}, \quad (10)$$

then there exists $\hat{u} \in C^\infty$ s.t. \hat{u} is a solution of the EBM and

$$F_q(\hat{u}) = \inf \left\{ F_q(u) \mid u \in H^1, u \geq 0 \right\}.$$

In addition to this, if q belongs to a bounded interval, then u can be bounded uniformly with respect to q :

$$\exists M > 0 \text{ s.t. } \hat{u}(x) \leq M, \quad \forall x \in [-1, 1]. \quad (11)$$

A rigorous proof of the previous result can be found in Section 1.4. The proof relies on standard arguments from the direct method of calculus of variation exploiting the fact that the outgoing radiation in the EBM model prevents the temperature from being too high.

Concerning the existence of two local minimum points, let us describe a sufficient condition. Consider the potential function $\bar{\mathcal{R}}: \mathbb{R} \rightarrow \mathbb{R}$ coming from the space averaged model

$$\bar{\mathcal{R}}(u) = \frac{1}{2} \int_{-1}^1 \mathcal{R}(x, u) dx.$$

If the viscosity $\kappa > 0$ is sufficiently large and the function $\bar{\mathcal{R}}$ has a double well shape with sufficiently deep minimum values attained at the minimum points, then we are able to prove the existence of two minimum points for F_q . Further, it is possible to prove that the functional F_q satisfies a compactness condition known as Palais-Smale condition. This property and the Mountain Pass theorem give the possibility to deduce the existence of a third steady-state solution. Next, we characterise a situation in which there are three steady-state solutions, two of which are local minimisers ([50]). This is summarised in the following result, whose proof is given in Section 1.7.

Theorem 2. *Denote by $B_{H^1}(v, \rho) = \{u \in H^1 \mid \|u - v\|_{H^1} < \rho\}$ the open ball in H^1 with center v and radius $\rho > 0$. Assume $\bar{\mathcal{R}}$ has two non-negative minimum points $u_1 \neq u_2$, with $F_q(u_1) \geq F_q(u_2)$. Then, there exist $\omega > 0$ and $f, g \in O(\varepsilon^{-1})$ as $\varepsilon \rightarrow 0^+$ s.t. if $\bar{\varepsilon} > 0$ satisfies:*

- (i) $\bar{\mathcal{R}}''(u_i) > f(\bar{\varepsilon})$, for $i = 1, 2$,
- (ii) $\kappa > g(\bar{\varepsilon})$,
- (iii) $\bar{\varepsilon} \leq \omega$,

then F_q has two local minimum points \hat{u}_1, \hat{u}_2 such that:

- (a) $B_{H^1}(u_1, \bar{\varepsilon}) \cap B_{H^1}(u_2, \bar{\varepsilon}) = \emptyset$,
- (b) $\hat{u}_i \in B_{H^1}(u_i, \bar{\varepsilon})$, for $i = 1, 2$,
- (c) If $\|u - u_1\|_{H^1} = \bar{\varepsilon}$, then $F_q(u) \geq F_q(u_1) + \delta$, with $\delta = \delta(\bar{\varepsilon}) > 0$.

Note how the previous result can be also interpreted as giving sufficient conditions for the convergence of the stable solutions of a space-inhomogeneous EBM to the stable solution of the corresponding space-averaged model, as the diffusion becomes large.

0.1.2 Value Function and uniqueness for the functional minimiser

The key element of this section is the value function, which is given by:

$$V(q) = \inf \left\{ F_q(u) \mid u \in H^1, u \geq 0 \right\}.$$

From Section 0.1.1, we know that the previous infimum is indeed a minimum and so $V(q)$ can be interpreted as the minimum possible value attained by the potential functional over the possible temperature profiles u . Since a minimum point for F_q is also a stationary point for the functional, the value function can be evaluated numerically by computing the minimum of the three steady-state solutions u_S, u_M, u_W . Following this strategy, Figure 2 shows $q \mapsto F_q(u_*)$, with $u_* \in \{u_S, u_M, u_W\}$. Particularly, there exists a point q_3 s.t. u_S is the global minimum point of F_q for $q < q_3$, while u_W is the global minimum point for $q > q_3$. Further, for $q = q_3$ the function F_q has two different global minimum points u_S, u_W and $q = q_3$ correspond a non-differentiability point for V . In addition to this, the value function

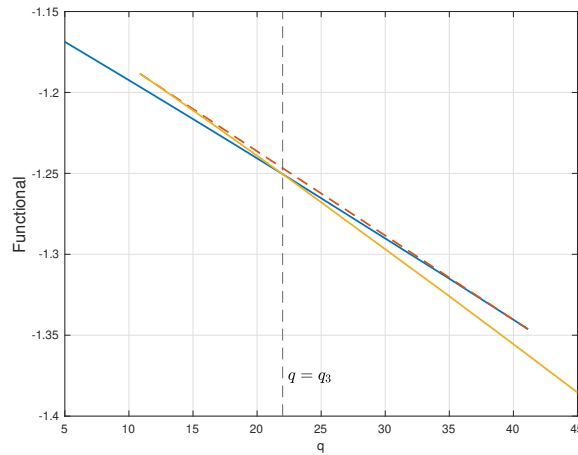


Figure 2: Potential functional F_q evaluated in the three steady-state solutions u_S, u_M, u_W . For $q < q_3$, u_S is the global minimum point, while u_W is a local minimum point. On the other hand, for $q > q_3$ the vice versa happens. Solid lines correspond to values of the functional attained on stable solutions, dashed lines for values corresponding to unstable ones.

appears to be concave, thus with a decreasing derivative, where it exists. Summarizing, the numerical evaluations of $V(q)$ suggest the following result, a rigorous proof of which is included in Sections 1.5, 1.6.

Theorem 3. *Assume q belongs to a bounded interval. Then:*

- (i) V is Lipschitz continuous.
- (ii) q is a non-differentiable point for V if and only if there is more than one minimiser for F_q .
- (iii) V is concave and V' is non-increasing.

See Lemma 22, Proposition 23, and Proposition 31 for the proof of the previous result.

We also see numerically that u_M is actually never a global minimiser for the specific functional F_q considered here, but we do not have a rigorous proof of this fact. Let's briefly discuss the proofs of the previous points. The proof of (i) follows from the facts that the sup-norm of the minimiser u_0 can be bounded uniformly in q and that, given a family $\{g_i\}_{i \in I}$ of L_i -Lipschitz functions g_i , then $\inf_{i \in I} g_i$ is Lipschitz if the constants L_i can be bounded uniformly. In our case, given $u \in H^1$ non-negative, we have

$$|F_{\mu_1}(u) - F_{\mu_2}(u)| \leq |\mu_1 - \mu_2| \int_{-1}^1 |u(x)| dx \leq 2M|\mu_1 - \mu_2|$$

where $M > 0$ is the constant appearing in Eq. (11). On the other hand, the proof of point (ii) is less straightforward, although being very similar to the one for the existence of a solution for the variational problem. The proof of point (iii) makes use of the concept of semiconcavity, a generalisation of that of concavity, which is fundamental in optimal control [16]. The main reason for the concavity of V though is that V is an infimum over functions that are affine in q . Hence the fact that q is additive is essential for this result. More details can be found in Section 1.5.

0.1.3 Value function graph and bifurcation diagram

An additional property of the value function can be observed when comparing the bifurcation diagram (Figure 3a) and the graph of the value function (Figure 3b).

Corollary 4. *If V is differentiable, then $V'(q) = -\int_{-1}^1 \hat{u}(x) dx$, where \hat{u} is the only minimiser for F_q .*

In other words, the part of the bifurcation diagram that corresponds to the global minimiser, represented by the sub-graph $(q, \frac{1}{2} \int_{-1}^1 \hat{u}, dx)$, can be determined based on the knowledge of V' , and vice versa. Figure 3 compares the bifurcation diagram to the graph of the value function, highlighting in magenta the corresponding parts of the two graphs. From the mathematical point of view, the previous result is a consequence of the proof of Theorem 3.

It is worth pointing out that by combining Theorem 3 and Corollary 4, a valuable property emerges, i.e., the global mean temperature of the functional minimiser is non-decreasing with respect to q . In other words, as the concentration of CO_2 rises, the global mean temperature increases. Additionally, through this monotonicity and Froda's theorem, we also establish that the global mean temperature is continuous, except for, at most, a countable number of upward jumps.

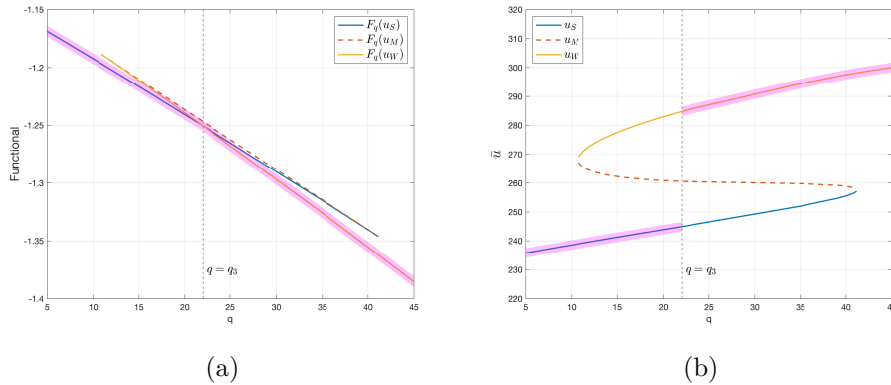


Figure 3: Comparison between the value function graph (left) and bifurcation diagram (right) for the 1D-EBM. The magenta-shaded area highlights the parts of the plots which are in one-to-one correspondence. (a) Functional F_q evaluated on steady-state solutions, as in Figure 2. (b) Steady-state solutions of the EBM for $q = 25$. In every point x of the space domain, the three steady-state solutions satisfy $u_S(x) < u_M(x) < u_W(x)$, with maximum temperature attained at the equator and minimum temperature attained at the poles.

0.2 A new 1D-EBM for climate change and extreme events

0.2.1 Motivation

The class of EBMs is well-regarded in the literature for its simplicity and its ability to describe climate dynamics in an elementary way, as noted in previous sections. Its application to paleoclimate investigations is widespread [81, 72, 30], with a particular focus on understanding how transitions can occur between the warm steady-state solution u_W of the EBM and the snowball climate u_S , and vice versa. This transition is a classic example of a tipping point in climate systems, referring to a significant non-linear shift in the climate or one of its subsystems, which can be triggered by a small variation in a climatic variable, such as global mean temperature (GMT) or carbon dioxide concentration.

There is scientific evidence, even if contested, that the snowball-warm climate tipping point occurred in the past. Regardless, the physical mechanism behind this bistability is simple and unquestionable: the solid-liquid phase transition of water. In fact, the fixed points for the 0D-EBM (1) are the temperature values where the absorbed radiation \bar{R}_a intersects the emitted radiation \bar{R}_e . The latter is proportional to the fourth power of the temperature, due to the Stefan-Boltzmann law, while the former is positive,

bounded, and increases with temperature T , as depicted in Figure 1a. The fact that \bar{R}_a and \bar{R}_e intersect three times, giving rise to two stable fixed points, is primarily due to the simple fact that ice melts at around 273 K, causing the ice-albedo feedback to break down.

But our main interest is the study of climate change, not the investigation of past climate. In the next paragraph, we will explain why the EBMs, as we have considered them so far, are not suitable for addressing this issue. To simplify, consider the stochastic 0D-EBM in (2); the same reasoning applies to the 1D-EBM (7). Since the global mean temperature T changes only slightly from year to year, it is reasonable to linearise the equation around the stable fixed point T_W of the deterministic model, corresponding to the present climate configuration of the Earth. In this way, we get

$$\bar{R}(T) = \bar{R}_a(T) - \bar{R}_e(T; q) = a + q + bT + o(T - T_W),$$

with $b < 0$ since T_W is stable. Thus, we obtain

$$\begin{aligned} \frac{dT}{dt} &= a_q + bT + \sigma dW_t, & a_q &= a + q, \\ T(0) &= T_0. \end{aligned} \tag{12}$$

The solution of the previous SDE is given by

$$T_t = T_0 e^{-tb} + a_q b (1 - e^{-tb}) + \sigma \int_0^t e^{-(t-s)b} dW_s.$$

It is a Gaussian process with a mean value of

$$\mathbb{E}[T_t] = T_0 e^{-tb} + a_q (1 - e^{-tb}),$$

and variance

$$\text{Var}(T_t) = \text{Var}\left(\sigma \int_0^t e^{-(t-s)b} dW_s\right) = \sigma^2 \int_0^t e^{-2(t-s)b} ds = \frac{\sigma^2}{2b} (1 - e^{-2tb}).$$

Thus, looking at the long-term behaviour of the mean and variance, we find

$$\lim_{t \rightarrow +\infty} \mathbb{E}[T_t] = a_q, \quad \lim_{t \rightarrow +\infty} \text{Var}(T_t) = \frac{\sigma^2}{2b}. \tag{13}$$

As expected, the mean depends on CO₂ concentration. The larger the value of q , the higher (on average) the global mean temperature. However, the same does not hold for the variance, which is independent of the concentration of carbon dioxide in the atmosphere. This is problematic because we would like a simplified model that demonstrates how temperature fluctuations increase with rising carbon dioxide (CO₂) concentrations.

Indeed, one of the most dramatic examples of climate change today is the increased frequency of extreme events. As pointed out by the IPCC

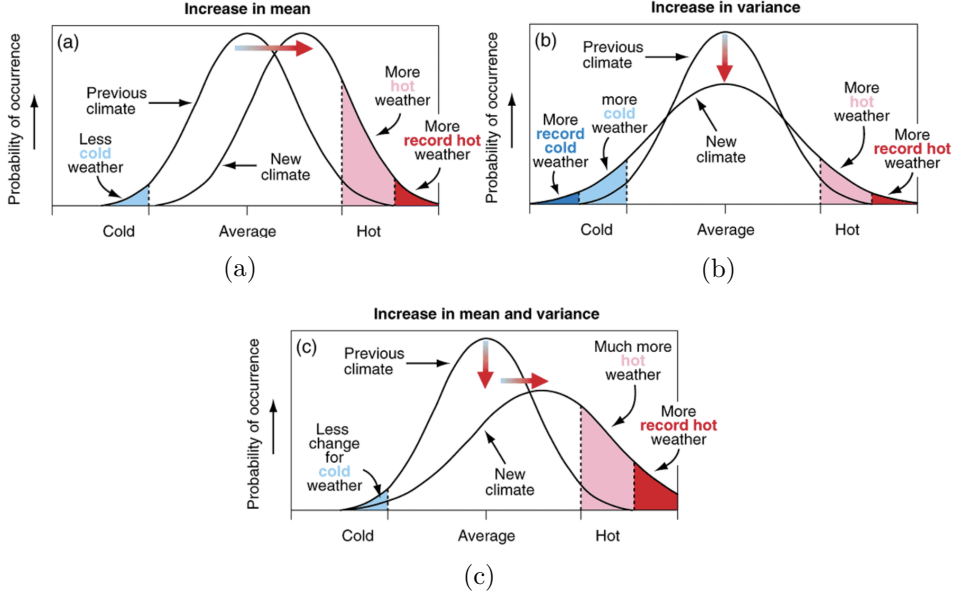


Figure 4: Schematic showing the effect on extreme temperatures when (a) the mean temperature increases, (b) the variance increases, and (c) both the mean and variance increase for a normal distribution of temperature. Reproduced from the IPCC Report on Climate Change 2001: The Scientific Basis ([45, Figure 2.32]).

Report ([45]), this can result from both an increase in mean temperature (which can be easily explained by an SDE model as in (12) and an increase in the variance of temperature, as shown in Figure 4. This phenomenon is not just speculative; it can be observed in real data, as shown in Figure 5a. The figure shows histograms of the daily mean temperature recorded in August for two different periods: from 1910 to 1940 (in blue) and from 1993 to 2023 (in red). In our view, explaining the joint increase of both mean value and variance is a challenging and, at present, completely open question.

The classical paradigm to explain the increase in the frequency of extreme events is given by a dynamical system approaching a bifurcation point, where random fluctuations are amplified near the bifurcation point ([23, 76, 54, 4, 56, 42, 8]). To explain this simply, we can again consider a linear EBM as in (12) but this time assuming that the coefficient b depends on the parameter q , i.e., $b_q = b_q(q)$ and the model is given by:

$$\frac{dT}{dt} = a_q + b_q \cdot T + \sigma dW_t, \quad a_q = a + q,$$

$$T(0) = T_0.$$

We can repeat the computations done previously starting from the explicit

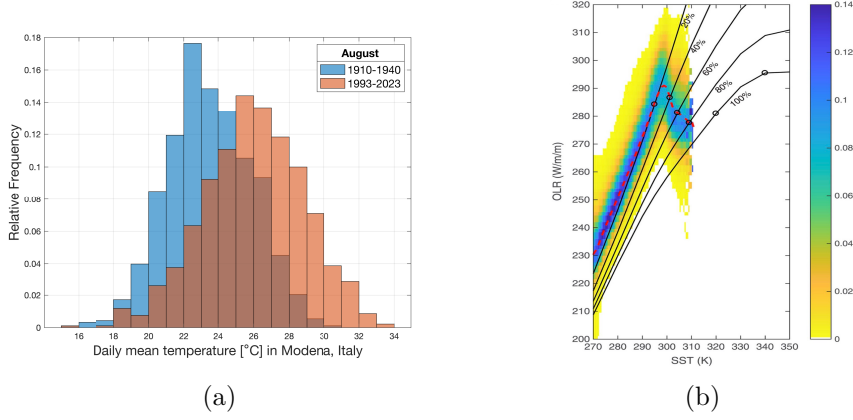


Figure 5: (a) Daily temperature recorded in August in Modena, Italy. The blue histogram shows the values for the time period 1910 – 1940 (blue), and the red histogram refers to 1993 – 2023 (red). Data provided by the Osservatorio Geofisico di Modena www.ossgeo.unimore.it. (b) Observational Outgoing Longwave Radiation (OLR) dependence on Sea Surface Temperature (SST), and SMART (SMART is a dataset for OLR measurements used in [27]) OLR output for various humidity values. The red dashed line is the mean. Reproduced with permission from Geophysical Research Letters 45, 19 (2018). Copyright 2018, John Wiley and Sons ([27, Figure 2a]).

solution

$$T_t = T_0 e^{-tb_q} + a_q b_q (1 - e^{-tb_q}) + \sigma \int_0^t e^{-(t-s)b_q} dW_s,$$

and getting to

$$\lim_{t \rightarrow +\infty} \mathbb{E}[T_t] = a_q, \quad \lim_{t \rightarrow +\infty} \text{Var}(T_t) = \frac{\sigma^2}{2b_q}.$$

If there exists a critical threshold q_* such that $b_q \rightarrow 0$ as $q \rightarrow q_*$, then we get $\lim_{t \rightarrow +\infty} \text{Var}(T_t) = +\infty$ as q approaches q_* .

The main question is whether the Earth is currently close to a bifurcation point, an issue that is speculated but not proven. Looking to the distant past, as noted earlier, it is clear that bifurcations took place, connecting a moderate climate like today’s with glacial climates. However, there is no clear indication that we are near a new bifurcation point leading to a warmer climate. One exception is in data near the Tropics: localised at that latitude, there is experimental evidence of potential bistability and a possible fast transition to a warmer climate ([27], see Figure 5b). However, data from regions outside the Tropics show different patterns. Therefore, we have developed a new 1D-EBM that incorporates these differences. Seen globally, as an infinite-dimensional dynamical system over the entire Earth,

the bistability in the Tropics does not introduce a new bifurcation to the model.

0.2.2 Model details and properties

We work with a Budyko-Sellers one-dimensional energy balance model (1D-EBM), in which a diffusion term modelling meridional heat transport is added as a driver of temperature evolution ([72]). The novelty of our model consists in adding, for the first time, a particular phenomenon that may happen at the Tropics. Indeed, one of the key mechanisms to stabilise Earth's temperature is the Planck feedback. It consists of increased outgoing longwave radiation (OLR) as surface temperature increases, thanks to the Stefan-Boltzmann law. But there exist cases, and our model highlights one of them, where this feedback can fail, as in the super-greenhouse effect (SGE) ([33, 9, 27]). This phenomenon is feedback between water vapour, surface temperature and greenhouse effect. Once the sea surface temperature or greenhouse gas concentration reaches a certain level, the increase in absorbed thermal radiation from the surface due to augmented evaporation with rising sea surface temperature (SST) outweighs the concurrent elevation in OLR, causing OLR to decline as SST increases.

More in detail, the model that we consider is almost identical to the 1D-EBM (4), better detailed in Section 1.1. Indeed, it is given by the following reaction-diffusion equation

$$\begin{aligned} C_T \partial_t u &= \partial_x (\kappa(x) u_x) + R_a(x, u) - R_e(x, u; q), \quad x \in [-1, 1], t \geq 0 \\ u(x, 0) &= u_0(x), \quad x \in [-1, 1], \\ u_x(-1, t) &= u_x(1, t) = 0, \quad t \geq 0, \end{aligned} \tag{14}$$

where again $C_T > 0$ denotes heat capacity, $\kappa(x) > 0$ is the diffusion function, R_a is the absorbed radiation, and R_e is the emitted radiation. It is worth underlying how the space dependence of this last term is the main novelty of this model. This novelty, driven by the SGE mentioned before, may lead to bistability for OLR locally in tropical regions. To capture this behaviour, we propose a model for OLR that varies with space and is symmetric with respect to latitude:

$$R_e(x, u; q) = q + |x| R_e^{pl}(u) + (1 - |x|) R_e^{eq}(u),$$

where R_e^{pl} and R_e^{eq} represent the OLR at the poles and equator, respectively. The function R_e smoothly transitions between polar and equatorial values, as shown in Figure 6, where different colours correspond to specific latitudes. More details on the terms and the parameters of the model can be found in Section 2.2.2.

The results obtained in Section 0.1, i.e. Theorems 1, 2, 3, and Corollary 4 still holds for this model. Indeed, the reaction-diffusion structure with a

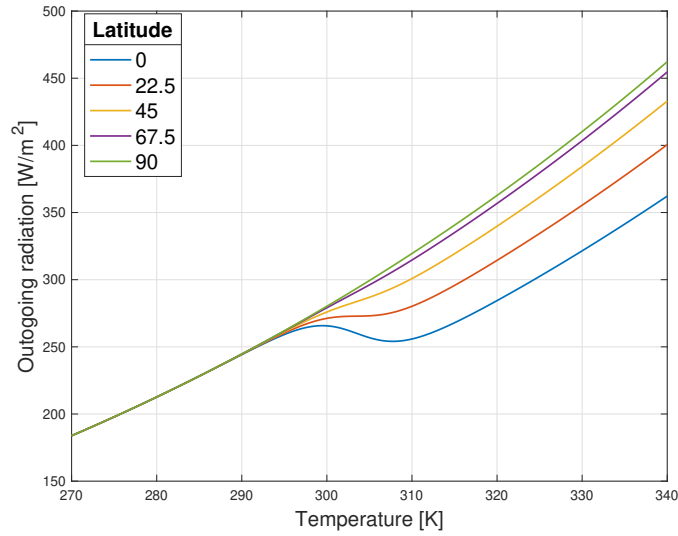


Figure 6: Representation of the Outgoing Longwave Radiation (OLR) $R_e = R_e(x, u; q)$ in (2.9) for $q = 0$. Different colours are used to represent the dependence on the space. At the tropics, the OLR presents the bistability due to the super-greenhouse effect shown in Figure 5. The bistable regimes progressively disappear as the space point moves to the poles, where the Stefan-Boltzmann law in (2.10) is applied to parametrise OLR.

space-heterogeneous reaction term is the same as the 1D-EBM (4). However, it is worth pointing out the bifurcation diagram of the model, which is shown in Figure 7. Although no new steady-state solutions are added to the model (in addition to the two classical saddle-node bifurcations that characterise EBMs), it can be observed a non-linear increase in the GMT of the warm steady-state solution u_W takes place for values of q close to 11. This increase is caused by the space-dependent emitted radiation with tropics bistability, since the same 1D-EBM without this feature does not show this behaviour (see Section 1.1, in particular Figure 1.1a).

0.2.3 Increase in extreme weather events frequency

It is well-established that human-induced greenhouse gas emissions have intensified the frequency and severity of climate extremes, particularly temperature fluctuations, since the pre-industrial period [73]. Despite various definitions of what constitutes an extreme event, no universally accepted standard exists [79]. A common approach defines an extreme weather event as one surpassing a specific threshold of a climate variable. To be able to investigate such a phenomenon, we extend the 1D-EBM in (14) by an additive space-time white noise with small intensity $\sigma > 0$, as in (7). In this framework, we consider as a proxy indicator for the frequency of extreme

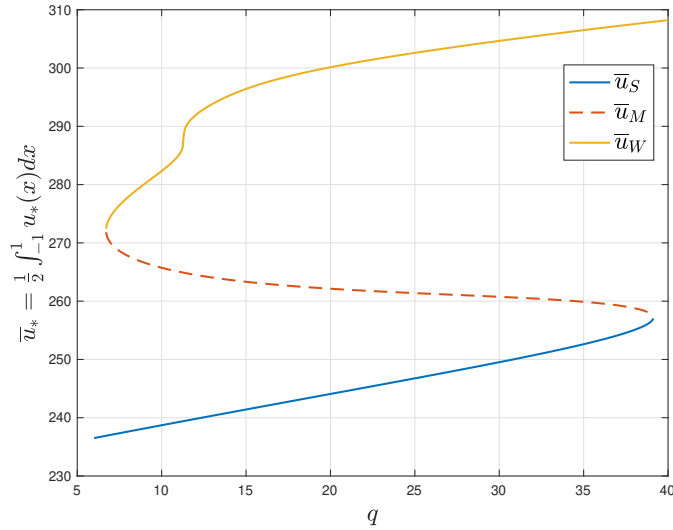


Figure 7: (b) Bifurcation diagram in the (q, \bar{u}_*) plan for the 1D-EBM (14), where u_* denotes a steady-state solutions and $\bar{u}_* = \frac{1}{2} \int_{-1}^1 u_*(x) dx$ is its global mean temperature (GMT). The S -shaped bifurcation diagram is characterised by the two classical saddle-node bifurcations around $q \approx 7$ and $q \approx 38$, and a non-linear (with respect to q) increase in the global mean temperature around $q \approx 11.3$.

weather events the variance of the solution, which we are going to better define later. In any case, our equation takes the form

$$\begin{aligned}
 C_T \partial_t u &= \partial_x (\kappa(x) u_x) + R_a(x, u) - R_e(x, u; q) \\
 &\quad + \sigma dW_t, \quad (x, t) \in [-1, 1] \times [0, T], \\
 u(x, 0) &= u_W(x), \quad x \in [-1, 1], \\
 u_x(-1, t) &= u_x(1, t) = 0, \quad t \in [0, T],
 \end{aligned} \tag{15}$$

where as initial condition we consider the warm steady-state solution u_W of the deterministic model, and $T = 500$ years. Indeed, we are interested in understanding the shape of the invariant measure ν around the actual climate, which is described by u_W . As can be expected, the invariant measure $\nu = \nu(q)$ is still Gibbs, with an explicit expression similar to (9). Indeed, as for the deterministic properties, all the stochastic properties of the model are preserved by the addition of the tropical instability correction. Anyway, the expression for the invariant measure ν is not useful, being non-linear, to get quantitative information. In particular, we would like to understand how much the fluctuations of the solution, i.e. the variance, are affected by the change in the CO_2 concentration.

Thus, we conduct a numerical simulation of the SPDE (15) using a finite difference method, which discretises both time and space into meshes.

Symbol	Meaning	Value
C_T	Heat capacity	$5 \cdot 10^7 \text{ J m}^{-2} \text{ K}^{-1}$
σ	Diffusion coefficient SPDE	0.2
T	Final time of simulation	500 yrs.
Δx	Space mesh size	0.01
Δt	Time mesh size	0.01
Δq	CO ₂ parameter mesh size (see (16))	$\approx 1.21 \cdot 10^{-2}$
q_0	First point in the CO ₂ mesh (see (16))	11.15
q_{29}	Last point in the CO ₂ mesh (see (16))	11.15

Table 1: Parameters and constants appearing in the model (15) and its numerical simulations (see Section 2.2.2 and Section 2.3.1 for more details on the parametrization of the terms and the numerical scheme, respectively).

Let $(x_i)_{i=1,\dots,n}$ and $(t_j)_{j=1,\dots,m}$ represent the spatial and temporal meshes, respectively. The solution $u(x, t)$ is approximated by a matrix $U = (u_{ij})_{ij}$, where u_{ij} denotes the temperature at spatial point x_i and time point t_j . Each simulation of the SPDE (15) is performed with a fixed value of the CO₂ parameter q . Different simulations vary by changes in the value of q , which is selected from the mesh $(q_k)_{k=0,\dots,29}$, where

$$q_k = 11.15 + \frac{k}{\Delta q}, \quad \Delta q = \frac{11.55 - 11.15}{29} \approx 1.21 \cdot 10^{-2}, \quad k = 0, \dots, 29. \quad (16)$$

For each spatial point $x_i \in [-1, 1]$, we compute the variance of the temperature over time. In other words, we measure how much the temperature fluctuates over the 500-year simulation period. Thus, we define our time-variance indicator as

$$\sigma_t^2(x_i) = \frac{1}{m} \sum_{j=1}^m (u_{ij} - \bar{u}_i)^2,$$

where $\bar{u}_i = \frac{1}{m} \sum_{j=1}^m u_{ij}$ represents the mean temperature at point x_i over time. Our simulations for σ_t^2 , shown in Figure 8a, reveal two primary behaviours in the variance. First, as the parameter q increases, the time variance σ_t^2 initially rises, reaching a peak around $q = 11.3069$, after which it begins to decline. This peak corresponds to the value of q that produces the greatest increase in global mean temperature (GMT), indicating a strong relationship between q and temperature variability. Second, the spatial profile of the variance is symmetric with respect to the centre of the domain, with local maxima occurring at three points: $x = 0$ (the equator) and $|x| \approx 0.8$ (sub-arctic regions). These maxima highlight regions where temperature fluctuations are particularly pronounced. In the next sections, we

are going to summarise our explanations of the two main properties of the time-variance: the spatial behaviour and behaviour with respect to carbon dioxide.

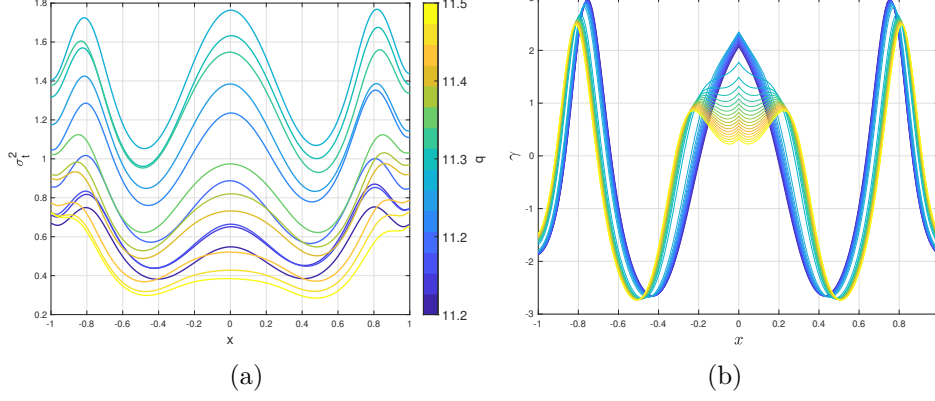


Figure 8: Indicators for the stochastic 1D-EBM (15) over the time interval $[0, T]$, with $T = 500$ yrs. (a) Time-variance indicator σ_t^2 . Different colours represent different values of q for which the stochastic 1D-EBM is simulated. (b) Local stability indicator γ , using the same colour scheme as in subfigure (a).

Local stability indicator - Spatial behaviour

To better understand why certain regions exhibit higher variance than others, we introduce a local stability indicator $\gamma(x)$, defined as:

$$\gamma(x) = \partial_u R(x, u_W(x)),$$

where $R(x, u) = R_a(x, u) - R_e(x, u; q)$ represents the net radiative forcing. In essence, $\gamma(x)$ measures the local stability of the temperature field: positive values of $\gamma(x)$ indicate instability, while negative values indicate stability in the absence of the diffusive coupling term $\kappa(x)u_x$.

First, our analysis shows that regions with high time variance also tend to exhibit positive values of $\gamma(x)$, indicating local instability, see Figure 8b. This suggests that time variance acts as a marker for regions where the climate system is most susceptible to fluctuations, particularly near the sub-arctic zones ($|x| \approx 0.8$) and the equatorial region ($x = 0$), where bistability and temperature gradients are strongest.

Second, we explain the presence of positive $\gamma(x)$ values as a consequence of the diffusion term in the model. Indeed, without diffusion, the warm steady-state solution at point x given by $u_W(x)$ it is just the minimiser, depending on x , of the potential functional of the system. In other words,

$$u_W(x) = \arg \min_{u \geq 0} \mathcal{R}(x, u),$$

with $\partial_u \mathcal{R} = R_e - R_a$. Thus, since u_W is a minimiser $\partial_u \mathcal{R}|_{(x, u_W(x))} = 0$. Further, under some mild regularity assumption, it follows that $\gamma(x) = \partial_u R|_{(x, u_W(x))} = \partial_u^2 \mathcal{R}|_{(x, u_W(x))} \leq 0$.

However, the addition of the diffusion term to the model introduces an additional complexity. The steady-state solution u_W is a minimiser of the functional

$$u \mapsto \int_{-1}^1 \mathcal{R}(x, u) dx + \frac{1}{2} \int_{-1}^1 \kappa(x) (u'(x))^2 dx.$$

Thus, the previous reasoning in the case $\kappa \equiv 0$ does not hold any more, and thus the local stability indicator may take positive values.

Local stability indicator - The effect of carbon dioxide

One of the key findings from our simulations is the peak in time variance at $q = 11.3069$, the previous increase, and the following decrease. To understand this phenomenon, we observe that as q increases, the steady-state temperature $u_W(x)$ rises, as can be guessed also by the calculation for the 0D case in (13) or the global mean temperature increase for u_W shown in the bifurcation diagram depicted in Figure 7. As the GMT rises, the temperature in the tropical area approaches the temperature interval in which the SGE effect is maximum. This leads to the increase of variance detected by σ_t^2 . However, once the tropical temperature exceeds this interval, the instability diminishes, leading to a reduction in variance.

We measure the instability of the SGE by averaging over the space domain the local stability indicator γ , i.e. we consider

$$\bar{\gamma}(q) = \int_{-1}^1 \gamma(x) dx = \int_{-1}^1 \partial_u R(x, u_W^{(q)}(x)) dx,$$

whose plot is shown in Figure 9. It closely follows the same trend as the time variance, peaking at $q = 11.3069$ and then declining.

0.3 A non-autonomous framework for weather, macroweather, and climate

Our work relies on considering a (stochastic) 1D-EBM depending on a slowly varying parameter $q(t)$, representing CO₂ concentration. In particular, the 1D-EBM has the form (we omit spatial dependence for clarity)

$$dT(t) = \bar{g}(T(t), q(t)) + \sigma dW(t), \quad (17)$$

where \bar{g} represents the radiation balance. Although it can be formulated with a single stochastic equation, we consider it an approximation of a more complex dynamic system that involves three different timescales: weather, macroweather, and climate. Weather operates on a daily to hourly scale,

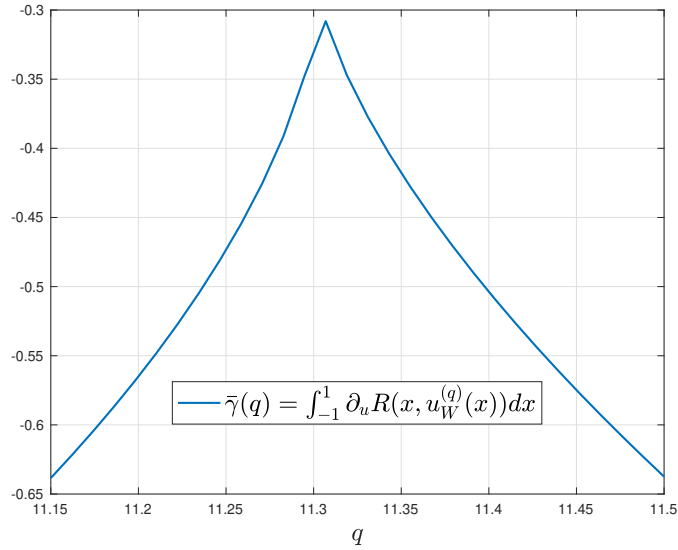


Figure 9: Average local stability indicator $\bar{\gamma}(q) = \int_{-1}^1 \partial_u R(x, u_W^{(q)}(x)) dx$. It increases, peaks at $q = 11.3069$, and then decreases.

macroweather on a scale of a few months to a few years, and climate on a scale of decades. While we simplify the model to focus on fewer timescales, it is important to emphasise the non-autonomous structure given by the time dependence of the CO_2 parameter $q(t)$.

The carbon dioxide concentration in the atmosphere varies on a longer timescale compared to macroweather: carbon dioxide in the atmosphere increased by 47% from 1850 to 2020, moving from 284 parts per million (ppm) to 412 ppm ([73]). For this reason, it is reasonable to consider the CO_2 parameter in the equation as fixed, i.e., not time-dependent, and study how the properties of the invariant measure change as a function of q . This is the *adiabatic*¹ approach to investigating the properties of the stochastic EBM. In other words, the stochastic equation we study is as follows:

$$dT(t) = \bar{g}(T(t), q) + \sigma dW(t). \quad (18)$$

The weather scale, based on Hasselmann’s work ([44]), is described by deterministic equations, where fast-changing variables represent fluid dynamics (such as velocity), and slower-changing variables like temperature evolve over months. Macroweather emerges when we change the scale to observe

¹In thermodynamics, a gas undergoes an adiabatic transformation during rapid expansion or compression. Although fast, the transformation is slow enough that the gas remains in a state of statistical equilibrium, preserving its entropy. Here, and throughout the text, we use the term “adiabatic” to refer to a variable, and the analysis of the associated equation, that varies much more slowly than the timescale of the system it is part of.

temperature variations over months and years. In this context, noise plays a critical role in driving these fluctuations, and stochastic processes become essential for accurately modelling these dynamics. At the macroweather scale, averaging approximations in the Freidlin-Wentzell style ([36]) help simplify the model by smoothing out short-term variations. However, this approach has limitations because it does not account for fluctuations, which was the pioneering idea of Hasselmann. He introduced noise to incorporate randomness into temperature dynamics on longer timescales than the weather, aligning with real-world temperature observations. We stress the importance of considering noise, delving into more details, in Subsections 2.1.1-2.1.4.

It is worth emphasizing that EBMs describe temperature on the macroweather timescale. This can be deduced by examining a linear 0D-EBM of the form:

$$C \frac{dT}{dt} = A - BT,$$

and considering the relaxation time of the model, $\tau_0 = \frac{C}{B}$. By plugging physically motivated values into the expression for τ_0 , it results in a macroweather timescale (see Section 2.2.1).

The third timescale is climate. In the adiabatic framework (18), we identify climate as the invariant measure of the stochastic EBM (in the non-autonomous framework (17), the invariant measure is time-dependent; see Section 2.1.5). In fact, climate is the result of the long-term evolution of the Earth's system, which began hundreds of millions of years ago from an initial condition whose significance has since been lost. The adiabatic approach we use in our analysis is also motivated by the fact that we consider the Earth's system on the macroweather timescale, where CO₂ slowly increases, and we track the invariant measure. Loosely speaking, we view our experience as a sample from the invariant measure. We observe an increasing number of extreme weather events each year because the invariant measure, i.e., the climate, now has a larger variance.

0.4 A fast-slow energy balance model

The following section contains an ongoing research and has two main goals. First, it aims to justify the inclusion of noise in the stochastic EBM, a key theme as it directly relates to understanding the origins of climate variability. This topic has been long discussed in the literature, and, following Hasselmann's foundational work, it is often attributed to the interaction of different timescales in climate dynamics, particularly the influence of fast processes on slower ones. We present a new derivation of the stochastic Stratonovich equation introduced by K. Hasselmann, sometimes referred to as the (N)-approximation for fast-slow climate equations (see [53, 63]), based on an approach *à la* Wong-Zakai.

The second goal is to enhance the model with a suitable multiplicative noise component. Thus far, we have considered an additive white noise in both space and time, which is a simplified and less realistic assumption (see [44, 3]). The modified stochastic EBM derived here will include a diffusion term that increases with temperature.

The starting point is a fast-slow system which, in a simplified way, it is assumed to be able to describe the interaction between a “slow” temperature component T , at a macroweather timescale, and a “fast” component Q_t , representing weather fluctuations. This latter component is modelled by solar radiation, defined as the power per unit area received from the Sun at Earth’s surface. This model is given by:

$$\begin{cases} dQ_t &= -\frac{1}{\tau}(Q_t - \bar{Q})dt + \frac{1}{\sqrt{\tau}}dW_t, \\ \frac{dT}{dt} &= Q_t\beta(T) + q - \varepsilon_0\sigma_0T^4. \end{cases} \quad (19)$$

The parameter $\tau > 0$ represents the separation among the timescales of the two processes in (19). Its magnitude is thus 10^{-2} , so quite small but not infinitesimal. This, as we will see, it is a key aspect of our discussion. The dynamics describing the evolution in time of temperature is the radiation balance between absorbed and emitted radiation, the classical mechanism driving EBMs. For simplicity of notation, we will rename the system as follows

$$\begin{cases} dX_t^\tau = -\frac{1}{\tau}(X_t^\tau - \bar{Q})dt + \frac{1}{\sqrt{\tau}}dW_t, & X_0^\tau = x, \\ dY_t^\tau = g(X_t^\tau, Y_t^\tau)dt, & Y_0^\tau = y, \end{cases} \quad (20)$$

where $g(x, y) = x\beta(y) - \alpha(y)$, and $\alpha(y) := q - \varepsilon_0\sigma_0y^4$. For the ease of notation, from now on we will denote the processes as X_t, Y_t , thus dropping the dependence on τ .

The following is the key result that we will use to derive a closed equation for the slow variable Y_t .

Lemma 5. *For each $t > 0$, it holds*

$$\lim_{\tau \rightarrow 0} \mathbb{E} \left| \frac{1}{\sqrt{\tau}} \int_0^t X_s ds - \frac{\bar{Q}t}{\sqrt{\tau}} - W_t \right|^2 = 0.$$

Now, we aim to derive a closed equation for the slow process Y_t . We heuristically invoke Lemma 5 to justify the following approximation:

$$X_t - \bar{Q} \approx \sqrt{\tau} \frac{dW(t)}{dt}. \quad (21)$$

This enables us derive the following equation for the slow process:

$$\begin{aligned} \frac{dY_t}{dt} &= (X_t - \bar{Q} + \bar{Q}) \beta(Y_t) + q - \varepsilon_0\sigma_0Y_t^4 \\ &= \bar{Q}\beta(Y_t) + q - \varepsilon_0\sigma_0Y_t^4 + \sqrt{\tau}\beta(Y_t) \frac{dW(t)}{dt}. \end{aligned} \quad (22)$$

Then, we perform an approximation inspired by the Wong-Zakai principle, although it does not fit exactly within that framework. Using this approximation, which we will comment on later, we replace the previous equation with the Stratonovich SDE:

$$d\tilde{Y}_t = \left(\bar{Q}\beta(\tilde{Y}_t) + q - \varepsilon_0\sigma_0\tilde{Y}_t^4 \right) dt + \sqrt{\tau}\beta(\tilde{Y}_t) \circ dW_t, \quad (23)$$

which can be converted to Ito form by applying the Ito-Stratonovich correction:

$$d\tilde{Y}_t = \left(\bar{Q}\beta(\tilde{Y}_t) + \frac{\tau}{2}\beta(\tilde{Y}_t)\beta'(\tilde{Y}_t) + q - \varepsilon_0\sigma_0\tilde{Y}_t^4 \right) dt + \sqrt{\tau}\beta(\tilde{Y}_t)dW_t. \quad (24)$$

Remark 6. *The most important consequence of the previous stochastic model is that the diffusion term is increasing, due to the co-albedo properties, with respect to temperature. Thus, the larger the temperature, the larger the variance of the solution, and thus the possibility of observing extreme weather events.*

It is worth recalling the Wong-Zakai principle, which underpins our derivation of the stochastic EBM (24) with Stratonovich noise. Loosely speaking, this principle states that if we approximate Brownian Motion (BM) with a smooth process, then take the limit of this smooth approximation, the resulting stochastic differential equation aligns with the Stratonovich rather than the Ito interpretation. A constructive example of a possible approximation of BM follows.

Lemma 7. *For $\varepsilon > 0$, consider the solution ξ_t^ε of the linear SDE*

$$d\xi_t^\varepsilon = -\frac{1}{\varepsilon}\xi_t^\varepsilon dt + \frac{1}{\varepsilon}dW_t, \quad \xi_0^\varepsilon = 0.$$

Then, setting $W_t^\varepsilon := \xi_t^\varepsilon$, we have $W_t^\varepsilon \xrightarrow[\varepsilon \rightarrow 0]{\mathbb{P}} W_t$.

Second, we state a version of the Wong-Zakai principle, which can, in any case, be strengthened, see [48, 84].

Theorem 8 (Wong-Zakai). *For $\varepsilon > 0$, let Y_t^ε be the solution of the ODE*

$$\frac{dY_t^\varepsilon}{dt} = b(Y_t^\varepsilon) + \sigma(Y_t^\varepsilon)\frac{dW_t^\varepsilon}{dt}.$$

Then, $Y_t^\varepsilon \xrightarrow[\varepsilon \rightarrow 0]{\mathbb{P}} Y_t$, where Y_t solves the SDE

$$dY_t = b(Y_t)dt + \sigma(Y_t) \circ dW_t.$$

Remark 9. We are not applying a true Wong-Zakai result to obtain (24). The Wong-Zakai principle (WZP) is a limiting result, which in our case would apply as $\tau \rightarrow 0$. However, there are at least two reasons why we must diverge from the WZP: (i) the physical interpretation of τ , and (ii) the differing scaling in our model compared to that used in WZP. First, the scaling parameter τ represents the timescale separation between the fast weather component (e.g., one day) and the slower macroweather component (e.g., six months or one year). Even though this ratio is small, it is far from zero. Furthermore, if we took $\tau \rightarrow 0$ in (21), we would obtain a deterministic closed equation for temperature in (22).

Second, our fast equation for solar radiation in (19) does not follow the scaling in the drift-diffusion coefficients required by Lemma 5. Specifically, our drift is scaled by $\frac{1}{\tau}$ and the diffusion by $\frac{1}{\sqrt{\tau}}$, whereas the fast process ξ^ε in WZP has both drift and diffusion scaled by $\frac{1}{\varepsilon}$. Nevertheless, we are confident that the scaling used for τ is correct for our setting. A primary reason is that, if we consider a SDE of the form

$$d\eta_t = b(\eta_t)dt + dW_t, \quad (25)$$

and we consider the rescaled fast process

$$\eta_t^\tau := \eta_{t/\tau},$$

then $(\eta_t^\tau)_t$ solves the SDE

$$d\eta_t^\tau = \frac{1}{\tau}b(\eta_t^\tau)dt + \frac{1}{\sqrt{\tau}}d\widetilde{W}_t, \quad (26)$$

where $(\widetilde{W}_t)_t$ is a Brownian Motion; in other words, if we first consider a solar radiation which satisfies an equation of the form (25), then on a faster timescale for the same process we get the $\frac{1}{\tau}, \frac{1}{\sqrt{\tau}}$ scaling from equations (26). Second, the variance of the (Gaussian) invariant measure for the solar radiation process X_t remains independent of τ , as we will explicitly calculate later in (3.1).

0.4.1 Link with Hasselmann's proposal

In this section, we briefly present Hasselmann's main contribution, in our opinion, to climate science, i.e. the conjecture that temperature (that we consider as representative climate variable) on a slow timescale (macroweather or climate timescale) satisfies a stochastic equation, provided that we that from a (realistic) fast-slow model describing the interaction between fast weather and slow climate.

Hasselmann's approach begins with a fast-slow ODE system:

$$\begin{cases} \dot{x} &= \frac{1}{\varepsilon}f(x, y), \\ \dot{y} &= g(x, y), \end{cases} \quad (27)$$

where $\varepsilon > 0$ is a scaling parameter that separates the fast weather component x from the slower climate (or macroweather) component y . To derive an equation for the slow variable y , we can apply the averaging principle (see [36]), which approximates y in (27) by a solution \bar{y} of the averaged equation

$$\dot{\bar{y}} = \bar{g}(\bar{y}), \quad (28)$$

where

$$\bar{g}(y) := \int g(x, y) \mu_y(dx).$$

This expression assumes that, for each fixed y , the fast equation

$$\dot{x} = \frac{1}{\varepsilon} f(x, y)$$

has a unique ergodic invariant measure μ_y . Determining this invariant measure in the deterministic case is complex, and not clearly understood. However, for the stochastic case, where the fast component has additional noise (such as an additive noise), the averaging principle is well studied, and we will focus on this in Section 0.4.2.

Hasselmann's pioneering insight was that the macroweather timescale solution is better represented by including fluctuations around the averaged dynamics. Specifically, he proposed that the slow variable y on an appropriate timescale satisfies an SDE of the form:

$$d\tilde{Y}_t = \bar{g}(\tilde{Y}_t) dt + A(\tilde{Y}_t) \circ dW_t, \quad (29)$$

where A is the diffusion term. By following Hasselmann's framework ([44, 3]), it can be shown that this equation, which we will refer to as *Hasselmann's equation*, reduces to (24) when starting from the fast-slow system (19). That is,

$$\bar{g}(y) = \int g(x, y) \mu(dx),$$

where μ is the invariant measure of the fast equation in (19), and $A(y) = \sqrt{\tau} \beta(y)$.

The following sections will demonstrate that both Hasselmann's equation (24) and our fast-slow model (19) are the same if we compute the: (i) deterministic zero-noise limits, (ii) Gaussian fluctuations around the averaged solution (zero-noise limit), and (iii) a large deviation principle. Our new contribution in the following sections consists in realising that equations (24) and (19) share the same characteristics given by (i), (ii), and (iii). Indeed, the use of the averaging principle, the Gaussian fluctuations, and the large deviations principle are rather classic in the probability field, as the results that we will present in the following (Theorem 10, and Propositions 11-14).

0.4.2 Averaging principle: deterministic limit

For a stochastic case fast-slow system in the form (19) the averaging principle is, in contrast to the deterministic case, well understood. In particular, up to technical assumptions (see [36, Chapter 7]), it can be proved the following result, in which we merge also the averaging result for the Hasselmann's equation.

Theorem 10 (Averaging Principle). *Let $T > 0$ and denote by $\mu(dx)$ the invariant measure for the fast equation in (19). Let $(\bar{Y}(t))_t$ be the solution of the ODE*

$$\dot{\bar{Y}}(t) = \bar{g}(\bar{Y}), \quad (30)$$

where

$$\bar{g}(y) := \int g(x, y) \mu(dx).$$

Consider $(Y_t^\tau)_t$ solution of the fast-slow system (19). Then, for any $\delta > 0$, it holds

$$\mathbb{P} \left(\sup_{0 \leq t \leq T} |Y_t^\tau - \bar{Y}(t)| > \delta \right) \xrightarrow{\tau \rightarrow 0} 0.$$

Similarly, if $(\tilde{Y}_t)_t$ is the solution of Hasselmann's equation (24), for any $\delta > 0$ it holds

$$\mathbb{P} \left(\sup_{0 \leq t \leq T} |\tilde{Y}_t - \bar{Y}(t)| > \delta \right) \xrightarrow{\tau \rightarrow 0} 0.$$

0.4.3 Gaussian fluctuations

In stochastic systems driven by small noise, the study of fluctuation processes provides insights into the behaviour of solutions near their deterministic limit. Fluctuations characterise the deviations from the deterministic trajectory, typically scaled by the inverse square root of the noise intensity, to observe how small perturbations influence the system's dynamics. This scaling follows the idea of the Central Limit Theorem in probability theory, where sums of independent random variables converge, after appropriate scaling, to a Gaussian distribution. Analogously, for SDEs, scaled fluctuation processes converge to a Gaussian process as the noise intensity tends to zero, capturing the an higher order behaviour of the SDE with respect to the averaged equation.

Here, we present the results regarding the Gaussian fluctuations for our model (19) and the Hasselmann stochastic EBM (24). For both results, which are classical, we do not focus on the assumptions but rather present the limiting equations and a sketch of the proofs. For the assumptions needed, we refer to [36, Chapter 7].

Proposition 11. *Consider the Gaussian fluctuations for the stochastic Hasselmann's EBM (24)*

$$Z_t^\tau := \frac{\tilde{Y}_t^\tau - Y_t^0}{\sqrt{\tau}} = \frac{\tilde{Y}_t^\tau - \bar{Y}(t)}{\sqrt{\tau}}.$$

Then, denoting by \xrightarrow{d} the convergence in distribution, it holds

$$(Z_t^\tau)_{t \in [0, T]} \xrightarrow[\tau \rightarrow 0]{d} (Z_t)_{t \in [0, T]}$$

where $(Z_t)_{t \in [0, T]}$ solves the SDE

$$\begin{aligned} dZ_t &= \bar{g}'(\tilde{Y}_t^0) Z_t dt + \beta(\tilde{Y}_t^0) dW_t \\ &= \bar{g}'(\bar{Y}(t)) Z_t dt + \beta(\bar{Y}(t)) dW_t. \end{aligned} \quad (31)$$

Proposition 12. *Let $(X_t^\tau, Y_t^\tau)_{t \in [0, T]}$ be the solution of the fast-slow system (19). Consider the fluctuations processes*

$$\zeta_t^\tau := \frac{Y_t^\tau - \bar{Y}(t)}{\sqrt{\tau}}, \quad \eta_t^\tau = \frac{X_t^\tau - \bar{Q}}{\sqrt{\tau}}.$$

Then, as $\tau \rightarrow 0$, we have

$$\zeta_t^\tau \xrightarrow[\tau \rightarrow 0]{\mathbb{P}} \zeta_t, \quad \forall t \in [0, T],$$

where $(\zeta_t)_t$ is the solution of

$$d\zeta_t = \bar{g}'(\bar{T}(t)) \zeta_t dt + \beta(\bar{T}(t)) dW_t,$$

and $\xrightarrow{\mathbb{P}}$ denotes convergence in probability.

0.4.4 Large deviations principle

In this section, we describe the large deviation principle (LDP), which, in our case, will inform us about the tails in the behaviour of the slow process describing temperature. Indeed, LDP provides a rigorous framework to quantify the asymptotic probabilities of deviations of the temperature variable Y_t^τ (or \tilde{Y}_t) from its typical behaviour, i.e. the averaged process $\bar{Y}(t)$. More in details, focusing on fast-slow system (19) (but the same intuition holds for the Hasselmann's equation (24)), if a LDP holds, then, given a continuous path $y(\cdot)$, we have

$$\mathbb{P}(Y^\tau(\cdot) \text{ is near } y(\cdot)) \approx \exp\left(-\frac{1}{\tau} I(y(\cdot))\right),$$

where I is called *rate function* or *action functional*. It captures the likelihood of observing deviations of Y_t^τ from the deterministic path $y(\cdot)$: the smaller the value of $I(y)$, the more likely Y_t^τ is to be found near $y(\cdot)$ in the limit $\tau \rightarrow 0$.

We start by recalling what is the rate function for an SDE with multiplicative noise, as Hasselmann's equation (24).

Proposition 13. *The solution $(\tilde{Y}_t)_t$ of the Hasselmann stochastic EBM*

$$d\tilde{Y}_t = \bar{g}(\tilde{Y}_t)dt + \sqrt{\tau}\beta(\tilde{Y}_t) \circ dW_t$$

satisfies a large deviation principle with rate function

$$I(y(\cdot)) = \frac{1}{2} \int_0^T \left| \frac{1}{\beta(y(t))} [\dot{y}(t) - \bar{g}(y(t))] \right|^2 dt. \quad (32)$$

The greatness of Hasselmann's insight was that he predicted an equation for the macroweather whose tails are analogous to those of the original slow-fast system.

Proposition 14. *The slow component Y_t in the fast-slow system (19) satisfies a large deviation principle with the same rate function defined in (32).*

Chapter 1

A class of space heterogeneous one-dimensional energy balance models

In this chapter, which covers the content of [24] and its Supplementary Material, we present rigorous proofs for the results outlined in Section 0.1 of the paper. This chapter is organised as follows. In Section 1.2, we recall the definition of the functional associated with the elliptic problem arising from the study of the stationary solutions of the EBM depending on an additive positive parameter q representing the carbon dioxide concentration. In Section 1.3, we make rigorous the link between the functional F_q which constitutes the variational problem and the Gibbs invariant measure of the stochastic 1D-EBM. In Section 1.4, we rigorously prove the existence of a global minimiser for the functional using the direct method from the calculus of variations. Furthermore, we establish the regularity, non-negativity, and boundedness of the minimiser. In Section 1.5, we characterise the uniqueness of the global minimiser in terms of the value function, i.e., the minimum, depending on q , among the values of the functional. Further, we show that the derivative of the value function is, up to the sign, the global mean temperature of the minimiser of the variational problem. Then, in Section 1.6 we prove that the value function is not only semiconcave but also concave. In particular, this last property implies that the global mean temperature of the variational problem minimiser is non-decreasing with respect to q . Lastly, in Section 1.7 we provide sufficient conditions to prove the existence of three steady-state solutions for the EBM. This relies on the use of the Mountain Pass Theorem and the direct method from the calculus of variations.

1.1 Model formulation

The fundamental mechanism of 1D-EBMs is that the temperature $u(t, x)$, averaged in the zonal direction, evolves in time due to: (i) the diffusion of energy between adjacent regions, (ii) the energy absorbed by the planet, and (iii) the energy emitted by the planet. The 1D-EBM we consider in this paper is a Seller type EBM where the absorbed radiation depends on an additive parameter ([6]). We only add a change in the diffusion term in order to get a non-degenerate parabolic PDE. Given an initial condition u_0 , the non-linear, parabolic, reaction-diffusion PDE governing the model is given by:

$$\begin{aligned} C_T \frac{\partial u}{\partial t} &= \partial_x [\kappa(x) \partial_x u] + R_a(x, u) - R_e(u; q), \quad t > 0, \quad x \in (-1, 1) \\ \kappa(-1)u_x(t, -1) &= \kappa(1)u_x(t, 1) = 0, \quad t \geq 0 \\ u(0, x) &= u_0(x), \quad x \in [-1, 1], \end{aligned} \tag{1.1}$$

where R_a and R_e represent the radiation absorbed and emitted by the planet per unit area, respectively. C_T is the heat capacity, and the differential term parametrises the meridional heat transport. The boundary conditions impose no flux at the poles. We now provide further details regarding the parameterisation of these terms. The values of the constants of the model can be found in Table 1.1.

Firstly, the absorbed radiation is assumed to have the form:

$$R_a(x, u) = Q_0(x)(1 - \alpha(u)),$$

where Q_0 is the solar radiation per unit area, and α is the albedo. The solar radiation is assumed to be

$$Q_0(x) = \hat{Q}_0 (c_1 - c_2 x^2), \quad c_i > 0$$

where \hat{Q}_0 is the mean solar radiation and c_i are constants. The albedo, which is the proportion of the incident light or radiation that is reflected by a surface, is parametrised by a smooth monotonically increasing function with a peak derivative in a reference temperature u_{ref} close to the melting point of ice. Specifically

$$\alpha(u) = \alpha_1 + (\alpha_2 - \alpha_1) \left[\frac{1 + \tanh(K(u - u_{ref}))}{2} \right]$$

where $K > 0$ is a rate parameter and $\alpha_1 > \alpha_2$ are respectively the ice-albedo and the water-albedo.

Second, the emitted radiation is modelled using the Stefan-Boltzmann law, in other words assuming that the Earth radiates as a black body. Under

this assumption, the energy radiated is proportional to the fourth power of its temperature and it is given by:

$$R_e(u; q) = \varepsilon_0 \sigma_0 u^4 - q.$$

where ε_0 and σ_0 are respectively the emissivity and Boltzmann's constant. The additive parameter q describes, in a simplified way, the radiative forcing by CO₂, i.e. the effect of atmospheric CO₂ on the energy budget [80]. It is worth explaining: (i) the additive structure of q , and (ii) its independence on the spatial variable x . About the first point, denote by C the global CO₂ concentration in part per million (ppm) and assume, just for explanation purposes, a dependence of the outgoing radiation both on u and C . To avoid confusion, we denote by $\hat{R}_e = \hat{R}_e(u, C)$ the outgoing radiation depending on temperature and CO₂ concentration. If we linearise \hat{R}_e w.r.t. temperature, we get:

$$\hat{R}_e(u, C) \approx A(C) + B(u - \hat{u}),$$

where \hat{u} is a reference temperature. In [65], three radiative transfer models are used in order to get that the dependence of the outgoing radiation which respect to changes in CO₂ is given by:

$$A(C) = A_1 - A_2 \cdot \ln \left(\frac{C}{C_0} \right),$$

where C_0 is a reference CO₂ concentration and $A_1, A_2 > 0$ are explicit constants. In conclusion

$$\hat{R}_e \approx A_1 + B(u - \hat{u}) - q, \quad q = A_2 \cdot \ln \left(\frac{C}{C_0} \right),$$

and thus the radiative forcing of CO₂ has an additive structure. About point (ii), we adopt the well-mixed hypothesis for CO₂. In other words, we assume that atmospheric CO₂ is globally homogeneous, thereby inducing a radiative forcing q independent of latitude [46]. This assumption overlooks the spatial pattern of CO₂ concentration, which affects many aspects of the climate system, such as the pole-ward heat transport [47]. It was the state-of-the-art assumption two decades ago, although today it is common to keep in consideration the spatial distribution of radiative forcing [46, 13, 86].

The third component of the model is the term $\partial_x (\kappa(x)u_x)$. It parametrises the meridional heat transport, that is the phenomenon resulting from the poleward transportation of heat by the Earth-atmosphere system due to the surplus of net radiation heating in the tropics and the deficit in the poleward regions. Usually, the diffusion function $\kappa(x)$ is assumed null at the poles, i.e. with a form such as $\kappa(x) = D(1 - x^2)$, where D is a diffusion constant. This choice is based on the paradigm of mimicking the conduction of heat on a sphere, see ([72]) for a derivation. On the other hand, it leads to mathematical difficulties in the treatment of the singular PDE arising, in

particular in the study of the corresponding variational problem, from which all our results follow. To avoid these difficulties, which at the moment remain an open problem to solve, we add as simplifying assumption that κ is non-degenerate and given by:

$$\kappa(x) = D(1 - x^2) + \delta, \quad D, \delta > 0.$$

We choose $\delta = 0.003$, but its value is not important for the results of this work and different choices can be made.

For the parabolic problem (1.1), the global existence and uniqueness of the solution can be demonstrated, given a regular initial condition ([82]). Furthermore, if the initial condition is non-negative, the solution remains non-negative for any time $t > 0$. This can be shown proving that $[0, +\infty)$ is an invariant region for Eq. (1.1), exploiting the fact that there exist $C_1, C_2 > 0$ such that $R(x, u; q) > C_1 > 0$ for all $x \in [-1, 1]$, $u \in [0, C_2]$ ([78]).

We recall the formulation of stochastic EBMs using the theory of SPDEs ([22]). Denote by Δ the Laplace operator with Neumann boundary conditions. Given an initial condition $u_0 \in H$, we consider the SPDE

$$\begin{aligned} \partial_t u &= \kappa \Delta u + Q_0(x) \beta(u) + q - R_e(u) + \varepsilon dW_t \\ u|_{t=0} &= u_0 \end{aligned} \tag{1.2}$$

where $\varepsilon > 0$ and $(W_t)_{t \geq 0}$ is a cylindrical Brownian motion on H . Under the minor cut-off modifications introduced in Section 0.1.1, it can be proved that the H -valued stochastic process $(u_t)_t$ which solves in mild sense (1.2) is unique and has continuous trajectories ([22]). In addition to this, there exists a unique Gibbs invariant measure

$$\nu(du) = \frac{1}{Z} \exp\left(-\frac{2}{\varepsilon^2} \int_{-1}^1 \mathcal{R}(x, u; q) dx\right) \mu(du), \tag{1.3}$$

where \mathcal{R} is as in Eq. (6), $\mu \sim \mathcal{N}(0, -\frac{\varepsilon^2}{2\kappa} \Delta^{-1})$ is a symmetric Gaussian measure on H with covariance $\mathcal{Q} = -\frac{\varepsilon^2}{2\kappa} \Delta^{-1}$ ([20, 21]). The covariance operator $\mathcal{Q}: H \rightarrow H$ is the unique linear operator such that $\int_H \langle h_1, \phi \rangle \langle h_2, \phi \rangle \mu(d\phi)$ for each $h_1, h_2 \in H$, where $\langle \cdot, \cdot \rangle$ denotes the scalar product in H . Further, it can be shown that \mathcal{Q} is symmetric, positive-definite and its eigenvalues $(\lambda_k)_{k \in \mathbb{Z}}$ satisfy $\sum_{k \in \mathbb{Z}} \lambda_k < \infty$. In the following lines, given a symmetric, positive-definite operator \mathcal{Q} such that $\sum_{k \in \mathbb{Z}} \lambda_k < +\infty$, we are going to explain how to construct an H -valued random variable X with law $\mathcal{N}(0, \mathcal{Q})$. Indeed, consider a sequence $(R_k)_{k \in \mathbb{Z}}$ of i.i.d. \mathbb{R} - $\mathcal{N}(0, 1)$ random variables defined on a probability space $(\Omega, \mathcal{F}, \mathbb{P})$. We can assume without loss of generality that the eigenvectors $(e_k)_{k \in \mathbb{Z}}$ associated to the eigenvalues $(\lambda_k)_{k \in \mathbb{Z}}$ form an orthonormal basis of H . Then, the H -valued random variable

$$X = \sum_{k \in \mathbb{Z}} \sqrt{\lambda_k} R_k e_k,$$

is well defined, i.e. the series defining X converges in $L^2(\Omega, \mathcal{F}, \mathbb{P}; H)$, and has law $\mathcal{N}(0, \mathcal{Q})$ [21, Proposition 2.18]. Further, the convergence also holds \mathbb{P} -a.s. in H [21, Proposition 2.13].

As mentioned in the introduction, this measure is concentrated on minimum points of the functional F_q . A heuristic explanation of this fact can be found in Section 0.1.1.

The stationary problem associated with the 1D-EBM is given by the elliptic equation:

$$\begin{aligned} (\kappa(x)u_x)' + Q_0(x)\beta(u) + q - \varepsilon_0\sigma_0u^4 &= 0, & x \in (-1, 1) \\ u'(-1) = u'(1) &= 0, & u(x) \geq 0. \end{aligned} \quad (1.4)$$

These solutions can be either stable or unstable, depending on the long-term behaviour of their infinitesimal perturbations. As pointed out in ([6]), if the reaction-diffusion equation was space-homogeneous, i.e. of the form:

$$\partial_t u = \kappa \Delta u + R(u), \quad (1.5)$$

then the stable steady-state solutions would correspond to constant functions, taking the same values as the stable fixed point of the ODE

$$y'(t) = R(y(t)).$$

A rigorous result in this direction has been shown in ([38]). Indeed, for a fixed double-well symmetric potential, it has been proved that: (i) if κ is large enough, the only steady-state solutions of (1.5) are the constants where the potential is critical, and (ii) the number of unstable steady-state solutions to (1.5) can be made arbitrary large as $\kappa \rightarrow 0$. Introducing a spatial dependence in $R = R(x, u)$ leads to a space-heterogeneous model. Depending on the space heterogeneity, it can exhibit any number of both stable and unstable steady-state solutions ([6]). The variational approach to the study of steady-state solutions provides a tool for characterizing the stable ones, which are the local minimum points of a functional.

In the following paragraph, we describe the properties of the solutions of (1.4). As the parameter q changes, numerical simulations for Eq. (1.4) suggest the existence of either one or three steady-state solutions. That is, there exists $q_1 < q_2$ s.t. Eq. (1.1) has one steady-state solution if $q < q_1$ or $q > q_2$, and the steady-state solutions are three if $q_1 \leq q \leq q_2$. In the latter case, we denote the solutions by $u_S \leq u_M \leq u_W$, corresponding respectively to the snowball climate, a middle climate and the warm climate. As an analogy, we denote by u_S the unique steady-state solution for $q < q_1$ and by u_W the unique one for $q > q_2$. Figure 1.1a shows the bifurcation diagram of the model in the (q, \bar{u}) plane, where $\bar{u} = \int_{-1}^1 u(x) dx$ denotes the average temperature. Figure 1.1b depicts the three steady-state solutions for $q = 25 \in (q_1, q_2)$.

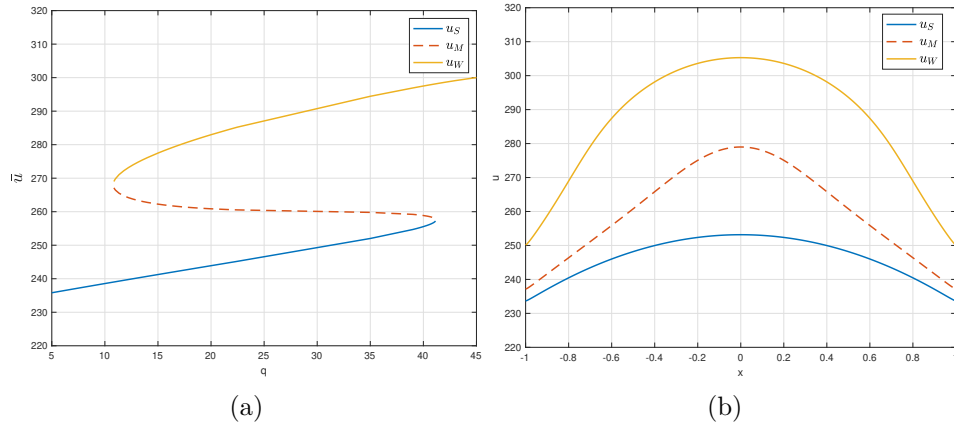


Figure 1.1: (a) Bifurcation diagram of the steady-state solutions in the (q, \bar{u}) plane, with $\bar{u} = \int_{-1}^1 u(x) dx$. Solid lines denote stable solutions u_S and u_W , while dashed lines the unstable solution u_M . (b) Steady-state solutions of the EBM for $q = 25$. In every point x of the space domain, the three steady-state solutions satisfy $u_S(x) < u_M(x) < u_W(x)$, with maximum temperature attained at the equator and minimum temperature attained at the poles.

A stability analysis can be conducted to determine the stability of the steady-state solutions. The results show that u_S and u_W are stable, while the middle climate u_M is unstable. Furthermore, it's worth noting that special values $q = q_1, q_2$ correspond to bifurcation points of saddle-node type, where the unstable solution u_M collides with either u_W (for $q = q_1$) or u_S (for $q = q_2$) and then disappears. These numerical findings regarding the number and stability of the steady-state solutions will be supported and validated using rigorous arguments, as in Section 0.1.1.

Symbol	Meaning	Value
D	Diffusivity constant	0.3
δ	Meridional heat transport perturbation constant	0.003
\hat{Q}_0	Mean solar radiation	341.3 W m^{-2}
ε_0	Emissivity	0.61
σ_0	Boltzmann's constant	$5.67 \cdot 10^{-8} \text{ W m}^{-2} \text{ K}^{-1}$
α_1	Ice albedo	0.7
α_2	Water albedo	0.289
K	Constant rate - albedo parametrization	0.1
u_{ref}	Reference temperature - albedo parametrization	275 K
C_T	Heat capacity	$5 \cdot 10^8 \text{ J m}^{-2} \text{ K}^{-1}$

Table 1.1: Parameters and constants appearing in the Seller EBM (1.1).

1.2 Functional definition

The 1D-EBM we consider has the form ([6]):

$$\begin{aligned} C_T \partial_t u &= \partial_x (\kappa(x) u_x) + Q_0(x) \beta(u) + q - \varepsilon_0 \sigma_0 u^4, \quad (t, x) \in [0, T] \times [-1, 1] \\ u_x(t, -1) &= u_x(t, 1) = 0, \quad t \geq 0, \\ u(0, x) &= u_0(x), \end{aligned}$$

where u_0 denotes the initial condition. The steady-state solutions to the previous problem are associated with the functional ([11, 71]):

$$F_q(u) = \int_{-1}^1 \varepsilon_0 \sigma_0 \frac{(u^5)_+}{5} - Q_0(x) B(u) - q u \, dx + \frac{1}{2} \int_{-1}^1 \kappa(x) [u'(x)]^2 \, dx.$$

In Section 0.1, we have illustrated some properties of the minimiser of the variational problem

$$\inf \left\{ F_q(u) \mid u \in H^1, u \geq 0 \right\}.$$

In this paragraph, we give the details of the definition of the radiation balance

$$R(x, u; q) = R_a(x, u) - R_e(u; q)$$

when u takes negative values, i.e. belongs to the unphysical range of temperature values. We recall that the radiation emitted is defined as a cut-off for negative value as in (8), i.e.

$$R_e(u; q) = \begin{cases} \varepsilon_0 \sigma_0 u^4 - q, & \text{if } u \geq 0 \\ -q, & \text{if } u < 0. \end{cases}$$

Denote by Ψ a primitive of R_e , i.e. $\Psi(u) = \varepsilon_0 \sigma_0 \frac{(u^5)_+}{5}$, where $(x)_+ = \max(x, 0)$. On the other hand, the co-albedo $\beta: \mathbb{R}_+ \rightarrow \mathbb{R}$ is extended to $\tilde{\beta}: \mathbb{R} \rightarrow \mathbb{R}$ as follows. Consider $\tilde{\beta}$ be s.t. $\tilde{\beta} \in C^\infty$ and

- (i) $\tilde{\beta}$ is monotonically increasing
- (ii) $\tilde{\beta}(u) \geq 0 \forall u \in \mathbb{R}$
- (iii) $\tilde{\beta}(u) = 0$ for $u \leq -M$, for some $M > 0$
- (iv) $\tilde{\beta}$ extends β for $u \geq 0$.

Denote by $B(u) := B_0 + \int_0^u \tilde{\beta}(v) dv$ a primitive of β , with B_0 s.t. $B(u) \geq 0 \forall u \in \mathbb{R}$. It will be useful in future to note that

$$0 \leq B(u) \leq |B_0| + |u| \quad \forall u. \tag{1.6}$$

In a similar way, we consider the extension of the Stefan-Boltzmann law given by:

$$\psi(u) = \begin{cases} \varepsilon_0 \sigma_0 u^4, & \text{if } u \geq 0 \\ 0, & \text{if } u < 0. \end{cases}$$

Lastly, since in our model we are assuming κ continuous and positive on $[-1, 1]$, we can also assume κ constant. Indeed, all the proofs, that in Chapter 1 are carried with constant κ , extended immediately to the non-constant case. In conclusion, the uniformly elliptic equation we are considering is given by:

$$\begin{aligned} 0 &= \kappa \Delta u + Q_0(x) \tilde{\beta}(u) + q - \psi(u), \\ u'(-1) &= u'(1) = 0, \end{aligned} \tag{1.7}$$

and the functional associated with its solution is

$$F_q(u) = \int_{-1}^1 \Psi(u) - Q_0(x) B(u) - qu \, dx + \frac{\kappa}{2} \int_{-1}^1 [u'(x)]^2 \, dx.$$

1.3 Gibbs invariant measure and functional minimum point

In this section, we make rigorous the relation between F_q and the invariant measure ν of the stochastic EBM. In particular, we prove a result giving information about the concentration of ν around minimum points for F_q . We start by recalling the notation and some useful results.

First, we set

$$I(u) := \int_{-1}^1 \left(\varepsilon_0 \sigma_0 \frac{(u^5)_+}{5} - Q_0(x) B(u) - qu \right) dx.$$

Consider $H = L^2(-1, 1)$ and $E = C([-1, 1])$. Then, following the theory SPDE, the stochastic equation obtained by adding a cylindrical Brownian motion is a gradient SPDE of the form

$$dX_t = [AX_t + f(x, X_t)] dt + \varepsilon dW_t, \quad X|_{t=0} = x_0 \tag{1.8}$$

where $(W_t)_t$ is a cylindrical Wiener process on H and $A = \kappa \Delta$ is the Neumann Laplacian with constant viscosity $\kappa > 0$, i.e. $A: D(A) \subset H \rightarrow H$,

$$\begin{aligned} D(A) &= \left\{ u \in H^2(-1, 1) \mid u'(-1) = u'(1) = 0 \right\} \\ Au &= \kappa u'', \end{aligned} \tag{1.9}$$

and

$$f(x, u) = Q_0(x) \tilde{\beta}(u) + q - \varepsilon_0 \sigma_0 (u^4)_+$$

We refer to [20] for details about the properties of the previous SPDE. The mild solution X_t of (1.8) is \mathbb{P} -a.s valued in E . Further, applying the theory of invariant measure developed in [21], we get the following property.

Proposition 15. *The SPDE (1.8) has a unique Gibbs invariant measure ν . Further, $\nu \ll \mu$ with explicit formula:*

$$\nu(du) = \frac{1}{Z} \exp\left(-\frac{2}{\varepsilon^2} I(u)\right) \mu(du), \quad u \in H \quad (1.10)$$

where $\mu \sim \mathcal{N}\left(0, -\frac{\varepsilon^2}{2} A^{-1}\right)$ is a Gaussian measure on H .

Remark 16. *The Neumann Laplacian Δ is not invertible on $H = L^2(-1, 1)$ and the invariant measure theory applies for a strictly negative definite operator A on H . For this reason, we should consider the strictly negative operator*

$$\tilde{A} := \lambda Id - A, \quad \lambda > 0.$$

In this way, the functional takes the form:

$$\tilde{I}(u) = I(u) - \lambda \|u\|_2^2,$$

and the reaction term in the SPDE is given by:

$$F(x, u) = f(x, u) - \lambda u.$$

In conclusion, the invariant measure for the SPDE

$$d\tilde{X}_t = \left[\tilde{A}\tilde{X}_t + F(x, X_t) \right] dt + \varepsilon dW_t, \quad \tilde{X}_{|t=0} = \tilde{x}_0$$

is given by:

$$\tilde{\nu}(du) = \frac{1}{Z} \exp\left(-\frac{2}{\varepsilon^2} \tilde{I}(u)\right) \tilde{\mu}(du), \quad u \in H,$$

where $\tilde{\mu} \sim \mathcal{N}(0, -\frac{\varepsilon^2}{2} \tilde{A}^{-1})$ is a Gaussian measure on H . Since this change only complicates the notation in the proofs, we will keep writing A^{-1} but the reader should interpret the Laplacian with the shift described above, in order to get the rigorous meaning.

Second, keeping in mind the previous remark, we adopt from now on the notation:

$$\mathcal{Q} = -\frac{\varepsilon^2}{2\kappa} \Delta^{-1}, \quad \mu(du; v, \mathcal{Q}) \sim \mathcal{N}(v, \mathcal{Q}).$$

The following statement is a classical result about the equivalence of Gaussian measures. See [21] for more details.

Theorem 17 (Cameron-Martin). *The Gaussian measures $\mu(du; 0, \mathcal{Q})$ and $\mu(du; v, \mathcal{Q})$ on H are equivalent if and only if $v \in \mathcal{Q}^{1/2}(H)$. In this case:*

$$\frac{\mu(du; 0, \mathcal{Q})}{\mu(du; v, \mathcal{Q})} = \exp\left(-\langle \mathcal{Q}^{-1/2}u, \mathcal{Q}^{-1/2}v \rangle + \frac{1}{2} \|\mathcal{Q}^{-1/2}v\|_2^2\right). \quad (1.11)$$

In the following, we are going to recall the rigorous meaning for

$$\langle \mathcal{Q}^{-1/2}u, \mathcal{Q}^{-1/2}v \rangle_{L^2}.$$

Consider

$$W_z: \mathcal{Q}^{1/2}(H) \subset H \rightarrow L^2(H, \mu), \quad W_z(u) := \langle u, \mathcal{Q}^{-1/2}z \rangle_{L^2}.$$

It can be shown that:

- (i) W_z is an isometry,
- (ii) $\mathcal{Q}^{1/2}(H)$ is dense in H (here it is fundamental $\ker(\mathcal{Q}) = \{0\}$.)

In this way, W_z can be extended in a unique way to a map $W_z: H \rightarrow L^2(H, \mu)$. So, it should be interpreted as:

$$\langle \mathcal{Q}^{-1/2}u, \mathcal{Q}^{-1/2}v \rangle_{L^2} = W_{\mathcal{Q}^{-1/2}v}(u), \quad u \in H.$$

Remark 18. For our choice of the operator \mathcal{Q} , we have that the Cameron-Martin space is $\mathcal{Q}^{1/2}(L^2) = H^1$.

At this point, we move to prove the main result of this section. Given a Banach space X , we denote by

$$B_X(x_0, \rho) = \{x \in X \mid \|x - x_0\|_X < \rho\}$$

the open ball with center $x_0 \in X$ and radius $\rho > 0$.

Proposition 19. Let $C > 0$, $r > 5$ and $v \in H^{2,2}(-1, 1)$. Consider the set

$$B_C(v, \eta) := B_{L^2}(v, \eta) \cap B_{L^r}(v, C).$$

Then,

$$(i) \quad \nu(B_C(v, \eta)) \xrightarrow{C \rightarrow +\infty} \nu(B_{L^2}(v, \eta))$$

$$(ii) \quad \mu(B_C(0, \eta)) \xrightarrow{C \rightarrow +\infty} \mu(B_{L^2}(0, \eta))$$

(iii) For each $C > 0$, it holds

$$\frac{\nu(B_C(v, \eta))}{\mu(B_C(0, \eta))} = \frac{1}{Z} \exp\left(-\frac{2}{\varepsilon^2} \left(F_q(v) + O(\eta^\theta)\right)\right),$$

where $\theta \in (0, 1)$ satisfies

$$\frac{1}{5} = \frac{\theta}{2} + \frac{1-\theta}{r}.$$

Proof. Assume for simplicity $\kappa = 1$.

(i)-(ii) Observe that for $v_1 \in L^2 \cap L^r$, we have:

$$B_{C_1}(v_1, \eta) \subset B_{C_2}(v_1, \eta), \quad \text{if } C_1 \leq C_2$$

and

$$B_{L^2}(v_1, \eta) = \left(\bigcup_{C>0} B_C(v_1, \eta) \right) \cup \{u \in L^2 \mid \|u\|_r = \infty\}.$$

Denote by $B = \{u \in L^2 \mid \|u\|_r = \infty\}$. If we are able to prove:

$$\mu(B) = 0,$$

then we get (i) and (ii) thanks to the continuity of measures on an increasing sequence of sets. Since $\mu \sim \mathcal{N}(0, -\frac{\varepsilon^2}{2} \Delta^{-1})$, then

$$\mu = M \sum_{n=1}^{\infty} \frac{Z_n}{n} e_n$$

where $\{Z_n\}_n$ are i.i.d. $\mathcal{N}(0, 1)$ defined on the probability space $(\Omega, \mathcal{F}, \mathbb{P})$, $\{e_n\}_n$ is an orthonormal basis of $H = L^2(-1, 1)$ and $M > 0$ is a constant. The previous series is convergent in $L^2((\Omega, \mathcal{F}, \mathbb{P}); H^s)$, for all $s < 1/2$; indeed

$$\begin{aligned} \|\mu\|_{H^s}^2 &= \left\| M \sum_n \frac{Z_n}{n} (-\Delta)^s e_n \right\|_2^2 = \left\| M \sum_n \frac{Z_n}{n} n^s e_n \right\|_2^2 = M^2 \sum_n M \frac{Z_n^2}{n^2} n^{2s} \\ &= \sum_n \frac{Z_n^2}{n^{2-2s}}. \end{aligned}$$

Taking the expected values, we get

$$\mathbb{E} \|\mu\|_{H^s}^2 = M^2 \sum_n \frac{1}{n^{2-2s}} < \infty \leftrightarrow s < 1/2.$$

The Sobolev embedding $H^s(-1, 1) \hookrightarrow L^p$, holds for each $p < \infty$ if s is close to $1/2$. This leads to $\mu(B) = 0$.

(iii) We start by using the explicit formula (1.10) in order to get

$$\frac{\nu(B_C(v, \eta))}{\mu(B_C(0, \eta))} = \frac{1}{Z} \frac{\int_{B_C(v, \eta)} \exp\left(-\frac{2}{\varepsilon^2} I(u)\right) \mu(du; 0, \mathcal{Q})}{\mu(B_C(0, \eta); 0, \mathcal{Q})}. \quad (1.12)$$

Using the Cameron-Martin formula (1.11), we have

$$\mu(du; 0, \mathcal{Q}) = \exp\left(-W_{\mathcal{Q}^{-1/2}v} + \frac{1}{2} \|\mathcal{Q}^{-1/2}v\|_2^2\right) \mu(du; v, \mathcal{Q})$$

for each $v \in Q^{1/2}(L^2) = H^1$. Since

$$Q^{-1/2}u = \frac{\sqrt{2}}{\varepsilon} (-\Delta)^{1/2},$$

and for $v \in H^2$

$$W_{Q^{-1/2}v}(u) = \langle u, Q^{-1/2}Q^{-1/2}v \rangle = \frac{2}{\varepsilon^2} \langle u, v'' \rangle$$

we arrive to

$$\mu(du; 0, \mathcal{Q}) = \exp\left(-\frac{2}{\varepsilon^2} \langle u', v' \rangle + \frac{1}{\varepsilon^2} \|v'\|_2^2\right) \mu(du; v, \mathcal{Q}).$$

Plugging the previous identity into (1.12), we deduce:

$$\frac{\nu(B_C(v, \eta))}{\mu(B_C(0, \eta))} = \frac{1}{Z} \frac{\int_{B_C(v, \eta)} \exp\left[-\frac{2}{\varepsilon^2} \left(I(u) + \langle u', v' \rangle - \frac{1}{2} \|v'\|_2^2\right)\right] \mu(du; v, \mathcal{Q})}{\mu(B_C(0, \eta); 0, \mathcal{Q})}$$

Assume for a moment that we are able to prove:

$$-\frac{2}{\varepsilon^2} \left(I(u) + \langle u', v' \rangle - \frac{1}{2} \|v'\|_2^2\right) = -\frac{2}{\varepsilon^2} \left(F_q(v) + O(\eta^\theta)\right), \quad u \in B_C(v, \eta), \quad (1.13)$$

for $\theta \in (0, 1)$. Then,

$$\begin{aligned} \frac{\nu(B_C(v, \eta))}{\mu(B_C(0, \eta))} &= \frac{1}{Z} \exp\left(-\frac{2}{\varepsilon^2} \left(F_q(v) + O(\eta^\theta)\right)\right) \frac{\mu(B_C(v, \eta); v, \mathcal{Q})}{\mu(B_C(0, \eta); 0, \mathcal{Q})} \\ &= \frac{1}{Z} \exp\left(-\frac{2}{\varepsilon^2} \left(F_q(v) + O(\eta^\theta)\right)\right), \end{aligned}$$

where we have used

$$\mu(B_C(v, \eta); v, \mathcal{Q}) = \mu(B_C(0, \eta); 0, \mathcal{Q}).$$

This concludes the proof. \square

It remains to prove (1.13).

Lemma 20. *If $u \in B_C(v, \eta)$ and $v \in H^2$ then there exists $\theta \in (0, 1)$ s.t.*

$$-\frac{2}{\varepsilon^2} \left(I(u) + W_{Q^{-1/2}v}(u) - \frac{1}{2} \|v'\|_2^2\right) = -\frac{2}{\varepsilon^2} \left(F_q(v) + O(\eta^\theta)\right).$$

Proof. Assume for simplicity $\kappa = 1$. We divide the proof into steps.

Step 1: $W_{Q^{-1/2}v}(u) = \langle v', v' \rangle + O(\eta)$, if $u \in B_C(v, \eta)$ and $v \in H^2$.

Indeed, since $v \in H^2$, we have $W_{Q^{-1/2}v}(u) = -\langle u, v'' \rangle$ and

$$\begin{aligned} |-\langle u, v'' \rangle - \langle v', v' \rangle| &= |-\langle u, v'' \rangle + \langle v, v'' \rangle| = |\langle v - u, v'' \rangle| \\ &\leq \|v - u\|_2 \|v''\|_{H^2} \leq \eta \|v''\|_{H^2}. \end{aligned}$$

Step 2 : $I(u) = I(v) + O(\eta^\theta)$, if $u \in B_C(v, \eta)$.

Observe that:

$$\begin{aligned} |I(u) - I(v)| &\leq \frac{\varepsilon_0 \sigma_0}{5} \int_{-1}^1 |(u^5)_+ - (v^5)_+| dx + \int_{-1}^1 Q_0(x) |B(u) - B(v)| dx \\ &\quad + q \int_{-1}^1 |u - v| dx \end{aligned}$$

By the properties of B and Q_0 , we get that there exists $M, M' > 0$ s.t.

$$\begin{aligned} \int_{-1}^1 Q_0(x) |B(u) - B(v)| dx + q \int_{-1}^1 |u - v| dx &\leq M \int_{-1}^1 |u - v| dx \leq M' \|u - v\|_2 \\ &\leq M' \eta. \end{aligned}$$

By the mean value theorem, we get that if $u, v \geq 0$ and $p \geq 1$, then

$$|u^p - v^p| \leq p \max\{|u|, |v|\}^{p-1} |u - v| \leq p(|u| + |v|)^{p-1} |u - v|.$$

By this inequality, we get

$$\int_{-1}^1 |(u^p)_+ - (v^p)_+| dx \leq p \int_{-1}^1 (u_+ + v_+)^{p-1} |u_+ - v_+| dx.$$

Let q_1 s.t. $\frac{1}{p} + \frac{1}{q_1} = 1$. By Holder's inequality, we deduce:

$$\begin{aligned} \int_{-1}^1 (u_+ + v_+)^{p-1} |(u)_+ - (v)_+| dx &\leq \left[\int_{-1}^1 (u_+ + v_+)^{q_1(p-1)} dx \right]^{1/q_1} \|u_+ - v_+\|_p \\ &\leq \|u_+ + v_+\|_p^{p/q_1} \|u_+ - v_+\|_p \\ &\leq (\|u\|_p + \|v\|_p)^{p/q_1} \|u - v\|_p. \end{aligned}$$

Choosing $p = 5$, by interpolation inequality there exists $\theta \in (0, 1)$ s.t.

$$\|u - v\|_p \leq \|u - v\|_2^\theta \|u - v\|_r^{1-\theta} \leq \eta^\theta C^{1-\theta}, \quad u \in B_C(v, \eta).$$

In this way, for $u \in B_C(v, \eta)$, we deduce

$$\begin{aligned} \int_{-1}^1 |u_+^5 - v_+^5| dx &\leq p (\|u\|_p + \|v\|_p)^{p/q_1} \|u - v\|_p \\ &\leq p (C + 2\|v\|_p)^{p/q_1} \eta^\theta C^{1-\theta} \\ &= O(\eta^\theta). \end{aligned}$$

□

1.4 Variational problem - existence

Given a Banach space X and a sequence $\{u_n\}_n \subseteq X$, we denote by $u_n \rightharpoonup u$ the weak convergence, while we reserve the symbol $u_n \rightarrow u$ for strong convergence. Further, $H^1 = H^{1,2}(-1,1)$ will denote the Sobolev Space on $[-1,1]$ with order 1 and exponent 2. The main result of this section is the following.

Theorem 1. *If $q > 0$, then there exists a global regular non-negative minimiser for F_q . In other words, if we consider the variational problem*

$$\inf \left\{ F_q(u) \mid u \in H^1, u \geq 0 \right\}, \quad (10)$$

then there exists $\hat{u} \in C^\infty$ s.t. \hat{u} is a solution of the EBM and

$$F_q(\hat{u}) = \inf \left\{ F_q(u) \mid u \in H^1, u \geq 0 \right\}.$$

In addition to this, if q belongs to a bounded interval, then u can be bounded uniformly with respect to q :

$$\exists M > 0 \text{ s.t. } \hat{u}(x) \leq M, \quad \forall x \in [-1,1]. \quad (11)$$

Proof. Let assume for simplicity $Q_0(x) = 1 \forall x$. This is not restrictive and the proof can be carried on in a similar way since

$$Q_0(x) > \delta > 0.$$

We divide the proof into steps.

Step 1: compactness. We consider the notion of convergence on \mathbb{X} given by:

$$u_n \xrightarrow{\mathbb{X}} u_\infty \quad \text{if and only if } u_n \rightarrow u_\infty \text{ uniformly in } [-1,1] \text{ and } u'_n \rightharpoonup u'_\infty \text{ in } L^2.$$

We want to verify the compactness of the sublevel sets of F_q . Let $\{u_n\}_n \subset \mathbb{X}$ and $M > 0$ s.t. $M \geq F_q(u_n) \forall n$. First, we observe

$$\begin{aligned} M \geq F_q(u_n) &\geq \int_{-1}^1 \varepsilon_0 \sigma_0 \frac{(u_n^5)_+}{5} - B(u_n) - q u_n dx \\ &= 2 \left[\varepsilon_0 \sigma_0 \frac{(u_n^5)_+}{5}(\xi_n) - B(u_n)(\xi_n) - q u_n(\xi_n) \right] \\ &\geq 2 \left[\varepsilon_0 \sigma_0 \frac{(u_n^5)_+}{5}(\xi_n) - B_0 - |u_n(\xi_n)| - q u_n(\xi_n) \right], \end{aligned}$$

where the first inequality follows from Lagrange Theorem and $\xi_n \in [-1,1]$. Since $v \mapsto \varepsilon_0 \sigma_0 (v^5)_+ / 5 - B(v) - qv$ explodes for $v \rightarrow \pm\infty$, we get the existence of $C_1 > 0$ s.t. $|u_n(\xi_n)| \leq C_1 \forall n$. Second, we get $\forall x \in [-1,1]$

$$|u_n(x)| \leq |u_n(\xi_n)| + |u_n(x) - u_n(\xi_n)| \leq C_1 + \|u'_n\|_2 |x - \xi_n|^{1/2}, \quad (1.14)$$

the second inequality follows from the fact that a function in H^1 is Holder-continuous. Third, since (1.6) holds, we have

$$\begin{aligned} M \geq F_q(u_n) &\geq \int_{-1}^1 -B(u_n) - u_n dx + \frac{1}{2} \|u'_n\|_2 \\ &\gtrsim -\|u_n\|_1 + \frac{1}{2} \|u'_n\|_2 \\ &\gtrsim -C_1 - \|u'_n\|_2 + \frac{1}{2} \|u'_n\|_2^2, \end{aligned}$$

where $a \gtrsim b$ if and only if exists $c > 0$ s.t. $a \geq c \cdot b$ and the last inequality follows from $\|u_n\|_1 \lesssim \|u_n\|_2$. The previous inequality of second order in the unknown $\|u'_n\|_2$ is verified if and only if

$$\|u'_n\|_2 \leq C_2, \quad (1.15)$$

for some $C_2 > 0$. Up to remaining the subsequence, we have $u'_n \rightharpoonup v$, for a $v \in H^1$. It remains to prove the uniform converge of u_n in $[-1, 1]$. Let's do it using the Ascoli-Arzelà theorem. We get equi-continuity from the properties of the Sobolev space. Indeed

$$|u_n(x) - u_n(y)| \leq \|u'_n\|_{L^2} |x - y|^{1/2} \quad \forall x, y \in [-1, 1]$$

and $\|u'_n\|_{L^2}$ is bounded thanks to weak convergence. Since (1.14) holds, we get also equi-boundedness. Then (up to remaining) $u_n \rightarrow u_\infty$ uniformly in $[-1, 1]$.

It remains to prove $u'_\infty = v$ in weak sense. Let $\phi \in C_c^\infty([-1, 1])$. Then, by weak derivative definition,

$$\int_{-1}^1 u_n \phi' dx = - \int_{-1}^1 u'_n \phi dx \quad \forall n,$$

and taking the limit on both sides of the equality (we use uniform convergence at left-hand side, and weak convergence at right-hand side)

$$\int_{-1}^1 u_\infty \phi' dx = - \int v \phi dx$$

Step 2: lower semi-continuity of F_q . Let $\{u_n\} \subset \mathbb{X}$ be s.t. $u_n \xrightarrow{\mathbb{X}} u$. Let F_1, F_2 be s.t.

$$F_q(u) = F_1(u) + F_2(u),$$

where

$$F_1(u) := \int_{-1}^1 \frac{\varepsilon_0 \sigma_0 (u^5)_+}{5} - B(u) - qu dx, \quad F_2(u) := \frac{\kappa}{2} \int_{-1}^1 (u')^2 dx$$

By uniform convergence, we have $\lim_{n \rightarrow \infty} F_1(u_n) = F_1(u)$; by lower semi-continuity of the L^2 norm w.r.t. weak convergence, we have $\liminf_{n \rightarrow \infty} F_2(u_n) \geq F_2(u)$.

In conclusion, F_q is lower semi-continuous and coercive. Then, $\exists \hat{u} \in \mathbb{X}$ minimum point for F_q in \mathbb{X} .

Step 3: regularity for \hat{u} The first variation of F_q in the point u in direction h is given by:

$$\delta F_q(u, h) = \int_{-1}^1 (\psi(u) - \tilde{\beta}(u) - q) h \, dx + \kappa \int_{-1}^1 u' h' \, dx.$$

Choosing $h \in C_c^\infty([-1, 1])$ and setting $\phi(t) := F_q(\hat{u} + th)$, it holds $\phi'(0) = 0$. So:

$$0 = \phi'(0) = \delta F_q(\hat{u}, h),$$

from which it follows

$$\int_{-1}^1 (\psi(\hat{u}) - \tilde{\beta}(\hat{u}) - q) h \, dx = -\kappa \int_{-1}^1 \hat{u}' h' \, dx. \quad (1.16)$$

Then

$$\kappa \hat{u}'' = \psi(\hat{u}) - \tilde{\beta}(\hat{u}) - q \quad (1.17)$$

in the weak sense. The right-hand side (RHS) is C^0 because $\hat{u} \in H^1$. Then $\hat{u}' \in C^1$ and $\hat{u} \in C^2$. Repeating the bootstrap argument, we get $\hat{u} \in C^\infty$.

Step 4: Neumann boundary conditions. Let $h \in C^\infty$. Following the same arguments above, we get to (1.16). Integrating by parts the RHS, we have:

$$\int_{-1}^1 (\psi(\hat{u}) - \tilde{\beta}(\hat{u}) - q - \hat{u}'') h \, dx = -\kappa (h(1)\hat{u}'(1) - h(-1)\hat{u}'(-1))$$

But the left-hand side of the previous equation is null thanks to (1.17). Choosing h s.t. $h(1) = 0$ and $h(-1) \neq 0$, it follows $\hat{u}'(-1) = 0$. In a similar way, we can get $\hat{u}'(1) = 0$.

Step 5: $\hat{u} \geq 0$. This can be proved by the following truncation argument. Assume there exists $x_0 \in [-1, 1]$ s.t. $\hat{u}(x_0) < 0$. Consider the following points

$$\tau_1 := \sup \{x < x_0 \mid \hat{u}(x) = 0\}, \quad \tau_2 := \inf \{x > x_0 \mid \hat{u}(x) = 0\}.$$

Let \tilde{u} be the truncation to 0 of \hat{u} in $[\tau_1, \tau_2]$, i.e.

$$\tilde{u}(x) := \begin{cases} \hat{u}(x) & \text{if } x \in [\tau_1, \tau_2]^c, \\ 0 & \text{if } x \in [\tau_1, \tau_2]. \end{cases} \quad (1.18)$$

Then

$$\begin{aligned} F_q(\hat{u}) - F_q(\tilde{u}) &= \int_{\tau_1}^{\tau_2} \varepsilon_0 \sigma_0 \frac{(\hat{u}^5)_+}{5} - Q_0(x)B(\hat{u}) - q\hat{u}(x) \, dx \\ &\quad + \frac{\kappa}{2} \int_{\tau_1}^{\tau_2} [\hat{u}']^2 \, dx + \int_{\tau_1}^{\tau_2} Q_0(x)B(0) \, dx \\ &\geq \int_{\tau_1}^{\tau_2} Q_0(x) (B(0) - B(\hat{u})) - q\hat{u}(x) \, dx \\ &> 0 \end{aligned}$$

where the last inequality follows from the fact that $B(0) \geq -B(\hat{u}(x))$ and $q > 0$. This is a contradiction and thus $\hat{u}(x) \geq 0 \forall x \in [-1, 1]$. \square

Repeating again a truncation argument similar to the one used in the last part of the previous proof, we can conclude the proof of the previous result by showing that the minimiser is bounded from above.

Lemma 21. *Assume $q \in (0, b)$. Then, there exists $M > 0$ s.t. if $\hat{u} = \hat{u}(q)$ is the minimiser for F_q , then $\hat{u} \leq M$.*

Proof. Indeed, set $\mathcal{R}(x, u) := \varepsilon_0 \sigma_0 \frac{(u^5)_\pm}{5} - Q_0(x)B(u) - qu$. Note that the following inequalities hold

$$\begin{aligned} \mathcal{R}(x, u) &\geq \varepsilon_0 \sigma_0 \frac{u^5}{5} - \|Q_0\|_\infty B(u) - bu, \quad u \geq 0, \\ \mathcal{R}(x, v) &\leq \varepsilon_0 \sigma_0 \frac{v^5}{5}, \quad v \geq 0. \end{aligned}$$

So, if we set $G(x, u, v) := \mathcal{R}(x, u) - \mathcal{R}(x, v)$, we have, uniformly in x

$$G(x, u, v) \geq \varepsilon_0 \sigma_0 \left(\frac{u^5}{5} - \frac{v^5}{5} \right) - \|Q_0\|_\infty B(u) - bu.$$

Note that for each $v \geq 0$ fixed the term on the right-hand side diverges to $+\infty$ for $u \rightarrow +\infty$. So, given $v \geq 0$, there exists $M = M(v)$ s.t if $u \geq M(v)$, then $G(x, u, v) \geq 1 \forall x \in [-1, 1]$.

Let us pick $v = 1$. We want to prove that $\hat{u}(x) \leq M \forall x \in [-1, 1]$. Assume by contradiction that $\hat{u}(x_0) > M$ for some $x_0 \in [-1, 1]$. Set

$$\tau_1 := \sup \{x < x_0 \mid \hat{u} = M\}, \quad \tau_2 := \inf \{x > x_0 \mid \hat{u} = M\},$$

and consider the truncated minimiser

$$\tilde{u}(x) := \begin{cases} \hat{u}(x) & \text{if } x \in [\tau_1, \tau_2]^c, \\ M & \text{if } x \in [\tau_1, \tau_2]. \end{cases} \quad (1.19)$$

Then

$$F_q(\hat{u}) - F_q(\tilde{u}) \geq \int_{\tau_1}^{\tau_2} \mathcal{R}(x, \hat{u}(x)) - \mathcal{R}(x, M) dx = \int_{\tau_1}^{\tau_2} G(x, \hat{u}(x), M) dx.$$

Since by definition of τ_1 and τ_2 , it holds $\hat{u}(x) \geq M \forall x \in [\tau_1, \tau_2]$, then we conclude

$$F_q(\hat{u}) - F_q(\tilde{u}) > 0.$$

This is a contradiction and concludes the proof. \square

1.5 Variational problem - uniqueness

In this section we are going to characterise the uniqueness for the solution of the variational problem in terms of the value function, i.e. the minimum value attained by F_q on H^1 .

The *value function* V is defined as follows:

$$V(q) = \inf \left\{ F_q(u) : u \in H^1 \right\}.$$

First of all, from the last result in Section 1.4 follows the Lipschitz property for V .

Lemma 22. *Assume $q \in (0, b)$. Then, the value function $q \mapsto V(q)$ is Lipschitz continuous.*

Proof. First of all, observe that thanks to the non-negativity of the minimiser and Lemma 21 there exists $M > 0$ s.t.

$$V(q) = \inf \left\{ F_q(u) \mid 0 \leq u \leq M, u \in H^1 \right\}.$$

Second, given a family $\{f_i\}_{i \in I}$ of L_i -Lipschitz function f_i , we know that the infimum $\inf_{i \in I} f_i$ is Lipschitz as long as we can bound uniformly the constants L_i . In our case this is true. Indeed, given $u \in H^1$, $0 \leq u \leq M$, we have:

$$|F_{q_1}(u) - F_{q_2}(u)| = |q_2 - q_1| \int_1^1 |u(x)| dx \leq 2M|q_2 - q_1|.$$

This concludes the proof. \square

The main result of this section is the following. We immediately give its proof and postpone to the remaining part of the section the proof of auxiliary results.

Proposition 23. *Assume $q \in (0, b)$. Then, V is differentiable in μ if and only if there exists a unique minimiser for F_μ in H^1 . Further, if V is differentiable, then*

$$V'(\mu) = - \int_{-1}^1 \hat{u} dx,$$

with $\hat{u} \in \operatorname{argmin} \{F_\mu(u) : u \in H^1\}$.

Proof. \Rightarrow) Let's consider the auxiliary function

$$W : \mathbb{R} \times (H^1 \cap \{u \geq 0\}) \rightarrow \mathbb{R}$$

given by:

$$W(q, u) := F_q(u) - V(q).$$

As preliminary remarks, note that $W(q, u) \geq 0$ and, if $\hat{u} \in \operatorname{argmin} \{F_q(u) : u \in H^1\}$, then $W(q, \hat{u}) = 0$. The existence of minimiser has been proved in Theorem 1. To prove uniqueness, assume that u_1, u_2 are two minimisers. Since (i) F_q is differentiable for each q , (ii) V is differentiable in μ by hypothesis and (iii) $W(\mu, u_i) = 0$, $i = 1, 2$, then

$$0 = \partial_q W(\mu, u_i) = - \int_{-1}^1 u_i(x) dx - V'(\mu).$$

Thus

$$- \int_{-1}^1 u_1(x) dx = - \int_{-1}^1 u_2(x) dx = V'(\mu).$$

Using Lemma 23, we know that also $u_1 \wedge u_2$ is a minimiser. With the same reasoning above, it holds

$$- \int_{-1}^1 u_1(x) dx = - \int_{-1}^1 u_2(x) dx = - \int_{-1}^1 u_1 \wedge u_2(x) dx$$

Since $u_i \geq u_1 \wedge u_2 \geq 0$, the previous identities can hold only if $u_1 = u_2$.

\Leftarrow) Assume that, given μ , $\exists!$ \hat{u} minimiser for F_μ . Let $\{h_n\}_n$ be a sequence s.t. $h_n \rightarrow 0$. Let's denote by u_q a minimiser for F_q , i.e.

$$u_q \in \operatorname{argmin} \{F_q(u) : u \in H^1\},$$

Then, set $u_n := u_{\mu+h_n}$. We are going to show that $V'(\mu) = - \int_{-1}^1 \hat{u} dx$, i.e.

$$\lim_{n \rightarrow \infty} \frac{V(\mu + h_n) - V(\mu)}{h_n} = - \int_{-1}^1 \hat{u} dx.$$

First, observe that by definition of the value function, we have

$$\begin{aligned} \frac{V(\mu + h_n) - V(\mu)}{h_n} &= \frac{F_{\mu+h_n}(u_n) - F_\mu(\hat{u})}{h_n} \\ &\leq \frac{F_{\mu+h_n}(u_*) - F_\mu(\hat{u})}{h_n} \\ &= - \int_{-1}^1 \hat{u} dx. \end{aligned}$$

Hence

$$\lim_{n \rightarrow \infty} \frac{V(\mu + h_n) - V(\mu)}{h_n} \leq - \int_{-1}^1 \hat{u} dx.$$

On the other hand,

$$\begin{aligned} \frac{V(\mu + h_n) - V(\mu)}{h_n} &= \frac{F_{\mu+h_n}(u_n) - F_\mu(\hat{u})}{h_n} \\ &\geq \frac{F_{\mu+h_n}(u_n) - F_\mu(u_n)}{h_n} \\ &= - \int_{-1}^1 u_n dx. \end{aligned}$$

It follows that:

$$\frac{V(\mu + h_n) - V(\mu)}{h_n} \geq - \int_{-1}^1 \hat{u} dx + \int_{-1}^1 (\hat{u} - u_n) dx$$

But the second integral on the right-hand side converges to zero as $n \rightarrow +\infty$ thanks to Lemma 25. This concludes the proof. \square

In order to complete the proof of the previous result, we need to verify some auxiliaries lemmas. First, let's prove that the infimum of two minimisers for F_q is still a minimiser.

Lemma 24. *If u_1, u_2 are minimisers for F_q in H^1 , then also $u_1 \vee u_2$ and $u_1 \wedge u_2$ are minimisers.*

Proof. For simplicity of notation, set $\mathcal{R}(x, u) := \varepsilon_0 \sigma_0 \frac{u^5}{5} - Q_0(x)\beta(u) - qu$. Further, we divide the proof into steps.

Step 1: $F_q(u_1 \wedge u_2) \geq F_q(u_1 \vee u_2)$.

We start observing that:

$$\begin{aligned} F_q(u_1 \wedge u_2) &= \frac{\kappa}{2} \int_{u_1 \geq u_2} (u_2')^2 dx + \int_{u_1 \geq u_2} \mathcal{R}(x, u_2) dx \\ &\quad + \frac{\kappa}{2} \int_{u_1 < u_2} (u_1')^2 dx + \int_{u_1 < u_2} \mathcal{R}(x, u_1) dx \\ &\geq F_q(u_1) \\ &= \frac{\kappa}{2} \int_{u_1 \geq u_2} (u_1')^2 dx + \int_{u_1 \geq u_2} \mathcal{R}(x, u_1) dx \\ &\quad + \frac{\kappa}{2} \int_{u_1 < u_2} (u_1')^2 dx + \int_{u_1 < u_2} \mathcal{R}(x, u_1) dx \end{aligned}$$

where the inequality holds since u_1 is a minimiser. So, we deduce

$$\frac{\kappa}{2} \int_{u_1 \geq u_2} (u_2')^2 dx + \int_{u_1 \geq u_2} \mathcal{R}(x, u_2) dx \geq \frac{\kappa}{2} \int_{u_1 \geq u_2} (u_1')^2 dx + \int_{u_1 \geq u_2} \mathcal{R}(x, u_1) dx. \quad (1.20)$$

In a similar way, we get

$$\frac{\kappa}{2} \int_{u_1 < u_2} (u_1')^2 dx + \int_{u_1 < u_2} \mathcal{R}(x, u_1) dx \geq \frac{\kappa}{2} \int_{u_1 < u_2} (u_2')^2 dx + \int_{u_1 < u_2} \mathcal{R}(x, u_2) dx. \quad (1.21)$$

Indeed, the previous inequality follows bounding from below $F_q(u_1 \wedge u_2)$ with $F_q(u_2)$ and comparing the terms on both sides of the inequality. Now, adding together Eq. (1.20) and Eq. (1.21), we obtain the claimed relation between $F_q(u_1 \wedge u_2)$ and $F_q(u_1 \vee u_2)$:

$$\begin{aligned}
 F_q(u_1 \wedge u_2) &= \frac{\kappa}{2} \int_{u_1 \geq u_2} (u_2')^2 dx + \int_{u_1 \geq u_2} \mathcal{R}(x, u_2) dx \\
 &+ \frac{\kappa}{2} \int_{u_1 < u_2} (u_1')^2 dx + \int_{u_1 < u_2} \mathcal{R}(x, u_1) dx \\
 &\geq \frac{\kappa}{2} \int_{u_1 \geq u_2} (u_1')^2 dx + \int_{u_1 \geq u_2} \mathcal{R}(x, u_1) dx \\
 &+ \frac{\kappa}{2} \int_{u_1 < u_2} (u_2')^2 dx + \int_{u_1 < u_2} \mathcal{R}(x, u_2) dx \\
 &= F_q(u_1 \vee u_2).
 \end{aligned}$$

Step 2: $F_q(u_1 \vee u_2) \geq F_q(u_1 \wedge u_2)$.

This inequality can be obtained by repeating the step above starting with $F_q(u_1 \vee u_2)$ instead of $F_q(u_1 \wedge u_2)$.

Step 3: $F_q(u_1) = F_q(u_1 \wedge u_2) = F_q(u_1 \vee u_2)$.

The last identity follows from Step 1 and Step 2. To get the first identity, let's observe that in our case

$$F_q(u_1) + F_q(u_2) = F_q(u_1 \wedge u_2) + F_q(u_1 \vee u_2). \quad (1.22)$$

The previous identity can be verified by writing

$$F_q(v) = \frac{\kappa}{2} \int_{u_1 \geq u_2} (v')^2 dx + \frac{\kappa}{2} \int_{u_1 < u_2} (v')^2 dx + \int_{u_1 \geq u_2} \mathcal{R}(x, v) dx + \int_{u_1 < u_2} \mathcal{R}(x, v) dx,$$

for $v = u_1, u_2, u_1 \wedge u_2, u_1 \vee u_2$. Then, it just consists in checking that Eq. (1.22) holds. At this point, since $F_q(u_1) = F_q(u_2)$ (because u_1, u_2 are minimisers) and $F_q(u_1 \wedge u_2) = F_q(u_1 \vee u_2)$ (thanks to Step 1 and Step 2), Eq. (1.22) can be rewritten as:

$$2F_q(u_1) = 2F_q(u_1 \wedge u_2).$$

□

Second, we need to verify that the space integral of a sequence of minimisers behaves in a continuous way as the parameter q approaches a point where the uniqueness hold for the variational problem.

Lemma 25. *Assume $q \in (0, b)$ and that there exists an unique minimiser \hat{u} for F_μ in H^1 . Consider a sequence q_n s.t. $q_n \rightarrow \mu$. Then,*

$$\int_{-1}^1 u_n dx \rightarrow \int_{-1}^1 \hat{u} dx,$$

with $u_n \in \operatorname{argmin} \{F_{q_n} : u \in H^1\}$.

Proof. We divide the proof into several steps. Some of them will involve repeating part of the direct method used to solve the variational problem considered in Theorem 1.

Step 1: there exists $u_\infty \in H^1$ and a subsequence $(n_k)_k$ s.t. $u_{n_k} \rightarrow u_\infty$ uniformly in $[-1, 1]$ and $u'_{n_k} \rightharpoonup u'_\infty$ weakly in L_2 .

Indeed, since V is continuous thanks to Lemma 22, we have:

$$F_{q_n}(u_n) = V(q_n) \rightarrow V(\mu) = F_\mu(\hat{u}).$$

In this way, we infer the existence of $M > 0$ s.t. $F_{q_n}(u_n) \leq M \forall n$. At this point, we are in the same hypothesis of the proof for Theorem 1 - Step 1. Following that reasoning, we get the claimed statement.

Step 2: $F_\mu(u_n) \rightarrow F_\mu(\hat{u})$.

Since \hat{u} is a minimiser for F_μ , we have:

$$F_\mu(u_n) \geq F_\mu(\hat{u}) \quad \forall n.$$

To get the thesis, we fix $\varepsilon > 0$ and we will verify that for n large enough it holds

$$F_\mu(u_n) \leq F_\mu(\hat{u}) + \varepsilon.$$

Indeed

$$\begin{aligned} |F_\mu(u_n) - F_\mu(\hat{u})| &\leq |F_\mu(u_n) - F_{q_n}(u_n)| + |F_{q_n}(u_n) - F_\mu(\hat{u})| \\ &\leq |\mu - q_n| \|u_n\|_1 + |V(q_n) - V(\mu)|. \end{aligned}$$

Thanks to Lemma 21, the term $\|u_n\|_1$ is bounded uniformly in n . Further, by the continuity of V we conclude that the right-hand side converges to 0 for $n \rightarrow \infty$.

Step 3: $u_\infty = \hat{u}$.

By proof of Theorem 1 - Step 2, we know that if $u_{n_k} \rightarrow u_\infty$ uniformly in $[-1, 1]$ and $u'_{n_k} \rightharpoonup u'_\infty$ weakly in L^2 , then

$$\liminf_k F_\mu(u_{n_k}) \geq F_\mu(u_\infty).$$

Further, since the sequence $F_\mu(u_n)$ is convergent to $F_\mu(\hat{u})$, we get

$$F_\mu(\hat{u}) = \lim_n F_\mu(u_n) = \liminf_k F_\mu(u_{n_k}) \geq F_\mu(u_\infty).$$

Thus, by the uniqueness of the minimiser for F_μ , we conclude $\hat{u} = u_\infty$.

Step 4: $u_n \rightarrow \hat{u}$ unif. in $[-1, 1]$. In particular, $\lim_{n \rightarrow \infty} \int_{-1}^1 u_n dx = \int_{-1}^1 \hat{u} dx$.

Take a subsequence u_{n_k} of u_n . We can use the same reasoning of Step 1 and get that there exists a subsubsequence $u_{n_{k_h}}$ s.t. $u_{n_{k_h}} \rightarrow u_\infty$ uniformly in $[-1, 1]$. But with the same reasoning in Step 3, it follows $u_\infty = \hat{u}$. Since the limit does not depend on n_{k_h} , we get the claimed statement. \square

Remark 26. Note that the previous result is equivalent to say that V' is continuous, where it is defined.

1.6 Value function - semiconcavity, concavity and non-increasing derivative

In Section 1.5, we introduced the value function V as a tool for characterizing the uniqueness of the variational problem through its differentiability. In this section, our objective is to establish the semiconcavity of V . Subsequently, we will demonstrate that V is also concave. This, in turn, implies that its derivative is non-increasing wherever it is defined. The explicit expression for V' provided in Proposition 23 allows us to say that this last property is equivalent to state that the map $q \mapsto \int_{-1}^1 \hat{u}(x)dx$, where $\hat{u} \in \operatorname{argmin} \{F_q(u) \mid u \in H^1\}$, is non-decreasing on the set where V' is well-defined. This set is the complement of a countable set.

First, we start by recalling the definition and the basic properties of semiconcave functions. More details can be found in [16].

Definition 27. *Let $A \subseteq \mathbb{R}$. A function $g: A \rightarrow \mathbb{R}$ is semiconcave if there exists a non-decreasing upper semicontinuous function $\omega: \mathbb{R}_+ \rightarrow \mathbb{R}_+$ such that $\lim_{\rho \rightarrow 0^+} \omega(\rho) = 0$ and*

$$\lambda g(q_1) + (1 - \lambda)g(q_2) - g(\lambda q_1 + (1 - \lambda)q_2) \leq \lambda(1 - \lambda)|q_1 - q_2|\omega(|q_1 - q_2|),$$

for any pair $q_1, q_2 \in A$, such that the segment $[q_1, q_2]$ is contained in A and for any $\lambda \in [0, 1]$. We call ω a modulus of semicontinuity for g in A .

As in the case of Lipschitz functions, taking the infimum of a family of semiconcave functions, the semiconcavity is preserved, provided that the functions have the same modulus.

Lemma 28. *[16, Proposition 2.1.5] Let $\{g_i\}_{i \in I}$ be a family of functions defined on A and semiconcave with the same modulus ω . Then the function $g := \inf_{i \in I} g_i$ is also semiconcave in A with the same modulus of ω , provided $g > -\infty$.*

If a semiconcave function has a modulus satisfying a limiting property, we retrieve the classical notion of concavity.

Lemma 29. *[16, Proposition 2.1.9] Let $g: A \rightarrow \mathbb{R}$ be semiconcave with A open and with a modulus ω such that*

$$\lim_{\rho \rightarrow 0^+} \frac{\omega(\rho)}{\rho} = 0.$$

Then g is concave on all convex subsets of A .

Second, we recall some elementary properties from convex analysis. More details can be found in [75]. Given $g: A \rightarrow \mathbb{R}$, with $A \subset \mathbb{R}$ convex, we denote by:

$$g'_-(q) = \lim_{h \rightarrow 0^-} \frac{g(q+h) - g(q)}{h}, \quad g'_+(q) = \lim_{h \rightarrow 0^+} \frac{g(q+h) - g(q)}{h},$$

respectively the *left* and *right derivative* of g in q . The following lemma summarises some basic results for a concave function.

Lemma 30. *Let $g: A \rightarrow \mathbb{R}$ be a concave function. Then the following statements hold.*

- (i) g is differentiable at all but at most countably many points.
- (ii) g'_- and g'_+ are well defined and, respectively, left and right continuous.
- (iii) For each $q_1 < q_2 \in \text{Int}(A)$, we have:

$$g'_+(q_2) \leq g'_-(q_2) \leq g'_+(q_1) \leq g'_-(q_1).$$

Lastly, we are able to present the main result of the section.

Proposition 31. *Let $b > 0$ and consider the value function $V: (0, b) \rightarrow \mathbb{R}$. The following statements hold.*

- (i) Let ω be a non-decreasing upper semicontinuous function $\omega: \mathbb{R}_+ \rightarrow \mathbb{R}_+$ such that $\lim_{\rho \rightarrow 0_+} \omega(\rho) = 0$. Then the value function is semiconcave with modulus ω .
- (ii) The value function is concave.
- (iii) There exists a countable set $S \subseteq (0, b)$ such that V is differentiable on $S^c \cap (0, b)$ and its derivative V' is non-increasing on $S^c \cap (0, b)$.

Proof. (a) Since $V(q) = \inf_{u \in H^1} F_q(u)$, thanks to Lemma 28 it is sufficient to prove that, given $u \in H^1$, the map $q \mapsto F_q(u) = F(q)$ is semiconcave. This is true since F_q is an affine function which respect to q and thus its modulus is also independent of u .

(b) It is a direct application of Lemma 29.

(c) Since V is concave, it is sufficient to recall the properties expressed in Lemma 30 and remember that V is differentiable in q if and only if $V'_-(q) = V'_+(q)$, and in that case the derivative is equal to the side derivatives. \square

We conclude the section highlighting how the properties of the value function's derivative reflect on the global mean temperature of the variational problem's minimiser.

Remark 32. *By Froda's theorem, a monotone function can have only jump discontinuities and further they can be at most countable. Since V'_-, V'_+ are monotone thanks to Lemma 30 and*

$$V'(q) = - \int_{-1}^1 \hat{u}(x) dx,$$

where $\hat{u} \in \operatorname{argmin} \{F_q(u) \mid u \in H^1\}$, we get that the global mean temperature, depending on q , is monotone increasing and continuous, except for at most a countable number of jumps. Further, the jumps coincide with the points in the set S from Proposition 31 where the value function V is not differentiable.

Lastly, we demonstrate the applicability of this result to other reaction-diffusion equations. We use as an example a spatially heterogeneous Allen-Cahn equation (ACE), already considered in [6]. For an initial condition u_0 , this model is given by:

$$\begin{aligned} \partial_t u &= \frac{1}{100} \Delta u + u(1 - u^2) + q + \frac{1}{2} \cos(\pi x), \quad x \in (-1, 1), \quad t > 0, \\ u_x(t, -1) &= u_x(t, 1) = 0, \quad t \geq 0, \\ u|_{t=0} &= u_0. \end{aligned} \tag{1.23}$$

The associated elliptic problem is

$$\begin{aligned} 0 &= \frac{1}{100} \Delta u + u(1 - u^2) + q + \frac{1}{2} \cos(\pi x), \quad x \in (-1, 1), \\ u'(-1) &= u'(1) = 0. \end{aligned} \tag{1.24}$$

In this case, the potential functional takes the form

$$J_q(u) = \int_{-1}^1 \frac{u^4(x)}{4} - \frac{u^2(x)}{2} - u(x)(q + \frac{1}{2} \cos(\pi x)) \, dx,$$

and all the properties discussed in Section 0.1.1 and 0.1.2 can be extended to this equation. Specifically, Theorems 1, 2 and 3 hold. But in this case, the structure of the bifurcation diagram is more complex, even if symmetric which respect to $q = 0$. Indeed, through numerical experiments, it is possible to deduce the existence of $0 < q_4 < q_5$ such that: (a) for $|q| > q_5$ or $|q| < q_4$, there exists a single steady-state solution, which is stable, (b) for $q_4 < |q| < q_5$, there are three steady-state solutions, two of which are stable while the third is unstable. Further, $q = q_4, q_5$ are bifurcation points of saddle-node type. We denote by u_1 the steady-state solution for $q < -q_5$, by u_2, u_3 the steady-state solutions appearing at the bifurcation point $q = -q_5$ and existing for $-q_5 < q < -q_4$ in addition to u_1 and by u_4, u_5 the steady-state solutions appearing at $q = q_4$ and existing for $q_4 < q < q_5$ in addition to u_3 . Regarding the potential functional J_q , in this case there exists $q_6 \in (q_4, q_5)$ such that u_1 is the global minimum point for the functional for $q < -q_6$ and u_3 is the global minimum point for $-q_6 < q < q_6$, while u_5 becomes the global minimum point for $q > q_6$. A picture for the bifurcation diagram just described and the value function is shown in Figure 1.2. Note that $q = \pm q_6$ are the only values of the parameter q for which the value function is not differentiable and also the only points in which the global minimiser of the variational problem is not unique.

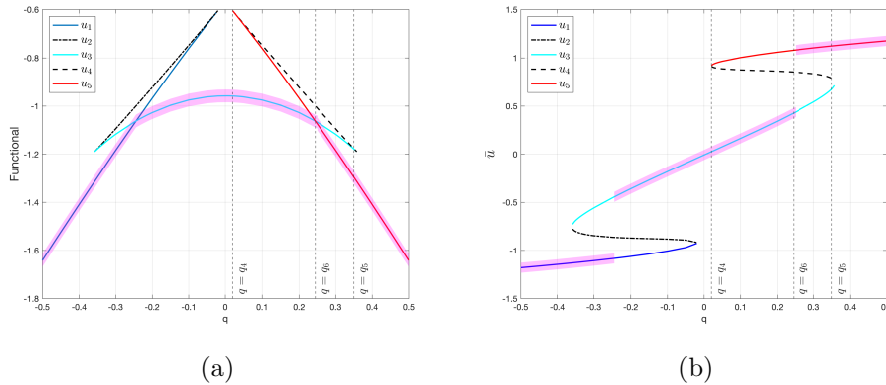


Figure 1.2: Comparison between the value function and the bifurcation diagram for the non-homogeneous ACE. The magenta-shaded area highlights the parts of the plots which are in one-to-one correspondence. (a) Potential functional evaluated on the steady-state solutions: u_1 is the global minimum point for $q < -q_6$, u_3 is the global minimum point for $-q_6 < q < q_6$, u_5 is the global minimum point for $q > q_6$. Note that $q = \pm q_6$ are the non-differentiability point for the value function, corresponding to non-uniqueness of the minimiser. (b) Bifurcation diagram.

1.7 Mountain Pass Theorem and existence of at least three steady-state solutions

In this section, we are going to use the Mountain pass theorem (MPT) from the calculus of variation to show the existence of at least three solutions to the elliptic problem (1.7). First, we start by checking that the functional F_q satisfies the compactness condition (Palais-Smale) needed in the hypothesis of the MPT. Second, we are going to show how numerical simulations suggest the existence of two (local) minimum points for F_q corresponding to u_S and u_W ; thus, the MPT gives us the existence of a third critical point, that corresponds to u_M thanks to numerical simulations. Third, we are giving sufficient hypotheses in order to prove the existence of the two local minimum points mentioned before; the existence of these two local minimum points is again obtained using the direct method.

Let $(X, \|\cdot\|)$ be a reflexive Banach space, $\Phi \in C^1(X, \mathbb{R})$ be a functional and Φ' denote the first variation of Φ .

Definition 33. *The functional Φ satisfies the Palais-Smale condition ((PS)-condition) if any sequence $\{u_n\}_n \subset X$ s.t.*

$$\Phi(u_n) \text{ is bounded and } \Phi'(u_n) \rightarrow 0,$$

admits a convergent subsequence.

The previous one is a compactness condition needed in order to use the Mountain pass theorem, which loosely speaking affirms the existence of a mountain pass between two valleys. See [50] for more details.

Theorem 34 (Mountain pass). *If Φ satisfies the (PS)-condition, $\Phi(0) = 0$ and*

$$\begin{aligned} \exists \rho, \alpha > 0 \text{ s.t. } \Phi(x) \geq \alpha \quad \forall x \text{ with } \|x\| = \rho, \\ \exists x_1 \text{ s.t. } \|x_1\| > \rho \text{ and } \Phi(x_1) \leq 0 \end{aligned}$$

then, $\exists x_2$ s.t. $\Phi(x_2) = c \geq \alpha$ and x_2 is a stationary point for Φ . Further,

$$c = \inf_{\gamma \in \Gamma} \max_{u \in \gamma([0,1])} \Phi(u)$$

where:

$$\Gamma = \{\gamma \in C([0, 1], X) : \gamma(0) = 0, \gamma(1) = x_2\}.$$

At this point, we already know from Theorem 1 the existence of a global minimiser for F_q . On the other hand, numerical simulations suggest the existence of a second local minimiser. Indeed, the second variation $\delta^2 F_q$ of the functional F_q in the point u in direction h is given by:

$$\delta^2 F_q(u, h) = \int_{-1}^1 [4u^3 h - Q_0(x)\beta'(u)h - \kappa h''] h dx.$$

We denote by:

$$\lambda_1(u) \leq \lambda_2(u) \leq \dots,$$

the eigenvalues of the second variation

$$h \mapsto 4u^3 h - Q_0(x)\beta'(u)h - \partial_x (\kappa(x)h').$$

We numerically evaluate the eigenvalues of the second variations in the three steady-state points $u_S \leq u_M \leq u_W$. The results, which are shown in Figure 1.3, tell us that u_S and u_W are strict local minimum points, except at the bifurcations points. This is because the smallest eigenvalues λ_1 for u_S and u_W is positive, hence the second variation in u_S and u_W is positive definite. From this, we get numerical evidence for the existence of a second minimiser. At this point, the Mountain pass theorem guarantees the existence of a third steady-state point, that from our numerical simulations corresponds to u_M , if we are able to prove the (PS)-property for F_q . This is what we are going to check in the following.

Let X be a reflexive Banach space and X^* its dual space. Given $x_n, x \in X$, denote by $x_n \rightharpoonup x$ the weak convergence in X .

Definition 35. *A: $X \rightarrow X^*$ is of type $(S)_+$ if any $\{x_n\}_n \subset X$ s.t. $x_n \rightharpoonup x$ and $\limsup_{n \rightarrow +\infty} \langle A(x_n), x_n - x \rangle \leq 0$ imply $x_n \rightarrow x$ in X .*

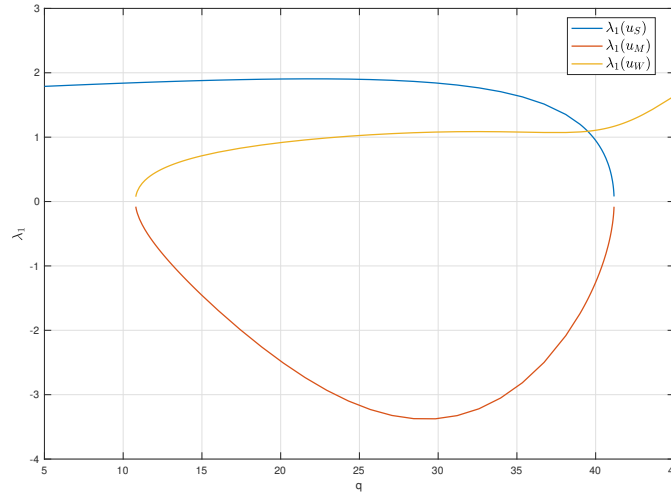


Figure 1.3: Smallest eigenvalue λ_1 for the second variation in u_S, u_M, u_W .

Let $X = W_n^{1,2} = W_n^{1,2}(-1, 1)$, i.e. the Banach space

$$W_n^{1,2}(-1, 1) = \left\{ u \in W^{1,2}(-1, 1) : u = \lim_{n \rightarrow \infty} u_n \text{ in } W^{1,2}, \right. \\ \left. u_n \in C^\infty([-1, 1]), u_n'(-1) = u_n'(1) = 0 \right\}.$$

Further, let $A: X \rightarrow X^*$ be the operator given by:

$$\langle A(u), v \rangle = \int_{-1}^1 u'v' dx,$$

where $\langle \cdot, \cdot \rangle = X^* \langle \cdot, \cdot \rangle_X$ denotes the duality pairing. We need to recall the following property of the operator A .

Proposition 36 ([1]). *The operator A is of type $(S)_+$.*

At this point, we are able to check the Palais-Smale condition for the functional F_q .

Proposition 37. *The functional $F_q: W_n^{1,2} \rightarrow \mathbb{R}$ satisfies the (PS)-condition.*

Proof. Consider $\{u_n\}_n \subseteq W_n^{1,2}$ and assume there exist $M > 0$ and a sequence $\{\varepsilon_n\}_n$ s.t.

$$|F_q(u_n)| \leq M, \quad \|F_q'(u_n)\|_{(W_n^{1,2})^*} \leq \varepsilon_n, \quad (1.25)$$

where $\varepsilon_n > 0$, $\varepsilon_n \rightarrow 0$ and

$$\langle F_q'(u), v \rangle = \int_{-1}^1 (\psi(u)\varepsilon_0\sigma_0 - q - \tilde{\beta}(u)) v dx - \langle A(u), v \rangle \\ := \int_{-1}^1 f(x, u)v dx - \langle A(u), v \rangle.$$

The proof is divided in two steps.

Step 1: u_n is bounded in $W_n^{1,2}$.

This first step is a corollary of the proof of Theorem 1. Indeed, in that proof, we assume $F_q(u_n) \leq M$ and we prove the boundedness of $\|u_n\|_\infty$ thanks to (1.14) and the boundedness of $\|u'_n\|_2$ thanks to (1.15).

Step 2: $\exists n_k$ s.t. $u_{n_k} \rightarrow u$ in $W_n^{1,2}$.

Up to subsequence, by the previous point we get $u_n \rightharpoonup u$ for some $u \in W_n^{1,2}$. Since the embedding $W_n^{1,2} \hookrightarrow L^2$ is compact, we deduce, again up to a subsequence, that $u_n \rightarrow u$ in L^2 . By (1.25), we have:

$$|\langle A(u_n), v \rangle - \langle f, v \rangle_{L^2}| \leq \varepsilon_n \quad \forall v \in W_n^{1,2}.$$

So, we can choose $v = u_n - u \in W_n^{1,2}$ and get

$$|\langle A(u_n), u - u_n \rangle| \leq |\langle F'_q(u_n), u - u_n \rangle| + |\langle f, u - u_n \rangle_{L^2}| \leq \varepsilon_n + \|f\|_2 \|u_n - u\|_2.$$

Taking the limits on both sides of the previous inequality we get:

$$\lim_{n \rightarrow \infty} \langle A(u_n), u - u_n \rangle = 0.$$

Since the operator A is of type $(S)_+$, we conclude $u_n \rightarrow u$ in $W_n^{1,2}$. \square

We conclude the section by giving sufficient conditions to have at least three solutions for the elliptic PDE (1.7). We introduce

$$\bar{\mathcal{R}}: \mathbb{R} \rightarrow \mathbb{R}, \quad \bar{\mathcal{R}}(u) = \frac{1}{2} \int_{-1}^1 \mathcal{R}(x, u) dx.$$

where we recall that \mathcal{R} is such that:

$$F_q(u) = \frac{k}{2} \|u'\|_2^2 + \int_{-1}^1 \mathcal{R}(x, u(x)) dx.$$

The assumptions we need in order to get our results are basically three: (1) the space-averaged EBM with potential $\bar{\mathcal{R}}$ has (at least) two stable steady-state solutions, (2) the viscosity $\kappa > 0$ of the 1D-EBM is sufficiently large, (3) the two wells in the potential functional $\bar{\mathcal{R}}$ corresponding to the two minimum points are sufficiently deep.

Theorem 2. *Denote by $B_{H^1}(v, \rho) = \{u \in H^1 \mid \|u - v\|_{H^1} < \rho\}$ the open ball in H^1 with center v and radius $\rho > 0$. Assume $\bar{\mathcal{R}}$ has two non-negative minimum points $u_1 \neq u_2$, with $F_q(u_1) \geq F_q(u_2)$. Then, there exist $\omega > 0$ and $f, g \in O(\varepsilon^{-1})$ as $\varepsilon \rightarrow 0^+$ s.t. if $\bar{\varepsilon} > 0$ satisfies:*

(i) $\bar{\mathcal{R}}''(u_i) > f(\bar{\varepsilon})$, for $i = 1, 2$,

(ii) $\kappa > g(\bar{\varepsilon})$,

(iii) $\bar{\varepsilon} \leq \omega$,

then F_q has two local minimum points \hat{u}_1, \hat{u}_2 such that:

(a) $B_{H^1}(u_1, \bar{\varepsilon}) \cap B_{H^1}(u_2, \bar{\varepsilon}) = \emptyset$,

(b) $\hat{u}_i \in B_{H^1}(u_i, \bar{\varepsilon})$, for $i = 1, 2$,

(c) If $\|u - u_1\|_{H^1} = \bar{\varepsilon}$, then $F_q(u) \geq F_q(u_1) + \delta$, with $\delta = \delta(\bar{\varepsilon}) > 0$.

Proof. The proof consists in repeating the direct method used to prove Theorem 1 and applying it to the set $H^1 \cap B_{H^1}(u_i, \bar{\varepsilon})$. Indeed, thanks to Lemma 38, we can find $\bar{\varepsilon} > 0$ s.t. $B_{H^1}(u_1, \bar{\varepsilon}) \cap B_{H^1}(u_2, \bar{\varepsilon}) = \emptyset$, $\hat{u}_i \in B_{H^1}(u_i, \bar{\varepsilon})$ and

$$\|u - u_i\|_{H^1} = \bar{\varepsilon} \implies F_q(u) - F_q(u_i) \geq \delta > 0, \quad \delta = \delta(\bar{\varepsilon}). \quad (1.26)$$

Now, we consider the set

$$\mathbb{X}_i = H^1 \cap \overline{B_{H^1}(u_i, \bar{\varepsilon})},$$

where we stress the fact that $\overline{B_{H^1}(u_i, \bar{\varepsilon})}$ denotes the closed ball in H^1 . Considering a sequence $\{u_{n,i}\}_n$, we want to show that the sublevel sets of F_q are compact in \mathbb{X}_i under the following notion of convergence:

$$u_{n,i} \xrightarrow{\mathbb{X}_i} u_\infty \quad \text{if and only if } u_{n,i} \rightarrow u_\infty \text{ uniformly in } [-1, 1] \text{ and } u'_{n,i} \rightharpoonup u'_\infty \text{ in } L^2.$$

Repeating the argument in the proof of Theorem 1, we get the existence of $u_{\infty,i} \in H^1$ s.t. $u_{n,i} \xrightarrow{\mathbb{X}_i} u_{\infty,i}$. Thanks to the uniform convergence, we have

$$\|u_{\infty,i} - u_i\|_{H^1}^2 = \|u_{\infty,i} - u_i\|_2^2 + \|u'_{\infty,i}\|_2^2 = \lim_n \|u_{n,i} - u_i\|_2^2 + \|u'_{\infty,i}\|_2^2.$$

Second, for each n it holds

$$\bar{\varepsilon}^2 \geq \|u_{n,i} - u_i\|_{H^1}^2 = \|u_{n,i} - u_i\|_2^2 + \|u'_{n,i}\|_2^2.$$

Then, using the inferior lower-semi-continuity of the norm, we get:

$$\begin{aligned} \bar{\varepsilon}^2 &\geq \liminf_n \left(\|u_{n,i} - u_i\|_2^2 + \|u'_{n,i}\|_2^2 \right) = \|u_{\infty,i} - u_i\|_2^2 + \liminf_n \|u'_{n,i}\|_2^2 \\ &\geq \|u_{\infty,i} - u_i\|_2^2 + \|u'_{\infty,i}\|_2^2 = \|u_{\infty,i} - u_i\|_{H^1}^2. \end{aligned}$$

Hence $u_{\infty,i} \in \overline{B_{H^1}(u_i, \bar{\varepsilon})}$. Since F_q is lower semi-continuous, we get the existence of \tilde{u}_i minimum point for F_q in \mathbb{X}_i . But thanks to the property (1.26), we deduce $\|\hat{u}_i - u_i\|_{H^1} < \bar{\varepsilon}$. Hence \tilde{u}_i are local minimum points for F_q in H^1 . □

Lemma 38. *Assume $\bar{\mathcal{R}}$ has a minimum point \hat{u} . Then, there exists $\omega > 0$ and $f, g \in O(\epsilon^{-1})$ as $\epsilon \rightarrow 0^+$ s.t. if $\epsilon > 0$ satisfies:*

$$(i) \quad \bar{\mathcal{R}}''(\hat{u}) > f(\epsilon),$$

$$(ii) \quad \kappa > g(\epsilon),$$

$$(iii) \quad \epsilon = \|u - \hat{u}\|_{H^1} \leq \omega,$$

then $F_q(u) \geq F_q(\hat{u}) + \delta$, with $\delta = \delta(\epsilon) > 0$.

Proof. Let $u \in H^1$ s.t. $\|u - \hat{u}\|_{H^1} = \epsilon$. Since $\epsilon^2 = \|u - \hat{u}\|_2^2 + \|u'\|_2^2$, we divide the proof in two cases according to the magnitude of $\|u - \hat{u}\|_2^2$ and $\|u'\|_2^2$.

Case 1: $\|u'\|_2^2 \geq \epsilon^2/2$ and $\|u - \hat{u}\|_2^2 \leq \epsilon^2/2$.

Since $\mathcal{R}(x, v)$ is locally Lipschitz in v uniformly in x , there exists $L = L(\mathcal{R}, \hat{u}) > 0$ and $\omega = \omega(\mathcal{R}, \hat{u}) > 0$ s.t.

$$|\mathcal{R}(x, v) - \mathcal{R}(x, \hat{u})| \leq L|v - \hat{u}|, \quad |u - \hat{u}| \leq \omega, \quad x \in [-1, 1].$$

Thus, if $\|u - \hat{u}\|_\infty \leq \|u - \hat{u}\|_{H^1} = \epsilon \leq \omega$, it holds

$$\int_{-1}^1 |\mathcal{R}(x, u(x)) - \mathcal{R}(x, \hat{u})| dx \leq L\|u - \hat{u}\|_1 \leq \sqrt{2}L\|u - \hat{u}\|_2 \leq L\epsilon$$

Using the previous inequality and the bound on $\|u'\|_2^2$, we have

$$F_q(u) - F_q(\hat{u}) \geq -\left| \int_{-1}^1 \mathcal{R}(x, u(x)) - \mathcal{R}(x, \hat{u}) dx \right| + \frac{k}{2}\|u'\|_2^2 \geq -L\epsilon + \kappa \frac{\epsilon^2}{4},$$

and thus $g(\epsilon) := \frac{4L}{\epsilon}$.

Case 2: $\|u'\|_2^2 \leq \epsilon^2/2$ and $\|u - \hat{u}\|_2^2 \geq \epsilon^2/2$.

Let's consider $\bar{u} = \frac{1}{2} \int_{-1}^1 u(x) dx$. We start by pointing out two useful inequalities. First

$$|\bar{u} - \hat{u}| = \left| \frac{1}{2} \int_{-1}^1 u(x) dx - \hat{u} \right| = \left| \frac{1}{2} \int_{-1}^1 u(x) - \hat{u} dx \right| \leq \|u - \hat{u}\|_\infty \quad (1.27)$$

Second, for each $x \in [-1, 1]$, it holds:

$$|u(x) - \bar{u}| = \left| \frac{1}{2} \int_{-1}^1 (u(x) - u(y)) dx \right| \leq \frac{1}{2} \|u'\|_2 \cdot \int_{-1}^1 |x - y|^{1/2} dy \leq \sqrt{2} \|u'\|_2, \quad (1.28)$$

where the first inequality follows from the Holder properties of the Sobolev space H^1 . At this point, the estimate on the value of the functional at u can be done considering

$$F_q(u) - F_q(\hat{u}) \geq \int_{-1}^1 \mathcal{R}(x, u(x)) - \mathcal{R}(x, \hat{u}) dx$$

and using a Taylor expansion for \mathcal{R} . Indeed,

$$\begin{aligned} \mathcal{R}(x, u(x)) &= \mathcal{R}(x, \hat{u}) + \mathcal{R}_u(x, \hat{u})(u(x) - \hat{u}) + \mathcal{R}_{uu}(x, \hat{u}) \frac{(u(x) - \hat{u})^2}{2} \\ &\quad + O(\|u - \hat{u}\|_\infty^3). \end{aligned}$$

Performing the decomposition

$$u(x) - \hat{u} = (u(x) - \bar{u}) + (\bar{u} - \hat{u}),$$

we observe that:

$$\int_{-1}^1 \mathcal{R}_u(x, \hat{u})(\bar{u} - \hat{u}) dx = (\bar{u} - \hat{u}) \int_{-1}^1 \mathcal{R}_u(x, \hat{u}) dx = (\bar{u} - \hat{u}) 2\bar{\mathcal{R}}'(\hat{u}) = 0$$

and thus

$$\begin{aligned} \int_{-1}^1 \mathcal{R}(x, u(x)) - \mathcal{R}(x, \hat{u}) dx &= \int_{-1}^1 \mathcal{R}_u(x, \hat{u})(u(x) - \bar{u}) dx \\ &\quad + \int_{-1}^1 \mathcal{R}_{uu}(x, \hat{u}) \frac{(u(x) - \hat{u})^2}{2} dx \\ &\quad + O(\|u - \hat{u}\|_\infty^3) \end{aligned} \quad (1.29)$$

The absolute value of the first term on the right-hand side can be bounded thanks to (1.28) and Holder's inequality. Indeed

$$\begin{aligned} \left| \int_{-1}^1 \mathcal{R}_u(x, \hat{u})(u(x) - \bar{u}) dx \right| &\leq \|\mathcal{R}_u(\cdot, \hat{u})\|_\infty \|u - \bar{u}\|_1 \leq 2\sqrt{2} \|\mathcal{R}_u(\cdot, \hat{u})\|_\infty \|u'\|_2 \\ &\leq 2 \|\mathcal{R}_u(\cdot, \hat{u})\|_\infty \varepsilon. \end{aligned}$$

Now, need to estimate the second term on the RHS of (1.29). Adding and subtracting $\bar{\mathcal{R}}''(\hat{u})$, we have:

$$\begin{aligned} \int_{-1}^1 \mathcal{R}_{uu}(x, \hat{u}) \frac{(u(x) - \hat{u})^2}{2} dx &= \frac{1}{2} \int_{-1}^1 \bar{\mathcal{R}}''(\hat{u})(u - \hat{u})^2 dx \\ &\quad + \frac{1}{2} \int_{-1}^1 \left(\mathcal{R}_{uu}(x, \hat{u}) - \bar{\mathcal{R}}''(\hat{u}) \right) (u - \hat{u})^2 dx. \end{aligned} \quad (1.30)$$

The first term on the RHS is large thanks to the central assumption of Case 2. In fact

$$\frac{1}{2} \int_{-1}^1 \bar{\mathcal{R}}''(\hat{u})(u - \hat{u})^2 dx = \frac{\bar{\mathcal{R}}''(\hat{u})}{2} \|u - \hat{u}\|_2^2 \geq \bar{\mathcal{R}}''(\hat{u}) \frac{\varepsilon^2}{4}.$$

The absolute value of the second term on the RHS of (1.30) can be bounded using Holder's inequality as follows:

$$\begin{aligned} \left| \frac{1}{2} \int_{-1}^1 \left(\mathcal{R}_{uu}(x, \hat{u}) - \bar{\mathcal{R}}''(\hat{u}) \right) (u - \hat{u})^2 dx \right| &\leq \frac{1}{2} \left\| \bar{\mathcal{R}}''(\hat{u}) - \mathcal{R}_{uu}(\cdot, \hat{u}) \right\|_\infty \|u - \hat{u}\|_2^2 \\ &\leq \left\| \bar{\mathcal{R}}''(\hat{u}) - \mathcal{R}_{uu}(\cdot, \hat{u}) \right\|_\infty \frac{\varepsilon^2}{2}. \end{aligned}$$

Chapter 2

A stochastic one-dimensional energy balance model for climate change

This chapter covers the content of [25], where we develop a three-timescale framework for modelling climate change and introduce a space-heterogeneous one-dimensional energy balance model. This model, addressing temperature fluctuations from rising carbon dioxide levels and the super-greenhouse effect in tropical regions, fits within the three-timescale setting and is given by a stochastic reaction-diffusion equations. Our results show how both mean and variance of temperature increase, without the system going through a bifurcation point. This study aims to advance the conceptual understanding of the extreme weather events frequency increase due to climate change.

More in detail, this chapter is organised as follows. In Section 2.1, we introduce the non-autonomous framework for weather, macroweather, and climate, with a particular focus on the latter two. We outline the scale separation between them and provide their tentative definitions. This first, abstract part culminates in a link between macroweather and climate, justifying an adiabatic approach to studying the former in the presence of a non-autonomous dependence, such as CO_2 concentration in the atmosphere. In Section 2.2, we begin by recalling the key concepts of EBMs, starting with the zero-dimensional version in Section 2.2.1. We discuss why EBMs are suitable for describing macroweather and how they can explain the increase in global mean temperature (GMT) due to rising CO_2 concentrations. In Section 2.2.2, we introduce our new 1D-EBM, detailing the parametrisation of all the terms of the parabolic partial differential equation (PDE). Section 2.2.3 describes the deterministic properties of the model, such as the existence of one or more steady-state solutions and their dependence on the CO_2 parameter. In Section 2.2.4, we discuss the stochastic extension of the model

and its properties, including the existence of an explicit invariant measure. Section 2.2.5 presents the main results of the second part. We demonstrate how our model predicts an increase in the variance of temperature fluctuations under CO₂ in the current climate configuration, without introducing new bifurcation points. We use both numerical tools and theoretical arguments to explain and understand this phenomenon. Finally, Section 2.3 details the finite-difference scheme used for numerical simulations and some spectral properties needed to deduce the existence of the invariant measure for the stochastic problem.

2.1 The non-autonomous scheme with three timescales

In Section 2.2 below, we introduce a stochastic EBM with suitable space dependence, and a slowly varying parameter corresponding to CO₂ concentration, in order to investigate the time-change of fluctuations, as also discussed in the Introduction. There are three different timescales involved in this modelling. We could skip the first one by just mentioning [44], and restrict ourselves to two timescales only, but at the same time we want to insist on the non-autonomous structure of the modelling, hence it is convenient to enlarge the discussion a bit.

In the modelling we have in mind, there are three timescales, called:

- weather, where variations are visible at the timescale of hours/day (variables will be denoted by $V_w(t)$, $T_w(t)$ etc.);
- macroweather, where variations are visible at the timescale of months/year (variables will be denoted by $V_{mw}(t)$, $T_{mw}(t)$ etc.);
- climate, changing at the timescale of dozens of years (probability measures and their expected values characterise this level, still changing in time).

Subdivision and attribution of a precise timescale are not strict.

Remark 40. *The reader will realise that, for the purpose of Section 2.2, we could start from Subsection 2.1.5. Let us then explain why we think that Subsections 2.1.1-2.1.4 are also very important. As already said, a main purpose of this work is to identify possible explanations for an increase in variance, when a parameter changes. In a sentence, the two main ingredients are a noise in the system equations and a suitable non-linearity which amplifies the variations of the noise in a different way for different values of the parameter. The noise, then, is crucial. Subsections 2.1.1-2.1.4 are devoted to explaining its origin.*

2.1.1 The weather timescale

Following [44], it is natural to model the weather scale by deterministic equations, ordinary equations for simplicity of notation (but the ideas are the same for PDEs); randomness can be introduced but it is not strictly necessary, except maybe for a description of the uncertainty about initial conditions and parameters, not included in the present discussion. Following [44], we distinguish the main physical variables in fast and slow ones, according to a system of the form

$$\begin{aligned}\partial_t V_w &= f(V_w, T_w) \\ \partial_t T_w &= \epsilon g(V_w, T_w, q(\epsilon t)) \\ q(t) &\text{ slowly varying}\end{aligned}$$

for a small $\epsilon > 0$. Here V_w changes in unitary time (corresponding to hours/day), and T_w varies very slowly (monthly, say). In addition, the slow variable is influenced by a slow time-change of structure, described by the time-varying parameters $q(\epsilon t)$. The function $q(t)$ is assumed to be slowly varying, hence $q(\epsilon t)$ is *super-slowly varying* (from here the three timescales arise).

The parameter $\tau = \frac{1}{\epsilon}$ corresponds to the typical reaction time of the slow variables, measured in the unitary time of V . Appreciable changes of T happen in a time of order τ , at the weather scale.

With great simplification, we may think that V collects the fluid dynamic variables (the fluid Velocity plus other related variables), which are very unstable and rapidly changing at the daily level, while T represents Temperature. In this case, the unit of time at the weather level is of the order of hours, and $\tau = \frac{1}{\epsilon}$ is of the order of a few months, hence e.g. of order 100. On the contrary, the time-change of CO₂ concentration, call it τ_{CO_2} , is of the order of a dozen of years, hence e.g. of order 10000 in the weather scale. With these figures, $q(t)$ has a relaxation time of 100 and $q(\epsilon t)$ of order 10000.

2.1.2 Macroweather timescale for T

Then we change the scale and set

$$\tilde{T}_{mw}(t) = T_w\left(\frac{t}{\epsilon}\right)$$

so that we observe variations of $\tilde{T}_{mw}(t)$ in unitary time. We call this the macroweather timescale. It holds

$$\partial_t \tilde{T}_{mw}(t) = g\left(V_w\left(\frac{t}{\epsilon}\right), \tilde{T}_{mw}(t), q(t)\right).$$

Let us recall that, at this timescale, q varies very slowly. Let us look for a simplification of this equation, where V_w does not appear any more.

2.1.3 The averaging approximation

Let us heuristically describe the averaging approximation, which can be made rigorous under proper assumptions for suitable systems, see [36].

At the integral level, we have

$$\tilde{T}_{mw}(t) - \tilde{T}_{mw}(t_0) = \int_{t_0}^t g\left(V_w\left(\frac{s}{\epsilon}\right), \tilde{T}_{mw}(s), q(s)\right) ds.$$

If $t - t_0$ is small, let us use the reasonable approximation

$$\begin{aligned} &\sim \int_{t_0}^t g\left(V_w\left(\frac{s}{\epsilon}\right), \tilde{T}_{mw}(t_0), q(t_0)\right) ds \\ &= (t - t_0) \frac{1}{t - t_0} \int_{t_0}^t g\left(V_w\left(\frac{s}{\epsilon}\right), \tilde{T}_{mw}(t_0), q(t_0)\right) ds. \end{aligned}$$

Then, if $\epsilon \ll t - t_0$, we heuristically invoke an ergodic theorem and approximate

$$\sim (t - t_0) \int g\left(v, \tilde{T}_{mw}(t_0), q(t_0)\right) \nu_{\tilde{T}_{mw}(t_0)}(dv)$$

where $\nu_\tau(dv)$ is invariant for

$$\partial_t V = f(V, \tau).$$

Setting

$$\bar{g}(\tau, q) = \int g(v, \tau, q) \nu_\tau(dv)$$

we may write

$$= (t - t_0) \bar{g}\left(\tilde{T}_{mw}(t_0), q(t_0)\right)$$

and then again approximate it to

$$\sim \int_{t_0}^t \bar{g}\left(\tilde{T}_{mw}(s), q(s)\right) ds.$$

Hence we get the simplified model

$$\partial_t \bar{T}_{mw}(t) = \bar{g}\left(\bar{T}_{mw}(t), q(t)\right).$$

2.1.4 Hasselmann's proposal

However, in our case, this simplification is not realistic. If ϵ is of order $\frac{1}{100}$, then $t - t_0$ is of order one, because we need the validity of the approximation

$$\frac{1}{t - t_0} \int_{t_0}^t g\left(V_w\left(\frac{s}{\epsilon}\right), a, b\right) ds \sim \int g(v, a, b) \nu_a(dv).$$

But on a time of order one, we observe variations of $\tilde{T}_{mw}(t)$, we said above, hence the approximation

$$\int_{t_0}^t g\left(V_w\left(\frac{s}{\epsilon}\right), \tilde{T}_{mw}(s), q(s)\right) ds \sim \int_{t_0}^t g\left(V_w\left(\frac{s}{\epsilon}\right), \tilde{T}_{mw}(t_0), q(t_0)\right) ds$$

is not so strict (on the contrary, it is excellent for the $q(s) \sim q(t_0)$ approximation).

We need to keep fluctuations into account at the macroweather scale. A phenomenological way (Hasselmann's proposal) is to replace the model above by

$$dT_{mw}(t) = \bar{g}(T_{mw}(t), q(t)) dt + \sqrt{\epsilon}\sigma(T_{mw}(t), q(t)) \circ dW(t)$$

for a suitable "volatility" σ (Stratonovich integral \circ looks more appropriate). In [44], heuristic justifications are given, inspired for instance the random displacements of a Brownian particle in a fluid of molecules (which on their own are subject to a deterministic fast dynamics, coupled with the slow deterministic dynamic of the bigger particle). The Bremen school on Random Dynamical Systems and other research groups explored for some time rigorous justifications for this proposal, but a final answer is not known, see for instance [3, 52]. However, the observation of temperature time series at the timescale of month-year clearly shows some form of stochasticity and thus Hasselmann's proposal looks very appealing.

For our purposes below, adhering to Hasselmann's proposal is essential, since our results are the consequence of random perturbations of a non-linear system representing climate dynamics at the macroweather timescale, namely a stochastic version of the EBM. Random perturbations are often accepted just based on the generic justification of an unknown coupling with other segments of the physical system (which at the end of the story is the reason also here, namely the coupling with the fast variables) but Hasselmann's proposal is a more precise explanation.

Let us however advise the reader that we shall start, in our example below, from a stochastic PDE for the temperature macroweather-scale, given a priori, not derived precisely from the weather scale as described above. We want to concentrate on the consequences of particular non-linearities. Our model will have the simplified form

$$dT_{mw}(t) = \bar{g}(T_{mw}(t), q(t)) dt + \sqrt{\epsilon}\sigma dW(t)$$

with constant σ .

2.1.5 Macroweather and climate

As announced at the end of Subsection 2.1.4, our investigation starts from an equation of the form (stochastic differential equation or SPDE)

$$dT(t) = \bar{g}(T(t), q(t)) dt + \sigma dW(t) \quad (2.1)$$

$q(t)$ slowly varying

where we skip the subscripts but keep in mind that it is a macroweather model, we have skipped the factor $\sqrt{\epsilon}$ but we shall choose a small diffusion coefficient σ , and the non-linear function \bar{g} will be chosen by means of typical arguments related to EBM's. The slowly varying function $q(t)$ will describe the effect, in the model, of slowly varying CO₂-concentration, appreciated on a timescale of dozens of years.

The climate is a collection of statistical information from the time series of this model. If it were an autonomous system ($q(t)$ equal to a constant), we would invoke invariant measures. Due to the time-change in \bar{g} , we have to use the formalism of time-varying invariant measures. However, at the simulation level, we approximate this time-varying system by an adiabatic system parametrised by a parameter q :

$$dT(t) = \bar{g}(T(t), q) dt + \sigma dW(t)$$

and investigate its invariant measures, parametrised by q . The slow change of statistics for the true non-autonomous system is mimicked by the change of statistics when the parameter q is changed.

Concerning precisely the concept of climate, let us introduce some formalism. We again limit ourselves to stochastic differential equations (SDEs) on an Euclidean space \mathbb{R}^d (e.g. the space-discretisation of a stochastic partial differential equation, as in our main example below) but the concepts can be widely generalised, see for instance [34] for a non-autonomous abstract random dynamical system framework related to the weather-climate dichotomy (that we improve hereby introducing a third level, the macroweather). Call $\Pr(\mathbb{R}^d)$ the set of probability measures on Borel sets of \mathbb{R}^d . Consider the SDE (2.1) on the full real line of time. Assume that $W(t)$ is a d -dimensional two-sided Brownian motion defined on a Probability space $(\Omega, \mathcal{F}, \mathbb{P})$ with expectation \mathbb{E} . Assume that, for the Cauchy problem on the half line $[t_0, \infty)$ with initial condition T_0 at time t_0 , with arbitrary t_0 and T_0 , at least weak global existence and uniqueness in law holds, and denote the solution by $T^{t_0, T_0}(t)$, $t \in [t_0, \infty)$; assume $T_0 \mapsto T^{t_0, T_0}(t)$ is Borel measurable from \mathbb{R}^d to $\Pr(\mathbb{R}^d)$ endowed with the weak convergence of measures.

For all $t_0 < t$, we introduce the Markov semigroup $\mathcal{P}_{t_0, t}$ mapping $\Pr(\mathbb{R}^d)$ into $\Pr(\mathbb{R}^d)$ defined by the identity

$$\int_{\mathbb{R}^d} \phi(y) (\mathcal{P}_{t_0, t} \nu)(dy) = \mathbb{E} \int_{\mathbb{R}^d} \phi(T^{t_0, T_0}(t)) \nu(dT_0)$$

for every $\nu \in \text{Pr}(\mathbb{R}^d)$ and every bounded continuous test function ϕ on \mathbb{R}^d . One can prove that

$$\begin{aligned}\mathcal{P}_{r,t}\mathcal{P}_{s,r} &= \mathcal{P}_{s,t} \\ \mathcal{P}_{s,s} &= Id.\end{aligned}$$

Moreover, one can link the Markov operator for equation (2.1) to the Fokker-Planck equation

$$\partial_t f + \text{div}(\bar{g}(\cdot, q) f) = \frac{\sigma^2}{2} \Delta f$$

but we do not stress the rigorous results here.

The set of probability densities $\text{Pr}(\mathbb{R}^d)$ is the state-space for the climate. In other words, any $\nu \in \text{Pr}(\mathbb{R}^d)$ is a (possible) state for the climate. Further, fixed the times $t_0 < t$, the operator $\mathcal{P}_{t_0,t}$ defines the evolution, from t_0 to t , of the climate dynamics. Thus, we look for the climate concept inside the class of time-varying invariant measures which are invariant under the operator defining the climate dynamics, i.e. a family

$$\{\mu_t\}_{t \in \mathbb{R}} \subset \text{Pr}(\mathbb{R}^d)$$

such that

$$\mathcal{P}_{s,t}\mu_s = \mu_t \quad \text{for every } s \leq t.$$

Remark 41. *The concept of time-dependent invariant measure $\{\mu_t\}_{t \in \mathbb{R}}$ should not be confused with any solution of the Fokker-Planck equation. Similarly to the fact that, in many cases, the invariant measure μ of an autonomous system is the limit, as $t \rightarrow +\infty$, of the law of the solution $X_t^{x_0}$ starting at time $t = 0$ from the initial condition x_0 , independent of x_0 , the time-dependent invariant measure μ_t is expected to be, in many cases, the limit as $t_0 \rightarrow -\infty$ of the law of the solution $X_t^{t_0, x_0}$ starting at time t_0 from x_0 , independently of x_0 (property that we could call "pull-back convergence to the equilibrium").*

Two simple illustrative examples are the Ornstein-Uhlenbeck equations with periodic or linear growth. For the periodic equation

$$dX_t = -X_t dt + \sin(t) dt + dW_t$$

the unique time-dependent invariant measure μ_t is the law, 2π -periodic of the process

$$X_t := \int_{-\infty}^t e^{-(t-s)} \sin(s) ds + \int_{-\infty}^t e^{-(t-s)} dW_s.$$

For the linear growth equation (closer to our model with CO_2 increase)

$$dX_t = -X_t dt + t dt + dW_t$$

the unique time-dependent invariant measure μ_t is the law of the process

$$X_t := \int_{-\infty}^t e^{-(t-s)} s ds + \int_{-\infty}^t e^{-(t-s)} dW_s.$$

Under suitable assumptions for the stochastic equations, there are results of existence (easy, in particular relying on the existence of a compact global attractor) and also uniqueness (more difficult) for such invariant families. This part of the theory is in progress. When the invariant measure $\{\mu_t\}_{t \in \mathbb{R}}$ is unique, we call it "the climate".

When uniqueness does not hold or it is not known, the idea could be to look for families μ_t not only invariant but also with additional properties of interest for physical sciences or other reasons. A typical one could be a pull-back version of "convergence to equilibrium":

$$\mu_t = \lim_{s \rightarrow -\infty} \mathcal{P}_{s,t} \lambda \tag{2.2}$$

where λ is a "natural" measure, as a rotation invariant centred Gaussian measure on \mathbb{R}^d . For simplicity of understanding, the reader can assume that there is one and only one invariant family μ_t or one selected by the pull-back property above.

If $q(t)$ varies very slowly, we expect that also μ_t varies accordingly, and thus an adiabatic approach to the numerical computation of μ_t is reasonable, as already remarked above.

It is crucial to emphasise the following point. We believe that viewing climate as a time-dependent invariant measure, constructed in the pull-back sense, is not only a rigorous definition but also a physically meaningful one. Indeed, the current climate is the result of a long-term evolution that began in the distant past, where the dependence on the initial condition has been lost. This idea, together with the application to geophysical science of concepts from dynamical systems theory, developed in the 1990s ([18, 2]), began gaining traction approximately fifteen years ago ([41, 17]).

2.2 A new 1D-EBM with tropics bistability

2.2.1 The macroweather timescale and the global mean temperature increase due to CO₂ concentration

EBMs are elementary climate models where, in the simplest form, the temperature of the planet evolves according to the balance of the radiation absorbed and emitted by the Earth ([12, 77, 67, 40, 42]). Their ability to capture the essential dynamics of Earth's climate system while remaining computationally tractable makes EBMs valuable tools for understanding a wide range of climate phenomena, from the onset of ice ages to the impacts of greenhouse gas emissions on global temperatures ([29, 6]). There

exists a spectrum of complexity for this kind of model, starting from the zero-dimensional (0D) case, moving to the one-dimensional (1D) case, and arriving at higher-dimensional models ([72]). Before delving into the details of our 1D-EBM with space heterogeneous radiation balance, we illustrate (i) why an EBM has a macroweather timescale, and (ii) why an increase of CO₂ concentration in a stochastic 0D-EBM leads to an increase of GMT, but not the variance of the solution.

First, we consider a 0D-EBM for the global mean temperature $T = T(t)$ which given a positive initial condition T_0 , is an ODE of the form

$$\begin{aligned} C \frac{dT}{dt} &= Q_0 \beta + q - A - B \cdot (T - 273), \\ T(0) &= T_0. \end{aligned} \tag{2.3}$$

In this model, the radiation emitted R_e by the planet is assumed, according to Budyko empirical radiation formula ([12]), of the form

$$R_e(T) = A + B \cdot (T - 273) - q,$$

where A, B are positive constants that can be derived by a best-fit estimate with real data observations; $C > 0$ denotes the heat capacity per square meter, while Q_0 and β are respectively the global mean radiation and co-albedo. Lastly, the additive parameter $q > 0$ the effect of CO₂ concentration on the radiation balance ([72, 6, 24]). Denoting by T_* the unique stable fixed point of the model, i.e.

$$T_* = \frac{Q_0 \beta - A + q}{B} + 273,$$

the solution of Eq. (2.3) is given by

$$T(t) = T_* + (T_0 - T_*) e^{-t/\tau_0},$$

where $\tau_0 = C/B$ is the relaxation time, i.e. the timescale at which a deviation from the equilibrium temperature is reabsorbed. Considering an all-land planet, it is reasonable to consider the heat capacity as half the heat capacity at constant pressure of the column of dry air over a square meter, as pointed out in [72], leading to

$$C = 5 \cdot 10^7 \text{ J K}^{-1} \text{ m}^{-2}.$$

On the other hand, satellite data suggest ([72, 43])

$$B = 1.90 \text{ W m}^2 \text{ K}^{-1}.$$

This leads to a relaxation time of the order of one month, as

$$\tau_0 = \frac{C}{B} = 2.63 \cdot 10^7 \text{ s} \approx 30 \text{ days}.$$

It is worth pointing out that the hypothesis of an all-land planet is a huge simplification of reality. Indeed, the Earth's system has various components capable of storing heat efficiently, each with its own unique capacity ([42]). The value for C we have considered corresponds to the capacity of the atmospheric column. But, even considering a planet with a mixed-layer only ocean, the heat capacity would be 60 times larger (see [72]) i.e. in the order of a few years, remaining thus in the macro weather timescale.

Second, we force the model with a stochastic noise modelling the effect of fast terms with respect to the slow radiation balance terms of Eq. (2.3). Denote by $(W_t)_{t \geq 0}$ a Brownian motion, and consider the SDE given by:

$$\begin{aligned} CdT_t &= (Q_0\beta + q - A - BT_t) dt + \sigma dW_t, \\ T(0) &= T_0, \end{aligned} \quad (2.4)$$

where $\sigma > 0$ is the noise intensity. Denoting by $\tilde{A} = Q_0\beta + q - A$, the solution can be explicitly written, using a variation of parameters technique ([5]) as

$$T_t = T_0 e^{-t/\tau_0} + \frac{\tilde{A}}{\tau_0} (1 - e^{-t/\tau_0}) + \sigma \int_0^t e^{-(t-s)/\tau_0} dW_s.$$

The solution is a Gaussian process with a mean value

$$\mathbb{E}[T_t] = T(0)e^{-t/\tau_0} + \tilde{A} (1 - e^{-t/\tau_0}), \quad (2.5)$$

and variance

$$\begin{aligned} \text{Var}(T_t) &= \text{Var}\left(\frac{\sigma}{C} \int_0^t e^{-(t-s)/\tau_0} ds\right) = \frac{\sigma^2}{C^2} \int_0^t e^{-2(t-s)/\tau_0} ds \\ &= \frac{\sigma^2}{2BC} (1 - e^{-2t/\tau_0}). \end{aligned} \quad (2.6)$$

Further, the stochastic EBM in Eq. (2.4) has a unique Gaussian invariant measure $\nu \sim \mathcal{N}(\mu_\nu, \sigma_\nu^2)$, whose mean μ_ν and variance σ_ν^2 , can be obtained taking the limit for the time that tends to infinity in Eq. (2.5) and Eq. (2.6), leading to

$$\mu_\nu = \tilde{A} = \frac{Q_0\beta + q - A}{B}, \quad \sigma_\nu^2 = \frac{\sigma^2}{2BC}.$$

Thus, a change in the CO₂ concentration leads to a change in the mean value of the climate, i.e. the invariant measure, but not in its variability. Usually, the variability increase results from a critical transition, such as a saddle-node bifurcation, which arises in the model. This is the concept of bifurcation-induced tipping point, which leads to the critical slowing down behaviour of the system, resulting in an increase of variance and autocorrelation close to the bifurcation point ([23, 76, 4, 56]). However, the presence

of a bifurcation point for the global scale climate is questionable, and the presence of bistable regimes for climate components, sometimes called tipping elements such for the Atlantic meridional overturning circulation or polar ice sheets, is localised in space. For all these reasons, in Section 2.2.2, we will describe a new one-dimensional model with a local in-space change in the non-linear term that is able to explain the variance increase.

2.2.2 Model formulation

In this section, we propose a 1D-EBM with space-dependent radiation balance with local bistability in the outgoing radiation term. The new term does not lead to the addition of a new bifurcation in the model, even if results in a non-linear change in the global mean temperature w.r.t. CO₂ concentration, in comparison with a linear increase in the case of the non-space dependent emitted radiation case. However, by adding a noise component to the model, we detect an increase of fluctuations over time for those values of CO₂ concentration in which the non-linear behaviour of GMT is triggered. We connect the increase in fluctuations over time, that we denote *time variance*, to a local (in space) notion of *relaxation time*. The latter indicator in a sense gives information about the local stability of a space point for, in our case, a global stable temperature configuration.

The main characteristics of a 1D-EBM are that the temperature $u = u(x, t)$, depending on time t and space $x = \sin(\phi)$, where $\phi \in [-\pi/2, \pi/2]$ denotes latitude, are that it evolves according to the diffusion of heat, and the planet energy balance ([12, 77, 40, 14]). Our model, which is an extension of the one considered in [24], assumes that the temperature u satisfies the non-linear parabolic partial differential equation

$$\begin{aligned} C_T \partial_t u &= \partial_x (\kappa(x) u_x) + R_a(x, u) - R_e(x, u; q), \quad x \in [-1, 1], t \geq 0 \\ u(x, 0) &= u_0(x), \quad x \in [-1, 1], \\ u_x(-1, t) &= u_x(1, t) = 0, \quad t \geq 0. \end{aligned} \tag{2.7}$$

The heat capacity $C_T = 5 \cdot 10^{-7} \text{ J K}^{-1} \text{ m}^{-2}$ is considered uniform over the whole planet, which we assume is an all-land planet, as the one presented at the beginning of Section 2.2. The PDE is a reaction-diffusion type ([82, 78]). Classical results can be used to prove the global existence and uniqueness of the solution, given a regular initial condition ([82]). Further, it can be proved that $[0, +\infty)$ is an invariant region in the sense of [78], as pointed out in [24]. In the following, we are going to describe the terms governing its time evolution, while the values of the constants appearing in the parametrisations can be found in Table 2.1.

In scientific modelling, heat diffusion is often depicted assuming the planet as a thin shell. This leads to a non-constant diffusion coefficient of the form $\kappa(x) = D \cdot (1 - x^2)$, with $D > 0$, where the term $1 - x^2$ arises due

to the spherical setting ([72]). However, this choice introduces difficulties for the mathematical treatment, resulting in degenerate problems ([35, 15]). For instance, proving the existence of steady-state solutions requires the use of weighted Sobolev spaces. To address this issue, we introduce a simplifying perturbation that removes the singularity at the border ([24]). We consider the diffusion function given by:

$$\kappa(x) = D \cdot (1 - x^2) + \delta(x),$$

with $D = 0.3$ and $\delta \in C^\infty(-1, 1)$, $\delta(x) = 0$ if $|x| \leq \eta$, δ even and non-decreasing in $(0, 1)$. The radiation absorbed by the planet, denoted as R_a , is the product of a spatially dependent solar radiation function $Q_0(x) = \hat{Q}_0 \cdot (1 - x^2)$, where $\hat{Q}_0 > 0$, and a temperature-dependent co-albedo $\beta = \beta(u)$. The co-albedo $\beta(u) = 1 - \alpha(u)$, where α is parametrised by a smooth, non-increasing, bounded function ([6, 24])

$$\alpha(u) = \alpha_1 + \frac{\alpha_2 - \alpha_1}{2} \cdot [1 + \tanh(K \cdot (u - u_{ref}))], \quad (2.8)$$

with $0 < \alpha_1 < \alpha_2 < 1$, α_1 denotes ice albedo, α_2 denotes water albedo, $u_{ref} = 275$ K, and K is a parametrisation constant.

Third, we describe the modelling of the radiation emitted R_e , which is the main innovation of our model. Local bistability in the Outgoing Longwave Radiation (OLR) may arise in tropical regions due to a positive feedback loop involving surface temperature and moisture. This feedback, above a threshold of sea level pressure and GHG concentration, causes the atmosphere to become optically thick, thus reducing OLR ([27]).

To model this effect, we choose a space-dependent, latitude-symmetric Outgoing Longwave Radiation (OLR) of the form:

$$R_e(x, u; q) = q + |x| R_e^{pl}(u) + (1 - |x|) R_e^{eq}(u), \quad (2.9)$$

where R_e^{pl} and R_e^{eq} denote respectively the OLR at the pole and the equator. The convex combination between R_e^{pl} and R_e^{eq} Figure 6 shows the space-dependent OLR R_e , using different colours to represent distinct latitude points. We define them as:

$$R_e^{pl}(u) = \varepsilon_0^{pl} \sigma_0 u |u|^3, \quad (2.10)$$

where ε_0 is the emissivity constant, σ_0 is the Stefan-Boltzmann constant. On the other hand, at the poles, we reproduce the super-greenhouse effect by considering:

$$R_e^{eq}(u) = R_e^{pl}(u)g(u) + (1 - g(u))\varepsilon_0^{eq} \sigma_0 u |u|^3, \quad (2.11)$$

where g is a smooth transition function of the form

$$g(u) = \frac{1}{1 + e^{(u - u_{ref}^{SGE})K^{SGE}}},$$

where $u_{ref}^{SGE} = 303.2$ K and $K^{SGE} = 0.36$ are respectively a reference temperature and a constant in the transition velocity involved in the SGE parametrisation. Further, $\varepsilon_0^{eq} < \varepsilon_0^{pl}$ is an emissivity constant at the equator taking into account the OLR reduction due to the SGE. Note that the OLR at the poles and at the equator in Eq. (2.10)-(2.11) has been defined, just for mathematical convenience, in the physical meaningless range of negative Kelvin temperature.

Lastly, the additive positive parameter q models the effect of CO₂ concentration on the energy budget ([66, 6]). A higher q leads to lower radiation emitted back to space from the surface. We emphasise the reason behind considering a constant value for the CO₂ parameter q . Greenhouse gas concentration can be regarded as constant at a macroweather, i.e., monthly, timescale, by avoiding seasonality insertion since it evolves on a much larger timescale. For instance, the CO₂ concentration has increased by around 47% from 1850 to 2020, moving from 284 parts per million (ppm) to 412 ppm ([73]). In a first approximation, we assume that the spatial distribution of greenhouse gases is uniform over the globe. This assumption, although no longer the state of the art, was widespread at the turn of the century and is based on the well-mixing property of GHG. This means that since most GHGs, such as CO₂, have a large lifetime, many studies have been conducted using global average values for the spatial distribution ([65, 66, 45]).

Symbol	Meaning	Value
D	Diffusivity constant	0.45
\hat{Q}_0	Mean solar radiation	341.3 W m ⁻²
ε_0^{pl}	Emissivity at the poles	0.61
ε_0^{eq}	Emissivity at the equator	0.478
σ_0	Boltzmann's constant	$5.67 \cdot 10^{-8}$ W m ⁻² K ⁻¹
α_1	Ice albedo	0.7
α_2	Water albedo	0.289
K	Constant rate - albedo parametrisation	0.1
K^{SGE}	Constant rate - SGE parametrisation	0.1
u_{ref}	Reference temperature - albedo parametrisation	273 K
u_{ref}^{SGE}	Reference temperature - SGE parametrisation	303.2 K
C_T	Heat capacity	$5 \cdot 10^7$ J m ⁻² K ⁻¹

Table 2.1: Parameters and constants appearing in the 1D-EBM (2.7).

2.2.3 Deterministic properties of the model

In this section, we describe the deterministic properties of our model, as the number of steady-state solutions and their stability. The new feature of our model is the rise of a strong non-linear increase of GMT with respect to the greenhouse parameter q , in the proximity of the model configuration describing the actual climate of the Earth.

In general, in dynamical system theory, huge information is given by the study of the steady-state solutions of the model, which are, in a sense, the long-time behaviour solutions. More specifically, in our model these solutions consist of the non-negative solutions $u = u(x)$ of the following elliptic PDE:

$$\begin{aligned} 0 &= (\kappa(x)u')' + R_a(x, u) - R_e(x, u; q), \\ 0 &= u'(-1) = u'(1). \end{aligned} \quad (2.12)$$

A common way to prove the existence of at least one stable steady-state solution involves a variational approach by studying the minimization problem

$$\inf \left\{ F_q(u) \mid u \in H^{1,2}(-1, 1), u \geq 0 \right\}, \quad (2.13)$$

where:

$$F_q(u) = \int_{-1}^1 \mathcal{R}(x, u(x)) dx + \frac{1}{2} \int_{-1}^1 \kappa(x) [u'(x)]^2 dx, \quad (2.14)$$

with $\partial_u \mathcal{R} = R_e - R_a$ and $H^{1,2}(-1, 1)$ denoting the Sobolev space of order 1 and exponent 2 ([67, 71, 68, 11]). Applying the results from [24, Theorem 1 and Theorem 3], it is possible to gain information about the existence and uniqueness of a steady-state solution.

Proposition 42. *(i) There exists an unique minimiser $\hat{u} \in C^\infty([-1, 1])$ of the variational problem (2.13). Further, \hat{u} solves the elliptic problem (2.12) and it is stable for the dynamics of the 1D-EBM (2.7).*

(ii) The map $q \mapsto \frac{1}{2} \int_{-1}^1 \hat{u}(x) ds$ is non-decreasing.

Note how the second part of the previous result gives qualitative information on the behaviour of the GMT. Furthermore, if the diffusion coefficient is sufficiently large and the 0D-EBM, obtained by removing the diffusion term and averaging in space the radiation balance, is bistable, it can be rigorously proven the existence of a second stable steady-state solution and a third unstable one ([24]).

Given the non-linear nature of the problem, a rigorous demonstration of all properties of the model is not always possible. In this case, the problem can be overcome by using numerical simulations. In particular, for each fixed q , we numerically simulated the solutions of Eq. (2.12). As q varies, we obtained, according to the large literature on this kind of model, that there can be either 1 or 3 stationary solutions. In the former case, the solution is stable. In the latter case, two solutions are stable, one describing a "snowball" configuration u_S for Earth's temperature with ice all over its surface. The other describes a warm climate u_W , similar to the one in which we are living. Additionally, an unstable solution u_M , whose average global mean temperature (GMT) lies between the GMT of u_S and u_W also arises.

See Figure 2.1a for a graphical representation of the steady-state solutions in the bistable case.

In general, proving theoretically the results for such kinds of models is non-trivial due to the presence of non-linear terms in the energy budget parametrisation. The bifurcation diagram of the model in the (q, \bar{u}_*) plane, where u_* denotes a solution of the elliptic PDE, and $\bar{u}_* = \frac{1}{2} \int_{-1}^1 u_*(x) dx$ is its GMT, is depicted in Figure 2.1b. We highlight how the addition of a space-dependent OLR with tropics bistability does not introduce a new bifurcation. Thus, no new steady-state solutions are added or the stability of the already existing ones is altered. However, as highlighted in Figure 2.1c, a strong non-linear behaviour of the GMT for the warm solution u_W appears for the value of q in the neighbourhood of $q \approx 11.3$, a thing that does not happen if we remove the bistability in R_e ([24]). We aim to focus on that phenomenon, when a noise component, describing the weather effect, is added to the model. This is the main topic of Sections 2.2.4-2.2.5.

2.2.4 Stochastic properties of the model

As discussed in the previous paragraphs, the EBM presented in this work corresponds to a macroweather timescale. However, as far as it has been introduced, it lacks in taking into account the effect of fast components of Earth's system, such as atmospheric pressure, wind, and precipitation. In literature, this has been achieved elementary by adding a stochastic term, such as white noise, to the radiation budget ([44, 49, 32, 31]). Note that this addition is necessary to describe the increase in the frequency of rare events. In fact, while a deterministic EBM is useful for obtaining information on global mean temperature, it is not able to investigate fluctuations around it due to all phenomena, such as weather, not included in the radiation balance of the model.

We consider $H = L^2(-1, 1)$ and the stochastic EBM given by:

$$\begin{aligned} du_t &= [Au_t + R(x, u_t)] dt + \sigma dW_t, \\ u|_{t=0} &= u_0 \end{aligned} \tag{2.15}$$

where $(W_t)_t$ denotes a cylindrical Wiener process on H , $u_0 \in H$ is a non-negative initial condition and $A : D(A) \rightarrow L^2(-1, 1)$ is the operator

$$\begin{aligned} D(A) &= \left\{ u \in H^2(-1, 1) \mid u'(-1) = u'(1) = 0 \right\} \\ Au &= (\kappa(x)u')'. \end{aligned} \tag{2.16}$$

We would like to apply the invariant measure theory for gradient systems to deduce the existence, and uniqueness of an invariant measure and its explicit formula. This can not be applied to the operator A since it is invertible on $L^2(-1, 1)$. For this reason, we consider the operator

$$\tilde{A} = \lambda Id - A, \tag{2.17}$$

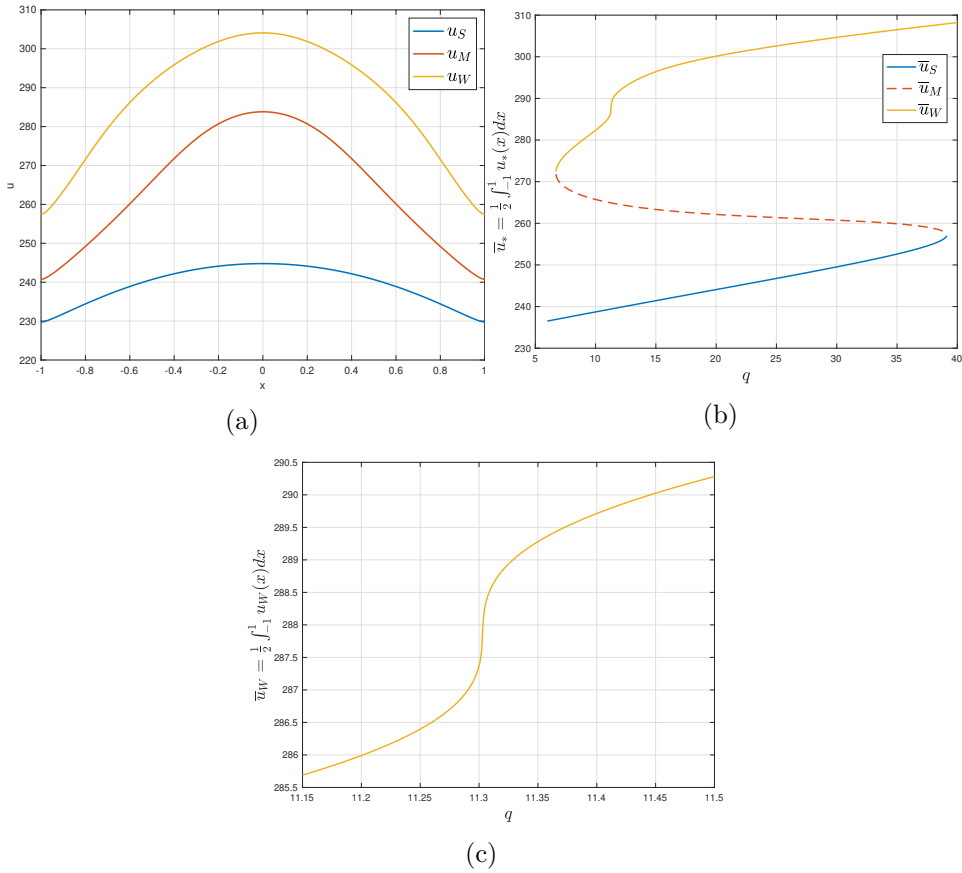


Figure 2.1: (a) Steady-state solutions for the 1D-EBM (2.7) for $q = 11.3$. Solid lines denote stable solutions, dotted lines denote unstable solutions. The snowball solution u_S is plotted in blue, the middle solution u_M in red, and the warm solution u_W in yellow. (b) Bifurcation diagram in the (q, \bar{u}_*) plan for the 1D-EBM (2.7), where u_* denotes a steady-state solutions and $\bar{u}_* = \frac{1}{2} \int_{-1}^1 u_*(x) dx$ is its global mean temperature (GMT). The S-shaped bifurcation diagram is characterised by the two classical saddle-node bifurcations around $q \approx 7$ and $q \approx 38$, and a non-linear (with respect to q) increase in GMT around $q \approx 22$. (c) Zoom of the bifurcation diagram around $q \approx 11.3$ and u_W .

where $\lambda > 0$ is a positive constant. By exploiting the Sturm-Liouville theory, it can be proved that $-\tilde{A}$ is a self-adjoint, negative definite operator, with eigenvalue $0 < \lambda_1 < \lambda_2 < \dots$, such that the trace of $Tr \left[(-\tilde{A})^{\beta-1} \right] < +\infty$, for some $\beta \in (0, 1)$. See Appendix 2.3.2 for a sketch of the proof of these facts. In this way, it is possible to deduce the following result ([21, 22, 24]).

Proposition 43. *Let $E = C([-1, 1])$. Then, there exists a unique \mathbb{P} -a.s. E -valued mild solution of the SPDE (2.15). Further, there exists a unique Gibbs invariant measure $\tilde{\nu}$, and $\tilde{\nu} \ll \tilde{\mu}$ with explicit formula*

$$\tilde{\nu}(du) = \frac{1}{Z} \exp\left(-\frac{2}{\sigma^2} \tilde{I}(u)\right) \tilde{\mu}(du), \quad (2.18)$$

where $\tilde{\mu} \sim \mathcal{N}\left(0, -\frac{\sigma^2}{2} \tilde{A}^{-1}\right)$ and

$$\tilde{I}_q(u) = \int_{-1}^1 \mathcal{R}(x, u(x)) dx - \frac{\lambda}{2} \|u\|_2^2.$$

We remark that the invariant measure $\tilde{\nu}$ is the object, in our context of stochastic EBM, that in Section 2.1.5 has been taken as the definition of climate. Then, it is worth pointing out the link between the invariant measure $\tilde{\nu}$ and the functional F_q building up the variational problem (2.13). Indeed, at least formally, we can write the Gaussian measure $\tilde{\mu}$ as

$$\tilde{\mu}(du) = \frac{1}{Z_1} \exp\left(-\frac{1}{2} \langle \mathcal{Q}^{-1}u, u \rangle\right) "du",$$

where Z_1 is a normalization constant, $\mathcal{Q} = -\frac{\sigma^2}{2} \tilde{A}^{-1}$ is the covariance operator of $\tilde{\mu}$, $\langle \cdot, \cdot \rangle$ denotes the scalar product on $H = L^2(-1, 1)$ and "du" is the formal notation for the Lebesgue measure on H . By an integration of parts, we deduce

$$-\frac{1}{2} \langle \mathcal{Q}^{-1}u, u \rangle = -\frac{2}{\sigma^2} \left(\frac{\lambda}{2} \|u\|_2^2 - \frac{1}{2} \langle \kappa(x)u', u' \rangle \right).$$

Hence, substituting back the formal expression for $\tilde{\mu}$ in Eq. (2.18), we conclude

$$\tilde{\nu}(du) \propto \exp\left(-\frac{2}{\sigma^2} F_q(u)\right) "du".$$

From this expression, we can deduce two important facts. First, the invariant measure of the stochastic EBM is concentrated on the global minimum points of the functional F_q . Second, the study of $\tilde{\nu}$ and its spread depending on q is as difficult as understanding how the functional F_q changes. For this reason, in Section 2.2.5, we will use numerical simulation to investigate how $\tilde{\nu}$ changes, depending on the adiabatic parameter q , as the CO_2 lies in the critical interval in Figure 2.1c.

2.2.5 Variance and extreme weather events increase

It is widely acknowledged that greenhouse gas emissions from human activities have led to more frequent and intense weather and climate extremes

since the pre-industrial era, particularly temperature extremes ([73]). Despite numerous definitions proposed to assess what constitutes an extreme event, there is currently no universally accepted definition ([79]). One commonly used definition considers an extreme weather event as one that exceeds a predefined threshold for a climate variable.

As it is well understood that such occurrences become more likely as the variance of that climate variable increases, we consider the time variance as a proxy indicator of extreme weather events for our EBM setting. As explained in Section 2.2.4, an explicit formula for the invariant measure of the stochastic EBM (2.4) exists. However, due to the presence of a non-linear term inside the Gibbs factor in Eq. (2.18), obtaining theoretical information is challenging. Thus, we rely on numerical simulations to capture the behaviour of the variance.

Specifically, given a fixed value of $q > 0$ and the warm steady-state solution $u_W = u_W^{(q)}$, we numerically integrate the stochastic PDE:

$$\begin{aligned} C_T \partial_t u &= \partial_x (\kappa(x) u_x) + R_a(x, u) - R_e(x, u; q) \\ &\quad + \sigma dW_t, \quad (x, t) \in [-1, 1] \times [0, T], \\ u(x, 0) &= u_W(x), \quad x \in [-1, 1], \\ u_x(-1, t) &= u_x(1, t) = 0, \quad t \in [0, T]. \end{aligned} \tag{2.19}$$

The simulation runs for $T = 500$ years to capture the properties of the invariant measure around the warm climate u_W , and we chose a noise intensity $\sigma = 0.2$. The finite difference method applied to simulate the equation is detailed in Appendix 2.3.1. Here, we describe what we mean by variance, its properties detected by numerical experiments, and our observations.

Given a space point $x \in [-1, 1]$ and a realization $\omega \mapsto u(\omega)$ of the solution of the Eq. (2.19), we consider the variance of the process $t \mapsto u_t(x, \omega) = u(x, t)$. We denote the numerical approximation of the solution by $U = (u_{ij})_{ij}$, where $u_{ij} = u(x_i, t_j)$, and $(x_i)_{i=1, \dots, n}$ and $(t_j)_{j=1, \dots, m}$ represent the spatial and temporal meshes, respectively, over the domain $[-1, 1]$ and $[0, T]$. The time-variance is calculated as

$$\sigma_t^2(x_i) = \frac{1}{m} \sum_{j=1}^m (u_{ij} - \bar{u}_i)^2,$$

where $\bar{u}_i = \frac{1}{m} \sum_{j=1}^m u_{ij}$. Figure 8a illustrates the time-variance indicator, with different colours representing different values of the parameter q .

We observe two distinct behaviours of the variance. First, depending on q , there is an increase in σ_t^2 , peaking at $q = 11.3069$, followed by a decrease. This peak corresponds to the q value that results in the largest increase in GMT, as shown in Figure 2.1c. Second, as expected, for a given value of q , the spatial profile of σ_t^2 is symmetric with respect to $x = 0$. Additionally, three local maximum points emerge one at $x = 0$ and the others at $|x| \approx 0.8$.

Our interpretation is that σ_t^2 identifies the highest fluctuating regions as those where the freezing water temperature is crossed (sub-arctic regions, $|x| = 0.8$), or where the SGE triggers bistability (tropical areas, $x = 0$).

To support this interpretation, it is useful to introduce the local stability indicator

$$\gamma(x) = \partial_u R(x, u_W(x)),$$

where $R(x, u) = R_a(x, u) - R_e(x, u; q)$. If the model were a simple Ordinary Differential Equation (ODE) without the coupling diffusion term, $\gamma(x)$ would be, up to a positive constant depending on C_T , the eigenvalue obtained by linearizing the reaction term around the stable steady-state temperature $u_W(x)$. Positive values of $\gamma(x)$ indicate local instability, while negative values indicate stability if the diffusion term is removed. Figure 8b presents the local stability indicator γ , with colours denoting different values of the parameter q . Notably, there is a clear relationship between time-variance and the local stability indicator: regions with high time-variance σ_t^2 coincide with areas of positive γ . This explains the spatial profile of σ_t^2 for a fixed value of q .

The reason for $\gamma(x) > 0$ at some points is due to the presence of the diffusion term. If $\kappa \equiv 0$, then u_W is not a minimiser of F_q , but instead solves the problem

$$u_W(x) = \arg \min_{u \geq 0} \mathcal{R}(x, u), \quad (2.20)$$

where $\partial_u \mathcal{R} = R_e - R_a$. Here, $\partial_u \mathcal{R}|_{(x, u_W(x))} = 0$, and since $u_W(x)$ is a minimum point, it follows $\partial_u^2 \mathcal{R}|_{(x, u_W(x))} = \partial_u R|_{(x, u_W(x))} \leq 0$. But with $\kappa(x) > 0$, $u_W(x)$ no longer satisfies Eq. (2.20), but instead is a minimiser of F_q , where the diffusion term appears in the second term on the right-hand side of Eq. (2.14). This term, which intuitively minimises the temperature gradient, allows for some points to fluctuate around a mean value that would be unstable if $\kappa \equiv 0$.

To understand why, given $x \in [-1, 1]$, the map $q \mapsto \sigma_t^2(x) = \sigma_t^{2,(q)}(x)$ increases until around $q = 11.3069$ and then decreases, we offer the following explanation. As q increases, the temperature $u_W(x)$ of the warm climate increases, as can be checked by numerical simulations and partially understandable from Proposition 42. This leads the temperature, especially in the tropical area, to approach the region where instability due to the SGE arises. Once the tropical temperature surpasses this region, the instability, and thus the variance, decreases. We support our statements as follows.

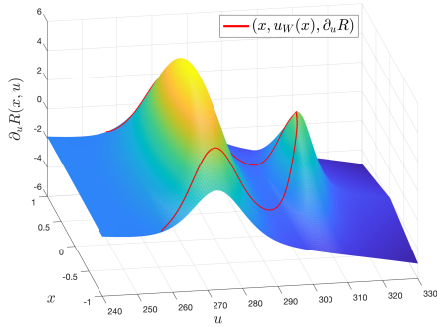
- (i) Figure 2.2 shows how the steady-state solution $u_W^{(q)}$ approaches unstable areas, defined by points (x, u) where $\partial_u R(x, u) > 0$. For $q_1 = 11.21$, $q_2 = 11.28$, and $q_3 = 11.4$, the map $(x, u) \mapsto \partial_u R(x, u_W(x))$ is presented, with the curve $x \mapsto (x, u_W(x), \partial_u R(x, u_W(x)))$ depicted in red. When the time variance peaks (i.e., $q = q_2$), the steady-state solution

values around the equator are close to the local maximum of $\partial_u R$, approximately close to $(x_M, u_M) = (0, 305)$. For $q = q_1$ and $q = q_3$, the equatorial steady-state value is smaller and larger than u_M , respectively.

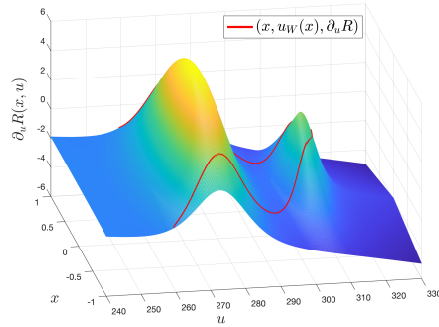
(ii) We consider the local mean stability indicator

$$\bar{\gamma}(q) = \int_{-1}^1 \gamma(x) dx = \int_{-1}^1 \partial_u R(x, u_W^{(q)}(x)) dx.$$

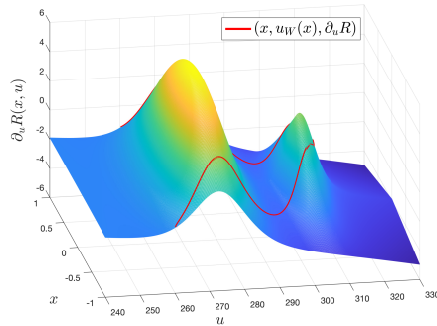
Its plot is shown in Figure 2.3a. Although providing only average information, it exhibits behaviour qualitatively similar to that of σ_t^2 for each fixed value of x , peaking at $q = 11.3069$.



(a) $q = 11.21$



(b) $q = 11.29$



(c) $q = 11.4$

Figure 2.2: Plot of the map $(x, u) \mapsto \partial_u R(x, u)$ and the curve $x \mapsto (x, u_W(x), \partial_u R(x, u_W^{(q)}(x)))$ in red, for different values of q .

Finally, we show the distribution of the solution $u(x, t)$ of the stochastic 1D-EBM (2.4) for the fixed space point $x = 0.6$ (similar results are observed for different space points). Figure 2.3b shows the distribution as a histogram,

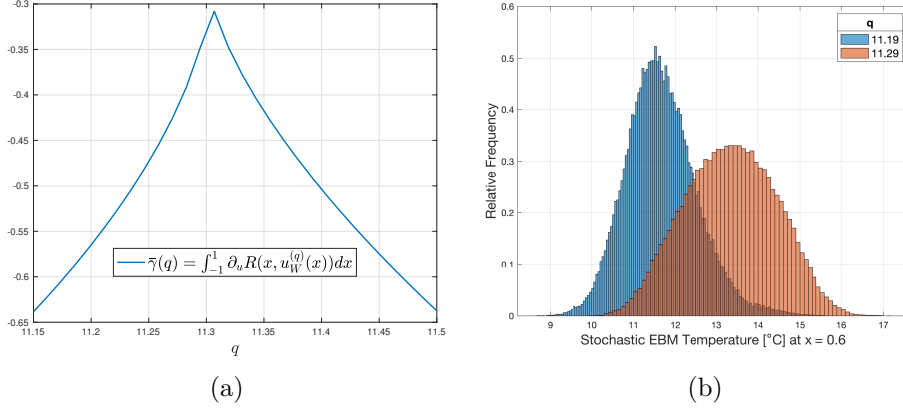


Figure 2.3: (a) Average local stability indicator $\bar{\gamma}(q) = \int_{-1}^1 \partial_u R(x, u_W^{(q)}(x)) dx$. It increases, peaks at $q = 11.3069$, and then decreases. (b) Histogram of the distribution of the solution of $t \mapsto u(\bar{x}, t)$ for the stochastic EBM (2.19) for $q = 11.19$ (blue) and $q = 11.29$ (red), at $\bar{x} = 0.6$.

comparing two distinct values of q . Blue depicts the results for $q = 11.2$, while red shows $q = 11.3$. From the plot, we deduce that our model captures the shift in the mean value and the increase in variance, correlating with the IPCC schematic climate change reproduction in Figure 4 and weather observations in Modena in Figure 5a.

2.3 Supplement information

2.3.1 Numerical methods

In this section, we describe the numerical method adopted to approximate the solutions of the stochastic PDE (2.19). We used an implicit Euler-Maruyama method, which is a small modification of the semi-implicit Euler-Maruyama method presented in [60, Section 10.5].

First, it is worth recalling that the numerical experiments presented in Section 2.2.5 are all performed for a fixed value of q , and using $u_W = u_W^{(q)}$ as initial condition of the parabolic stochastic problem (2.19). The constant q value is chosen from a mesh of the form

$$q_k = 11.15 + \frac{k}{\Delta q}, \quad \Delta q = \frac{11.55 - 11.15}{29} \approx 1.21 \cdot 10^{-2}, \quad k = 0, \dots, 29.$$

The steady-state solution u_W solves the elliptic problem (2.12). To numerically approximate it, we have applied the same finite difference scheme described in [24, Appendix A].

Second, we move to describe the numerical method for the parabolic problem. We denote by $R(x, u; q) = R_a(x, u) - R_e(x, u; q)$ the non-linear radiation budget, and the underline notation to denote a vector (e.g. $\underline{y} \in \mathbb{R}^4$). We consider two uniform meshes for the spatial domain $[-1, 1]$ and the time domain $[0, T]$, i.e.

$$x_i = -1 + i\Delta x, \quad i = 0, \dots, n, \quad \Delta x = \frac{2}{n},$$

and

$$t_j = j\Delta t, \quad j = 0, \dots, m, \quad \Delta t = \frac{T}{m} = \frac{500}{m}.$$

The number of points in the space and time mesh, respectively $n + 1$ and $m + 1$, are chosen in a way that $\Delta x = \Delta x = 0.01$. Then, the solution to the problem can be approximated by considering the system

$$\begin{aligned} C_T \frac{u_{i,j+1} - u_{i,j}}{\Delta t} &= \frac{u_{i-1,j+1}\kappa_{i-\frac{1}{2}} - u_{i,j+1}(\kappa_{i-\frac{1}{2}} + \kappa_{i+\frac{1}{2}}) + u_{i+1,j+1}\kappa_{i+\frac{1}{2}}}{\Delta x^2} \\ &+ R(x_i, u_{i,j+1}) + \sqrt{\frac{\Delta t}{\Delta x}} \sigma z_{i,j} \quad 0 \leq i \leq n, \quad 0 \leq j \leq m-1, \\ 0 &= \frac{u_{n+1,j} - u_{n-1,j}}{2\Delta x} = \frac{u_{1,j} - u_{-1,j}}{2\Delta x} \quad j = 1, \dots, m, \\ u_{i,0} &= u_W(x_i), \quad i = 0, \dots, n, \end{aligned}$$

where $u_{-1,j}, u_{n+1,j}$ are ghost points, $(z_{i,j})_{i,j}$ is a collection of independent identically distributed (i.i.d.) normal random variables, and $u_{i,j} = u(x_i, t_j)$, $\kappa_{i\pm\frac{1}{2}} = \kappa(x_{i\pm\frac{1}{2}})$, $x_{i\pm\frac{1}{2}} = x_i \pm \Delta x/2$. Since $u_{1,j} = u_{-1,j}$ and $u_{n+1,j} = u_{n-1,j}$, the previous system of equation can be rewritten as

$$(I_{n+1} - rA) \underline{u}^{j+1} = I_{n+1} \underline{u}^j + \frac{\Delta T}{C_T} R(\underline{u}^{j+1}) + \sqrt{\frac{\Delta t}{\Delta x}} \sigma \underline{Z}^j,$$

where I_{n+1} denotes the $(n+1) \times (n+1)$ identity matrix, $\underline{u}^j = (u_{0,j}, \dots, u_{n,j})^T$, $r = \frac{\Delta t}{C_T \Delta x^2}$, $R(\underline{y}) = (R(x_0, y_1), \dots, R(x_n, y_{n+1}))^T$, $(\underline{Z}^j)_j$ denotes a set of i.i.d. $\mathcal{N}(\underline{0}, I_{n+1})$ normal random vectors, and $A \in \mathbb{R}^{(n+1) \times (n+1)}$ is the tridiagonal matrix with diagonal $\underline{d} \in \mathbb{R}^{n+1}$, superdiagonal $\underline{d}_1 \in \mathbb{R}^n$, and subdi-

agonal $\underline{d}_{-1} \in \mathbb{R}^n$ given by

$$\begin{aligned} \underline{d}(i) &= \begin{cases} -(\kappa_{-1/2} + \kappa_{1/2}), & i = 1, \\ -(\kappa_{i-3/2} + \kappa_{i-1/2}), & i = 2, \dots, n, \\ -(\kappa_{n-1/2} + \kappa_{n+1/2}), & i = n+1, \end{cases} \\ \underline{d}_1(i) &= \begin{cases} \kappa_{-1/2} + \kappa_{1/2}, & i = 1, \\ \kappa_{i-1/2}, & i = 2, \dots, n, \end{cases} \\ \underline{d}_{-1}(i) &= \begin{cases} \kappa_{i-1/2} + \kappa_{1/2}, & i = 1, \dots, n, \\ -(\kappa_{n-1/2} + \kappa_{n+1/2}), & i = n. \end{cases} \end{aligned}$$

Thus, given the numerical approximation \underline{u}^j at time t_j , to advance the scheme at time t_{j+1} it is needed to solve the previous non-linear system of algebraic equations. To do this, we apply the Newton-Raphson Method (NRM), which we recall in the following. We consider the map $\underline{F}^j: \mathbb{R}^{n+1} \rightarrow \mathbb{R}^{n+1}$ defined as

$$\underline{F}^j(\underline{y}) = (I_{n+1} - rA)\underline{y} - \underline{u}^j - \frac{\Delta T}{C_T} R(\underline{y}) - \sqrt{\frac{\Delta t}{\Delta x}} \sigma \underline{Z}^j.$$

To approximate the vector $\underline{y} \in \mathbb{R}^{n+1}$ such that $\underline{F}^j(\underline{y}) = 0$, the NRM consider the following sequence

$$\begin{cases} \underline{y}^{k+1} &= \underline{y}^k - J_{F^j}(\underline{y}^k)^{-1} F^j(\underline{y}^k), \\ \underline{y}^0 &= \underline{u}^j, \end{cases}$$

where $J_{F^j} \in \mathbb{R}^{(n+1) \times (n+1)}$ is the Jacobian matrix of \underline{F}^j with respect to \underline{y} . Since the noise intensity $\sigma = 0.2$ is small, we expect that the choice $\underline{y}^0 = \underline{u}^j$ is a good initial guess of the solution. The iteration of the NRM are stopped when $\|\underline{F}^j(\underline{y}^k)\| \leq 10^{-10}$.

2.3.2 Spectral properties of the operator \tilde{A}

To apply the invariant measure theory, the operator $\tilde{A} = \lambda Id - A$ defined in Section 2.2.4 should satisfy the following assumptions (see [21, Section 11]):

- (i) \tilde{A} is self-adjoint and there exists $\omega > 0$ such that

$$\langle \tilde{A}x, x \rangle \leq -\omega|x|^2, \quad x \in D(A).$$

- (ii) There exists $\beta \in (0, 1)$ such that $Tr [(-\tilde{A})^{\beta-1}] < +\infty$.

We denote by $(\lambda_n)_n$ the eigenvalues of $-A$, where

$$\begin{aligned} D(A) &= \left\{ u \in H^2(-1, 1) \mid u'(-1) = u'(1) = 0 \right\} \\ Au &= (\kappa(x)u')'. \end{aligned} \quad (2.21)$$

Since A is a Sturm-Liouville regular operator, classical results assure the existence of the real eigenvalues λ_n , and furthermore, it can be proved

$$\lambda_1 < \lambda_2 < \dots < \lambda_n < \dots \rightarrow +\infty.$$

First, to check hypothesis (i) it is thus sufficient to prove that

$$\lambda_n \geq 0, \quad \forall n.$$

Indeed, by definition of eigenvalue, there exists an eigenfunction $v_n \in D(A)$ such that

$$Av_n = -\lambda_n v_n.$$

Multiplying the previous identity by v_n and integrating over the domain $[-1, 1]$, we get

$$\int_{-1}^1 [\kappa(x)v_n'(x)]' v_n(x) dx = -\lambda_n \int_{-1}^1 v_n(x)^2 dx.$$

Performing an integration by parts on the left-hand side, we deduce

$$- \int_{-1}^1 \kappa(x) (v_n'(x))^2 dx = -\lambda_n \int_{-1}^1 v_n(x)^2 dx.$$

In conclusion,

$$\lambda_n = \frac{\int_{-1}^1 \kappa(x) (v_n'(x))^2 dx}{\int_{-1}^1 v_n(x)^2 dx},$$

and our claim follows from the fact that $\kappa(x) > 0$ on $[-1, 1]$.

Second, the hypothesis (ii) is a consequence of the following asymptotic estimate for regular Sturm-Liouville problems ([37, Section 4]): there exist $B > 0$ and $n_0 > 0$ such that

$$\left[\frac{\left(n - \frac{1}{2}\right) \pi}{B} \right]^2 < \lambda_n < \left[\frac{\left(n + \frac{1}{2}\right) \pi}{B} \right]^2, \quad \forall n \geq n_0.$$

Chapter 3

Energy balance models from Hasselmann's perspective

The following chapter, which is based on an ongoing research, contains the proofs of the results presented in Section 0.4, whose main aim is to derive using a Wong-Zakai approach a closed equation for the fast-slow system (19). The resulting closed equation for macroweather is what we call *Hasselmann's equation*, since correspond to the equation, in our EBM setting, claimed by Hasselmann in [44].

The first result, that we restate, we need to prove is the one that give use the possibility to obtain a closed equation for Y_t from (19). Indeed, it state a limiting result for the fast process $(X_t)_t$, solution of (19), when the scaling parameter τ goes to 0.

Lemma 5. *For each $t > 0$, it holds*

$$\lim_{\tau \rightarrow 0} \mathbb{E} \left| \frac{1}{\sqrt{\tau}} \int_0^t X_s ds - \frac{\bar{Q}t}{\sqrt{\tau}} - W_t \right|^2 = 0.$$

Proof. For the ease of notation, we will denote the fast process as $(X_t)_t$, dropping its dependence on τ . It can be written explicitly as

$$\begin{aligned} X_t &= xe^{-t/\tau} + \frac{1}{\tau} \int_0^t \bar{Q} e^{-(t-s)/\tau} ds + \frac{1}{\sqrt{\tau}} \int_0^t e^{-(t-s)/\tau} dW_s \\ &= xe^{-t/\tau} + \bar{Q} (1 - e^{-t/\tau}) + \frac{1}{\sqrt{\tau}} \int_0^t e^{-(t-s)/\tau} dW_s \\ &= (x - \bar{Q}) e^{-t/\tau} + \bar{Q} + \frac{1}{\sqrt{\tau}} \int_0^t e^{-(t-s)/\tau} dW_s. \end{aligned}$$

Thus, integrating in time, we get

$$\begin{aligned} \int_0^t X_s ds &= \int_0^t \left[(x - \bar{Q}) e^{-s/\tau} + \bar{Q} + \frac{1}{\sqrt{\tau}} \int_0^s e^{-(s-r)/\tau} dW_r \right] ds \\ &= \tau (1 - e^{-t/\tau}) (x - \bar{Q}) + t\bar{Q} + \frac{1}{\sqrt{\tau}} \int_0^t \int_0^s e^{-(s-r)/\tau} dW_r ds. \end{aligned}$$

The last term on the RHS can be computed applying Fubini-Tonelli for stochastic integrals

$$\begin{aligned} \frac{1}{\sqrt{\tau}} \int_0^t \int_0^s e^{-(s-r)/\tau} dW_r ds &= \frac{1}{\sqrt{\tau}} \int_0^t \int_r^t e^{-(s-r)/\tau} ds dW_r \\ &= \sqrt{\tau} \int_0^t \left(1 - e^{-(t-r)/\tau}\right) dW_r \\ &= \sqrt{\tau} \left(W_t - \int_0^t e^{-(t-r)/\tau} dW_r\right). \end{aligned}$$

From the previous computations, we deduce

$$\begin{aligned} \mathbb{E} \left| \frac{1}{\sqrt{\tau}} \int_0^t X_s ds - \frac{\bar{Q}t}{\sqrt{\tau}} - W_t \right|^2 &= \mathbb{E} \left| \sqrt{\tau} \left(1 - e^{-t/\tau}\right) (x - \bar{Q}) - \int_0^t e^{-(t-r)/\tau} dW_r \right|^2 \\ &\leq 2\tau \left(1 - e^{-t/\tau}\right)^2 (x - \bar{Q})^2 + 2\mathbb{E} \left| \int_0^t e^{-(t-r)/\tau} dW_r \right|^2 \\ &= 2\tau \left(1 - e^{-t/\tau}\right)^2 (x - \bar{Q})^2 + 2 \int_0^t \int_0^t e^{-2(t-r)/\tau} dr \\ &= 2\tau \left(1 - e^{-t/\tau}\right)^2 (x - \bar{Q})^2 + 2\tau \left(1 - e^{-2t/\tau}\right). \end{aligned}$$

where the first inequality follows from the Jensen's inequality, and the following inequality by Ito-isometry. Taking the limits in τ , we conclude the proof. \square

Theorem 10 (Averaging Principle). *Let $T > 0$ and denote by $\mu(dx)$ the invariant measure for the fast equation in (19). Let $(\bar{Y}(t))_t$ be the solution of the ODE*

$$\dot{\bar{Y}}(t) = \bar{g}(\bar{Y}), \quad (30)$$

where

$$\bar{g}(y) := \int g(x, y) \mu(dx).$$

Consider $(Y_t^\tau)_t$ solution of the fast-slow system (19). Then, for any $\delta > 0$, it holds

$$\mathbb{P} \left(\sup_{0 \leq t \leq T} |Y_t^\tau - \bar{Y}(t)| > \delta \right) \xrightarrow{\tau \rightarrow 0} 0.$$

Similarly, if $(\tilde{Y}_t)_t$ is the solution of Hasselmann's equation (24), for any $\delta > 0$ it holds

$$\mathbb{P} \left(\sup_{0 \leq t \leq T} |\tilde{Y}_t - \bar{Y}(t)| > \delta \right) \xrightarrow{\tau \rightarrow 0} 0.$$

Proof. We only prove that the averaged drift \bar{g} takes the form

$$\bar{g}(y) = \bar{Q}\beta(y) + q - \varepsilon_0\sigma_0 y^4.$$

In other words, we prove that the averaged equation for the fast-slow system (19) and the Hasselmann's equation (24) are the same. Then, the uniform convergence in probability by the thesis is a consequence of the classical averaging principle (see [36, Chapter 7]).

To find the invariant measure $\mu(dx)$ for the fast component in (19), we consider the solution X^{t_0} of the fast equation starting at time t_0 with initial condition X_{t_0} , i.e., the solution of

$$dX^{t_0} = -\frac{1}{\tau} (X^{t_0} - \bar{Q}) dt + \frac{1}{\sqrt{\tau}} dW_t, \quad X^{t_0}(t_0) = X_{t_0}.$$

For $t_0 = 0$, the solution of this SDE takes the form

$$X^{t_0}(t) = (X_{t_0} - \bar{Q}) e^{-(t-t_0)/\tau} + \bar{Q} + \frac{1}{\sqrt{\tau}} \int_{t_0}^t e^{-(t-s)/\tau} dW_s.$$

Taking $t_0 \rightarrow -\infty$, we obtain the stationary solution of the fast equation:

$$X^{-\infty}(t) = \bar{Q} + \frac{1}{\sqrt{\tau}} \int_{-\infty}^t e^{-(t-s)/\tau} dW_s.$$

The distribution of $X^{-\infty}(t)$ represents the invariant measure μ , which is Gaussian with mean \bar{Q} and variance

$$\begin{aligned} \text{Var}(X^{-\infty}(t)) &= \mathbb{E} \left| \frac{1}{\sqrt{\tau}} \int_{-\infty}^t e^{-(t-s)/\tau} dW_s \right|^2 \\ &= \frac{1}{\tau} \int_{-\infty}^t e^{-2(t-s)/\tau} ds \\ &= \frac{1}{\tau} \left[\frac{\tau}{2} \cdot e^{-2(t-s)/\tau} \right]_{-\infty}^t \\ &= \frac{1}{2}. \end{aligned} \tag{3.1}$$

Thus, we obtain

$$\begin{aligned} \bar{g}(y) &= \int (x\beta(y) + q - \varepsilon_0\sigma_0y^4) \mu(dx) \\ &= \beta(y) \int x \mu(dx) + (q - \varepsilon_0\sigma_0y^4) \int 1 \mu(dx) \\ &= \beta(y)\bar{Q} + q - \varepsilon_0\sigma_0y^4. \end{aligned}$$

In conclusion, applying the averaging principle to our model (19) yields the deterministic 0D-EBM

$$\dot{\bar{Y}} = \bar{g}(\bar{Y}(t)). \tag{3.2}$$

□

Then, we move to provide the ideas of the proofs for the results regarding the fluctuations of \tilde{Y}_t and Y_t^τ .

Proposition 11. *Consider the Gaussian fluctuations for the stochastic Hasselmann's EBM (24)*

$$Z_t^\tau := \frac{\tilde{Y}_t^\tau - Y_t^0}{\sqrt{\tau}} = \frac{\tilde{Y}_t^\tau - \bar{Y}(t)}{\sqrt{\tau}}.$$

Then, denoting by \xrightarrow{d} the convergence in distribution, it holds

$$(Z_t^\tau)_{t \in [0, T]} \xrightarrow[\tau \rightarrow 0]{d} (Z_t)_{t \in [0, T]}$$

where $(Z_t)_{t \in [0, T]}$ solves the SDE

$$\begin{aligned} dZ_t &= \bar{g}'(\tilde{Y}_t^0) Z_t dt + \beta(\tilde{Y}_t^0) dW_t \\ &= \bar{g}'(\bar{Y}(t)) Z_t dt + \beta(\bar{Y}(t)) dW_t. \end{aligned} \quad (31)$$

Proof. The equation satisfied by \tilde{Y}_t^τ , for $\tau \geq 0$, is

$$dY_t^\tau = \bar{g}(\tilde{Y}_t^\tau) dt + \sqrt{\tau} \beta(\tilde{Y}_t^\tau) \circ dW_t = \left(\bar{g}(\tilde{Y}_t^\tau) + \frac{\tau}{2} \beta(\tilde{Y}_t^\tau) \beta'(\tilde{Y}_t^\tau) \right) dt + \sqrt{\tau} \beta(\tilde{Y}_t^\tau) dW_t.$$

Performing a Taylor expansion of the terms \bar{g}, β , we have

$$\begin{aligned} \bar{g}(\tilde{Y}_t^\tau) &= \bar{g}(\tilde{Y}_t^0) + \sqrt{\tau} \bar{g}'(\tilde{Y}_t^0) Z_t^\tau + O(\tau), \\ \beta(\tilde{Y}_t^\tau) &= \beta(\tilde{Y}_t^0) + \sqrt{\tau} \beta'(\tilde{Y}_t^0) Z_t^\tau + O(\tau). \end{aligned}$$

We compute now the differential of the Gaussian fluctuations

$$\begin{aligned} dZ_t^\tau &= \frac{1}{\sqrt{\tau}} (d\tilde{Y}_t^\tau - d\tilde{Y}_t^0) \\ &= \left(\bar{g}'(\tilde{Y}_t^0) Z_t^\tau + \frac{\sqrt{\tau}}{2} \beta(\tilde{Y}_t^\tau) \beta'(\tilde{Y}_t^\tau) + O(\sqrt{\tau}) \right) dt \\ &\quad + \left(\beta(\tilde{Y}_t^0) + \sqrt{\tau} \beta'(\tilde{Y}_t^0) Z_t^\tau + O(\tau) \right) dW_t \end{aligned}$$

Performing the limit $\tau \rightarrow 0$ in the previous equation and ignoring the higher order terms in τ , we get the SDE (11). \square

Proposition 12. *Let $(X_t^\tau, Y_t^\tau)_{t \in [0, T]}$ be the solution of the fast-slow system (19). Consider the fluctuations processes*

$$\zeta_t^\tau := \frac{Y_t^\tau - \bar{Y}(t)}{\sqrt{\tau}}, \quad \eta_t^\tau = \frac{X_t^\tau - \bar{Q}}{\sqrt{\tau}}.$$

Then, as $\tau \rightarrow 0$, we have

$$\zeta_t^\tau \xrightarrow[\tau \rightarrow 0]{\mathbb{P}} \zeta_t, \quad \forall t \in [0, T],$$

where $(\zeta_t)_t$ is the solution of

$$d\zeta_t = \bar{g}'(\bar{T}(t)) \zeta_t dt + \beta(\bar{T}(t)) dW_t,$$

and $\xrightarrow{\mathbb{P}}$ denotes convergence in probability.

Proof. The fast fluctuations process $(\eta_t^\tau)_t$ satisfies

$$d\eta_t^\tau = -\frac{1}{\tau}\eta_t^\tau dt + \frac{1}{\tau}dW_t.$$

Applying the Wong-Zakai principle from Theorem 8, we get that

$$\eta_t^\tau \xrightarrow[\tau \rightarrow 0]{\mathbb{P}} \widetilde{W}_t, \quad \forall t > 0,$$

where $(\widetilde{W}_t)_t$ is a Brownian motion, for which from now on we will denote again $(W_t)_t$. We introduce the notation $g(x, y) = x\beta(y) - \alpha(y)$, where g is the drift of the slow equation in (19). Then, the fluctuations of the slow process satisfy

$$\begin{aligned} d\zeta_t^\tau &= \frac{1}{\sqrt{\tau}} \left(dY_t^\tau - \dot{\bar{Y}}(t) \right) \\ &= -\frac{1}{\sqrt{\tau}} \left(\alpha(Y_t^\tau) - \alpha(\bar{Y}(t)) \right) + \frac{1}{\sqrt{\tau}} \left(X_t^\tau - \bar{Q} \right) \beta(Y_t^\tau) + \frac{1}{\sqrt{\tau}} \bar{Q} \left(\beta(Y_t) - \beta(\bar{Y}(t)) \right) \\ &= -\alpha'(\bar{Y}(t))\zeta_t^\tau + \beta(Y_t^\tau)\eta_t^\tau + \bar{Q}\beta'(\bar{Y}(t))\zeta_t^\tau + O(\sqrt{\tau}). \end{aligned}$$

Thus, using the convergences $Y_t^\tau \rightarrow \bar{Y}(t)$ and $\eta_t^\tau \rightarrow W_t$, we get the limiting stochastic equation for $\tau \rightarrow 0$ given by

$$\begin{aligned} d\zeta_t &= \left(-\alpha'(\bar{Y}(t)) + \bar{Q}\beta(\bar{Y}(t)) \right) \zeta_t + \beta(\bar{Y}(t))dW_t \\ &= \bar{g}'(\bar{Y}(t))\zeta_t dt + \beta(\bar{Y}(t))dW_t. \end{aligned}$$

In principle, in the previous equation we should have a Stratonovich integral, i.e.

$$d\zeta_t = \bar{g}'(\bar{Y}(t))\zeta_t dt + \beta(\bar{Y}(t)) \circ dW_t.$$

But in the case in which the integrand is deterministic, the Ito integral coincides with the Stratonovich integral. This is the thesis. \square

Lastly, we give the details on how to derive the rate function $I(y(\cdot))$ for the LDP for Hasselmann's equation and our fast-slow model.

Proposition 13. *The solution $(\tilde{Y}_t)_t$ of the Hasselman stochastic EBM*

$$d\tilde{Y}_t = \bar{g}(\tilde{Y}_t)dt + \sqrt{\tau}\beta(\tilde{Y}_t) \circ dW_t$$

satisfies a large deviation principle with rate function

$$I(y(\cdot)) = \frac{1}{2} \int_0^T \left| \frac{1}{\beta(y(t))} [\dot{y}(t) - \bar{g}(y(t))] \right|^2 dt. \quad (32)$$

Proof. The proof follows by considering the SDE in Ito form

$$d\tilde{Y}_t = \left(\bar{g}(\tilde{Y}_t) + \frac{\tau}{2}\beta(\tilde{Y}_t)\beta'(\tilde{Y}_t) \right) dt + \sqrt{\tau}\beta(\tilde{Y}_t)dW_t,$$

and neglecting the term higher order term $\frac{\tau}{2}\beta(\tilde{Y}_t)\beta'(\tilde{Y}_t)$. Then, it is a straightforward application of known results, see [26, Theorem 5.6.7]. \square

We now move to derive a large deviation principle for our fast-slow system. Let X be a metric space, and define

$$C_b(X) = \{f: X \rightarrow \mathbb{R} : f \text{ is continuous and bounded}\}.$$

Let $\{Z_\epsilon\}_\epsilon$ be a family of X -valued random variables with corresponding laws $\{\mu_\epsilon\}_\epsilon$. In what follows, we recall a generalization of the Gärtner-Ellis Theorem for exponentially tight measures¹ (for a detailed discussion, see [26, Theorem 4.4.2]).

Theorem 44. *Suppose the family $\{\mu_\epsilon\}_\epsilon$ is exponentially tight, and that for every $f \in C_b(X)$, the following limit defining Λ_f exists:*

$$\Lambda_f := \lim_{\epsilon \rightarrow 0} \epsilon \log \int_X e^{f(x)/\epsilon} \mu_\epsilon(dx) = \lim_{\epsilon \rightarrow 0} \epsilon \log \mathbb{E} \left[e^{f(Z_\epsilon)/\epsilon} \right].$$

Then, the family $\{\mu_\epsilon\}_\epsilon$ satisfies the LDP with a good rate function given by

$$I(x) = \sup_{f \in C_b(X)} (f(x) - \Lambda_f).$$

Keep in mind that we are not using the exact version of this result or focusing on the specific hypothesis, but we will apply its main idea to get the LDP for our fast-slow model, whose proof is adapted from [10].

Proposition 14. *The slow component Y_t in the fast-slow system (19) satisfies a large deviation principle with the same rate function defined in (32).*

Proof. In this proof, we will focus only on the key steps and main arguments. The detailed computations that link these stages are provided in auxiliary lemmas.

Given two initial conditions x, y , our fast-slow system has the form

$$\begin{cases} dX_t^x = \frac{1}{\tau} f(X_t^x) dt + \frac{1}{\sqrt{\tau}} dW_t, & X_0^x = x, \\ dY_t^{x,y} = g(X_t^x, Y_t^{x,y}) dt, & Y_0^{x,y} = y, \end{cases}$$

with $f(x) = -(x - \bar{Q})$, $g(x, y) = x\beta(y) + q - \epsilon_0\sigma_0 y^4$. Further, we denote by $\mu(dx) \sim \mathcal{N}(\bar{Q}, \frac{1}{2})$ the invariant measure for the fast process. Setting

$$u(t, x, y) := \mathbb{E} [\phi(X_t^x, Y_t^{x,y})],$$

¹A family of probability measures $\{\mu_\epsilon\}_\epsilon$ is *exponentially tight* if, for every $\alpha < \infty$, there exists a compact set $K_\alpha \subset X$ such that

$$\limsup_{\epsilon \rightarrow 0} \epsilon \log \mu_\epsilon(K_\alpha^c) < -\alpha.$$

we have that u satisfies the forward Kolmogorov equation

$$\begin{cases} \partial_t u = g(x, y) \partial_y u + \frac{1}{\tau} f(x) \partial_x u + \frac{1}{2\tau} \Delta_x u, \\ u(0, x, y) = \phi(x, y), \end{cases} \quad (3.3)$$

In particular, we choose the test function ϕ as $\phi(x, y) = \exp\left(\frac{1}{\tau}\psi(y)\right)$, for ψ test function. Indeed, our aim is to detect the large deviation of Y_t away from \bar{Y} , which we expect being exponentially small in τ^{-1} . In other words,

$$u(t, x, y) = \mathbb{E} \left[\exp \left(\frac{1}{\tau} \psi(Y_t^{x,y}) \right) \right]. \quad (3.4)$$

We look for a solution of the Kolmogorov equation of the form

$$u(t, x, y) = w(t, x, y) \exp \left(\frac{1}{\tau} \Lambda(t, x, y) \right). \quad (3.5)$$

Note that, at least heuristically, we have

$$\Lambda(t, x, y) = \lim_{\tau \rightarrow 0} \tau \log \mathbb{E} \left[\exp \left(\frac{1}{\tau} \psi(Y_t^{x,y}) \right) \right].$$

Thus, Λ plays the role of the scaled cumulant generating function of the Gärtner-Ellis Theorem, and for this reason we have used the same notation in Theorem 44.

Plugging the previous ansatz inside the Kolmogorov equation (3.3), we start by equalling the terms with the same order in τ , in order to get more information on Λ . In particular, the terms of order τ^{-3} lead to deduce that Λ is independent on x , hence $\Lambda = \Lambda(t, y)$, see Lemma 45a. In addition to this, observing the terms of order τ^{-1} we deduce two facts. First, Λ satisfies the following Hamilton-Jacobi equation (see Lemma 45b)

$$\begin{cases} \partial_t \Lambda(t, y) = H(y, \partial_y \Lambda), & t > 0, \\ \Lambda(0, y) = \psi(y), \end{cases} \quad (3.6)$$

where H is the Hamiltonian defined by

$$H(y, \theta) := \frac{1}{2} \int_{\mathbb{R}} (\partial_y \log(w))^2 \mu(dx) + \bar{g}(y) \theta, \quad \bar{g}(y) = \int g(x, y) \mu(dx). \quad (3.7)$$

Second, w satisfies the identity (see Lemma 45c)

$$wg(x, y) \partial_y \Lambda + f(x) \partial_x w + \frac{1}{2} \partial_x^2 w = \left[\frac{1}{2} \int_{\mathbb{R}} (\partial_y \log(w))^2 \mu(dx) + \bar{g}(y) \partial_y \Lambda \right] w. \quad (3.8)$$

By the structure of our fast-slow system, it is possible to explicitly compute the Hamiltonian H . Indeed, the key is to assume that w has the following form:

$$w(t, x, y) = \exp \left(xm(y, \theta) + x^2 N(y, \theta) \right), \quad (3.9)$$

with $m(y, \theta)$ and $N(y, \theta)$ to be determined later. Plugging the ansatz (3.9) inside Eq. (3.8), we deduce that (see Lemma 46a)

$$m(y, \theta) = \beta(y)\theta, \quad N(x, \theta) = 0.$$

In conclusion, the Hamiltonian H has the form (see Lemma 46b)

$$H(y, \theta) = \bar{g}(y)\theta + \frac{1}{2}\beta^2(y)\theta^2.$$

At this point, applying the Gärtner-Ellis Theorem (in the spirit of Theorem 44), we deduce that setting

$$\mathcal{L}(x, y) = \sup_{\theta} (x\theta - H(y, \theta)),$$

we can express the rate function of the LDP as

$$I(y(\cdot)) = \int_0^T \mathcal{L}(\dot{y}(t), y(t)) dt.$$

Since

$$\theta \mapsto x\theta - H(y, \theta) = -\frac{1}{2}\beta^2\theta^2 + \theta(x - \bar{g})$$

is a concave parabola, its maximum is attained in its vertex $\theta_* = \frac{x - \bar{g}(y)}{\beta^2(y)}$. Thus,

$$\mathcal{L}(x, y) = x\theta_* - H(y, \theta_*) = \theta_* \left(x - \bar{g} - \frac{1}{2}\beta^2\theta_* \right) = \frac{\theta_*}{2} (x - \bar{g}) = \frac{1}{2\beta^2(y)} (x - \bar{g}(y))^2,$$

and this leads to the thesis. \square

We complete the proof of the large deviations for the fast-slow system by proving the auxiliary results. The first one deals with some properties of the scaled moment generating function Λ and the function w appearing in the ansatz for the solution u of the Kolmogorov equation.

Lemma 45. *Consider u of the form*

$$u(t, x, y) = w(t, x, y) \exp\left(\frac{1}{\tau}\Lambda(t, x, y)\right).$$

If u is a solution of the Kolmogorov equation (3.3), then:

- (a) Λ is independent of x .
- (b) Λ satisfies the Hamilton-Jacobi equation (3.6).

(c) $w = w(t, x, y)$ satisfies the equation

$$wg(x, y)\partial_y\Lambda + f(x)\partial_x w + \frac{1}{2}\partial_x^2 w = \left[\frac{1}{2} \int_{\mathbb{R}} (\partial_y \log(w))^2 \mu(dx) + \bar{g}(y)\partial_y\Lambda \right] w, \quad (3.10)$$

where

$$\bar{g}(y) = \int g(x, y)\mu(dx).$$

Proof. (a) Calculating the partial derivative of u , the Kolmogorov equation takes the form

$$\begin{aligned} e^{\tau^{-1}\Lambda}\partial_t w + \tau^{-1}e^{\tau^{-1}\Lambda}w\partial_t\Lambda &= g \left(e^{\tau^{-1}\Lambda}\partial_y w + \tau^{-1}we^{\tau^{-1}\Lambda}\partial_y\Lambda \right) \\ &\quad + \tau^{-1}f \left(e^{\tau^{-1}\Lambda}\partial_x w + \tau^{-1}we^{\tau^{-1}\Lambda}\partial_x\Lambda \right) \\ &\quad + 2\tau^{-1} \left(e^{\tau^{-1}\Lambda}\partial_x^2 w + \tau^{-1}e^{\tau^{-1}\Lambda}\partial_x\Lambda\partial_x w \right) \\ &\quad + \tau^{-1}\partial_x we^{\tau^{-1}\Lambda}\partial_x\Lambda + \tau^{-2}we^{\tau^{-1}\Lambda}(\partial_x\Lambda)^2 \\ &\quad + \tau^{-1}we^{\tau^{-1}\Lambda}\partial_x^2\Lambda. \end{aligned}$$

Equalising the terms of order τ^{-3} , we deduce

$$0 = we^{\tau^{-1}\Lambda}(\partial_x\Lambda)^2.$$

Since $w > 0$, which follows from (3.4)-(3.5), we conclude

$$\partial_x\Lambda = 0,$$

and thus $\Lambda = \Lambda(t, y)$ is independent of x .

(b) Grouping the terms of order τ^{-1} , we get

$$e^{\tau^{-1}\Lambda}w\partial_t\Lambda = gwe^{\tau^{-1}\Lambda}\partial_y\Lambda + fe^{\tau^{-1}\Lambda}\partial_x w + \frac{1}{2}e^{\tau^{-1}\Lambda}\partial_x^2 w.$$

We can divide the identity by $e^{\tau^{-1}\Lambda}$, and we obtain

$$w\partial_t\Lambda = gw\partial_y\Lambda + f\partial_x w + \frac{1}{2}\partial_x^2 w. \quad (3.11)$$

Dividing both sides by $w > 0$, we get

$$\partial_t\Lambda = g\partial_y\Lambda + fw^{-1}\partial_x w + \frac{1}{2}w^{-1}\partial_x^2 w. \quad (3.12)$$

We denote by L_0, L_1 respectively the operators

$$L_0 = g(x, y)\partial_y, \quad L_1 = f(x)\partial_x + \frac{1}{2}\partial_x^2,$$

and by P the integral with respect to the invariant measure μ , i.e.

$$(P\phi)(y) = \int_{\mathbb{R}} \phi(x, y) \mu(dx).$$

We substitute the identity

$$fw^{-1}\partial_x w + \frac{1}{2}w^{-1}\partial_x^2 w = L_1 \log(w) + \frac{1}{2}(\partial_y \log(w))^2$$

into (3.12), and we get

$$\partial_t \Lambda = L_1 \log(w) + \frac{1}{2}(\partial_y \log(w))^2 + L_0 \Lambda. \quad (3.13)$$

Now, we exploit the facts that

$$PL_1 = 0$$

(it can be checked that $PL_1\phi = \frac{d}{dt}\mathbb{E}[\phi(X_t)] = 0$, where X_t is the stationary solution of the fast equation) and that

$$P\Lambda = \Lambda,$$

since Λ does not depend on x . Hence, applying P to both the sides of (3.13), we have

$$\begin{aligned} \partial_t \Lambda &= \frac{1}{2}P\partial_y \log(w) + PL_0\Lambda \\ &= \frac{1}{2} \int_{\mathbb{R}} (\partial_y \log(w))^2 \mu(dx) + \bar{g}(y)\partial_y \Lambda := H(x, \partial_y \Lambda), \end{aligned} \quad (3.14)$$

where we have denoted

$$\bar{g}(y) = \int g(x, y) \mu(dx).$$

(c) By comparing the RHS of (3.11) and the RHS of (3.14) multiplied by w , we get

$$wL_0\Lambda + L_1w = H(y, \partial_y \Lambda)w.$$

Writing explicitly the previous equation, we get (3.10). \square

Lastly, we show how it is possible to explicitly compute w and the Hamiltonian H .

Lemma 46. (a) Consider w of the form

$$w(t, x, y) = \exp\left(xm(y, \theta) + x^2N(y, \theta)\right).$$

Then, w is a solution of Eq. (3.10) such that $H(y, 0) = 0^2$ if and only if

$$m(y, \theta) = \beta(y)\theta, \quad N = 0.$$

²This represents an admissibility condition. Indeed the rate function $I = I(y(\cdot))$ describes the cost of deviating from the deterministic trajectory (which in our case satisfies $\bar{Y}(t) = \bar{g}(Y(t))$). The condition $H(y, 0) = 0$ ensures that $\bar{Y}(\cdot)$ has cost zero, or, in other words, that the deterministic trajectory does not contribute to the large deviation cost.

(b) The Hamiltonian H defined in (3.7) can be explicitly written as

$$H(y, \theta) = \bar{g}(y)\theta + \frac{1}{2}\beta^2(y)\theta^2,$$

with

$$\bar{g}(y) = \int_{\mathbb{R}} g(x, y)\mu(dx).$$

Proof. (a) We start by reporting the calculations of some terms appearing in Eq. (3.10):

$$\begin{aligned} \partial_x w &= w(m + 2xN), \\ \partial_x^2 w &= w(4N^2x^2 + 4Nmx + m^2 + 2N), \\ \partial_x \log(w) &= m + 2xN, \\ \int_{\mathbb{R}} (\partial_x \log(w))^2 \mu(dx) &= m^2 + 4mN\bar{Q} + 4N^2\bar{Q}^2 + 2N^2. \end{aligned}$$

Setting $\theta = \partial_y \Lambda$, Eq. (3.10) takes the form

$$\begin{aligned} \left[(x\beta(y) - \alpha(y))\theta - (x - \bar{Q})(m + 2xN) + 2N^2x^2 + 2Nmx + \frac{1}{2}m^2 + N \right] w = \\ \left[\frac{1}{2}m^2 + 2mN\bar{Q} + 2N^2\bar{Q}^2 + N^2 + \bar{g}\theta \right] w, \end{aligned}$$

where we have denoted $g(x, y) = x\beta(y) - \alpha(y)$. The previous one is an identity involving a polynomial of degree 2 in the variable x . Thus, its coefficients should be equal to zero, leading to the system

$$\begin{cases} -N + N^2 & = 0 \\ \beta\theta - m + 2Nm & = 0 \\ \bar{Q}m + N - 2mN\bar{Q} - 2N^2\bar{Q}^2 - N^2 - \bar{Q}\beta & = 0. \end{cases}$$

It can be checked that it admits two solutions

$$m(y, \theta) = \beta(y)\theta, \quad N = 0,$$

and

$$m(y, \theta) = -2\bar{Q} - \beta(y)\theta, \quad N = 1.$$

But the second one is not admissible, since it can be verified that $H(x, 0) = 0$ only if $N|_{\theta=0} = 0$.

(b) By substituting the calculations done in the first part of the proof, we conclude that the Hamiltonian is given by

$$H(y, \theta) = \frac{1}{2} \int_{\mathbb{R}} (\partial_y \log(w))^2 \mu(dx) + \bar{g}\theta = \frac{1}{2}m^2 + \bar{g}\theta = \frac{1}{2}\beta^2(y)\theta^2 + \bar{g}(y)\theta.$$

□

Conclusions

In the first chapter of this thesis, we have considered a one-dimensional energy balance model depending on a bifurcation parameter q , describing the effect of CO₂ concentration in the atmosphere and affecting the energy absorbed by the planet. Numerical simulations show that this model can exhibit either one or three asymptotic solutions, depending on the values of q . We began our analysis by introducing the potential functional F_q associated with the steady-state solutions. The functional F_q has significant implications, as it is closely linked to both the stability of steady-state solutions of the EBM and the invariant measure for the stochastic EBM obtained by perturbing the model with an additive Gaussian white noise. In particular, the invariant measure of the system concentrates on global minimisers of F_q , giving them exponentially larger weight than local minimisers. By analysing the first variation of F_q and applying standard arguments from the direct method of calculus of variations, we established that F_q possesses a global regular minimiser for all values of the parameter q . Furthermore, we provide sufficient conditions to prove the existence of at least three steady-state solutions for the 1D-EBM.

We then introduced the value function $V(q)$, which represents the minimum value attained by the potential functional among all possible temperature profiles. By evaluating $V(q)$ numerically using the steady-state solutions u_S, u_M, u_W , we observed that the function exhibits Lipschitz continuity and concavity. Furthermore, non-differentiability points of $V(q)$ coincide with points where multiple global minimisers exist for F_q . Lastly, when V is differentiable, its derivative is non-increasing and equal to the negative global mean temperature, i.e. $V'(q) = -\int_{-1}^1 \hat{u}(x) dx$, where \hat{u} is the minimiser for F_q . Moreover, as a consequence of the explicit expression for V' , the global mean temperature is non-decreasing with respect to q and it is continuous, except for a Lebesgue zero-measure set of upwards jumps. These are the non-differentiability points of V , corresponding to the case where two or more global minimisers, hence multiple climate equally probable, exist for the stochastic EBM. These findings, which we are able to prove rigorously, allow us to establish a correspondence between the bifurcation diagram and the graph of the value function. Additionally, we applied our results to a spatially inhomogeneous Allen-Cahn equation, to show how our

results still hold for more general space-inhomogeneous reaction-diffusion equations.

The diffusion function $\kappa = \kappa(x)$ that we have examined is non-degenerate at the boundary of the spatial domain. This is an assumption to simplify the study of the variation problem. At present, there remains a problem with how to extend our results to the case where κ is degenerate at the boundary.

Further, we have characterised climate as an invariant measure within a stochastic equation that describes temperature. The emission of CO_2 is considered a parameter influencing the shape of this invariant measure, particularly in relation to the points around which the measure is concentrated. From our perspective, the climate we are currently witnessing reflects changes in the invariant measure, representing a realization of a random variable with that invariant measure as its distribution. Moreover, we have demonstrated the monotonic relationship between global mean temperature and CO_2 . Finally, we have outlined simple conditions, adaptable to other multi-stable reaction-diffusion models, to establish the existence of three asymptotic climate states.

In the second chapter of the thesis, we have presented a non-autonomous framework to describe the scale separation between weather, macroweather, and climate. According to Hasselmann's proposal, weather is conceptualised as arising from a set of deterministic equations, describing variables such as temperature on a fast timescale, typically from an hour to one day. Macroweather, on the other hand, encompasses variations that are neither as short-term as weather nor as long-term as climate. We assume that temperature on a macroweather timescale satisfies a stochastic equation, reflecting the most original aspect of Hasselmann's work. Additionally, at the macro weather timescale, we include a non-autonomous term to model the atmospheric CO_2 concentration, which evolves on a timescale of years. Finally, we identify climate with the invariant measure arising from the stochastic equation at the macro weather level.

In addition to this, we have introduced a new 1D-EBM on a macroweather timescale, which can predict the increase in the number of extreme weather events associated with climate change. The novelty of our model relies on the parametrisation of the non-linear space-dependent radiation budget. Indeed, we have inserted the presence of the SGE, a phenomenon typical of tropical areas that may lead to an instability in the OLR. Our model includes a non-autonomous term $q = q(t)$, that in light of the first part, we have considered constant, that is the effect of the CO_2 concentration on the radiation balance. We have recalled the basic mathematical properties of our model, such as the existence of steady-state solutions, using also numerical simulations. Also, we have shown how the GMT of the steady state solution increases with increasing CO_2 concentration.

The most important results of our work are presented in Section 2.2.5, in

which we focus on the stochastic version of the 1D-EBM. In particular, we have exploited numerical simulations to study the changes in the invariant measure as the CO₂ concentration increases. To obtain this, we have performed numerical integration of the stochastic 1D-EBM on a time interval of 500 years and with the initial condition the warm steady-state solution u_W of the deterministic 1D-EBM, changing only q in different runs of the simulation. Given q , for each space point $x \in [-1, 1]$ we associate the extreme weather event frequency with the time variance $\sigma_t^2(x)$ of a trajectory of the stochastic 1D-EBM at point x . We explain the spatial behaviour of $\sigma_t^2(x)$, which presents two local maximum points for $x \approx \pm 0.8$ and one for $x = 0$, combining heuristic reasoning with empirical indicators. The informal explanation is that the presence of the diffusion term forces the stable warm stationary solution, and the oscillations around it due to noise, to take on values that are not stable if we were to consider the ODE obtained by removing the diffusion term. These regions of temperature, which are locally unstable, correspond to the areas where the variance σ_t^2 is highest. We also motivated the behaviour of $\sigma_t^2(x) = \sigma_t^2(q)(x)$ with respect to q , at fixed x . The variance observed in this way increases to a maximum value and then decreases. This is explained by the increase in GMT due to q and the presence of the diffusion term, leading the solution of the stochastic EBM to be increasingly in, and then out of, the region of instability due to the SGE.

Then, Chapter 3 provides valuable insights into the role of noise in stochastic EBMs by investigating the interplay between fast and slow processes in climate dynamics. The chapter's main conclusion is that, starting from a fast-slow model for weather-macroweather, the closed equation resulting for the macroweather has a diffusion term which is increasing with temperature. In other words, this is another explanation, different from the one presented in Chapter 2, of the increase of extreme weather events frequency associated to climate change.

Lastly, we are aware that our model, although based on physical laws, is largely phenomenological. In some parts of our model, we have included simplifications of convenience, such as in the perturbation of the diffusion function, which makes the problem non-singular and thus easier to deal with mathematically; in other parts, such as in the parametrisation of the space-dependent and tropic-restored OLR, we have followed the principle of simplicity. Other choices would certainly have been possible, but the elementary nature of the model leads us to avoid choices that are too fine or complex. Concerning open questions, understanding how the properties of the model change if more physical processes are considered, such as advection, is a problem we would like to address in the future, as well as the extension of our work to a two-dimensional setting.

Code and data availability

This work does not include any externally supplied code. All material in the text and figures was produced by the authors using standard mathematical and numerical analysis tools.

The code for the numerical simulations of Chapter 1 is available at Zenodo <https://zenodo.org/doi/10.5281/zenodo.10469450>, and the code for Chapter 2 is available at (<https://zenodo.org/doi/10.5281/zenodo.11609952>). The Modena temperature data, used in Chapter 2, were provided by the Geophysical Observatory of Modena, University of Modena and Reggio Emilia, Italy (www.ossgeo.unimore.it, [59]) and are available upon request.

Bibliography

- [1] Sergiu Aizicovici, Nikolaos S. Papageorgiou, and Vasile Staicu. Existence of multiple solutions with precise sign information for super-linear neumann problems. *Annali di Matematica Pura ed Applicata*, 188(4):679–719, February 2009.
- [2] Ludwig Arnold. *Random dynamical systems*. Springer Monographs in Mathematics. Springer-Verlag, Berlin, 1998.
- [3] Ludwig Arnold. Hasselmann’s program revisited: the analysis of stochasticity in deterministic climate models. In Peter Imkeller and Jin-Song von Storch, editors, *Stochastic Climate Models*, pages 141–157, Basel, 2001. Birkhäuser Basel.
- [4] Peter Ashwin, Sebastian Wieczorek, Renato Vitolo, and Peter Cox. Tipping points in open systems: bifurcation, noise-induced and rate-dependent examples in the climate system. *Philosophical Transactions of the Royal Society A: Mathematical, Physical and Engineering Sciences*, 370(1962):1166–1184, Mar 2012.
- [5] Paolo Baldi. *Stochastic Calculus*. Springer International Publishing, 2017.
- [6] Robbin Bastiaansen, Henk A Dijkstra, and Anna S von der Heydt. Fragmented tipping in a spatially heterogeneous world. *Environmental Research Letters*, 17(4):045006, mar 2022.
- [7] A. Berger, editor. *Climatic Variations and Variability: Facts and Theories*. Springer Netherlands, 1981.
- [8] Paolo Bernuzzi and Christian Kuehn. Bifurcations and early-warning signs for spdes with spatial heterogeneity. *Journal of Dynamics and Differential Equations*, pages 1–45, 2023.
- [9] Tom Beucler and Timothy W. Cronin. Moisture-radiative cooling instability. *Journal of Advances in Modeling Earth Systems*, 8(4):1620–1640, 2016.

- [10] Freddy Bouchet, Tobias Grafke, Tomás Tangarife, and Eric Vandeneijnden. Large deviations in fast-slow systems. *J. Stat. Phys.*, 162(4):793–812, 2016.
- [11] Haim Brezis. *Functional analysis, Sobolev spaces and partial differential equations*, volume 2. Springer, 2011.
- [12] Mikhail I Budyko. The effect of solar radiation variations on the climate of the earth. *tellus*, 21(5):611–619, 1969.
- [13] B. Byrne and C. Goldblatt. Radiative forcing at high concentrations of well-mixed greenhouse gases. *Geophysical Research Letters*, 41(1):152–160, January 2014.
- [14] P. Cannarsa, V. Lucarini, P. Martinez, C. Urbani, and J. Vancostenoble. Analysis of a two-layer energy balance model: Long time behavior and greenhouse effect. *Chaos: An Interdisciplinary Journal of Nonlinear Science*, 33(11):113111, 11 2023.
- [15] Piermarco Cannarsa, Martina Malfitana, and Patrick Martinez. Parameter determination for energy balance models with memory. *Mathematical Approach to Climate Change and its Impacts: MAC2I*, pages 83–130, 2020.
- [16] Piermarco Cannarsa and Carlo Sinestrari. *Semiconcave Functions, Hamilton—Jacobi Equations, and Optimal Control*. Birkhäuser Boston, 2004.
- [17] Mickaël D. Chekroun, Eric Simonnet, and Michael Ghil. Stochastic climate dynamics: random attractors and time-dependent invariant measures. *Phys. D*, 240(21):1685–1700, 2011.
- [18] Hans Crauel and Franco Flandoli. Attractors for random dynamical systems. *Probab. Theory Related Fields*, 100(3):365–393, 1994.
- [19] G. Da Prato and J. Zabczyk. *Ergodicity for Infinite Dimensional Systems*. London Mathematical Society Lecture Note Series. Cambridge University Press, 1996.
- [20] Giuseppe Da Prato. *Kolmogorov Equations for Stochastic PDEs*. Birkhäuser Basel, 2004.
- [21] Giuseppe Da Prato. *An Introduction to Infinite-Dimensional Analysis*. Springer Berlin Heidelberg, 2006.
- [22] Giuseppe Da Prato and Jerzy Zabczyk. *Stochastic Equations in Infinite Dimensions*. Cambridge University Press, April 2014.

- [23] Vasilis Dakos, Marten Scheffer, Egbert H. van Nes, Victor Brovkin, Vladimir Petoukhov, and Hermann Held. Slowing down as an early warning signal for abrupt climate change. *Proceedings of the National Academy of Sciences*, 105(38):14308–14312, 2008.
- [24] G. Del Sarto, J. Bröcker, F. Flandoli, and T. Kuna. Variational techniques for a one-dimensional energy balance model. *Nonlinear Processes in Geophysics*, 31(1):137–150, 2024.
- [25] G. Del Sarto and F. Flandoli. A non-autonomous framework for climate change and extreme weather events increase in a stochastic energy balance model. *Chaos: An Interdisciplinary Journal of Nonlinear Science*, 34(9):093122, 09 2024.
- [26] Amir Dembo and Ofer Zeitouni. *Large deviations techniques and applications*, volume 38 of *Stochastic Modelling and Applied Probability*. Springer-Verlag, Berlin, 2010. Corrected reprint of the second (1998) edition.
- [27] M. Dewey and C. Goldblatt. Evidence for radiative-convective bistability in tropical atmospheres. *Geophysical Research Letters*, 45(19):10,673–10,681, 2018.
- [28] Jesús Ildefonso Díaz. On the mathematical treatment of energy balance climate models. In Jesús Ildefonso Díaz, editor, *The Mathematics of Models for Climatology and Environment*, pages 217–251, Berlin, Heidelberg, 1997. Springer Berlin Heidelberg.
- [29] Dietmar Dommenges and Janine Flöter. Conceptual understanding of climate change with a globally resolved energy balance model. *Climate Dynamics*, 37(11–12):2143–2165, March 2011.
- [30] Brady Dortmans, William F Langford, and Allan R Willms. An energy balance model for paleoclimate transitions. *Climate of the Past*, 15(2):493–520, 2019.
- [31] Gregorio Díaz and Jesús Ildefonso Díaz. Stochastic energy balance climate models with legendre weighted diffusion and an additive cylindrical wiener process forcing, 2022.
- [32] J.I. Díaz, J.A. Langa, and J. Valero. On the asymptotic behaviour of solutions of a stochastic energy balance climate model. *Physica D: Nonlinear Phenomena*, 238(9):880–887, 2009.
- [33] Kerry Emanuel, Allison A. Wing, and Emmanuel M. Vincent. Radiative-convective instability. *Journal of Advances in Modeling Earth Systems*, 6(1):75–90, 2014.

- [34] Franco Flandoli, Umberto Pappalettera, and Elisa Tonello. Nonautonomous attractors and young measures. *Stochastics and Dynamics*, 22(02):2240003, 2022.
- [35] Giuseppe Floridia. Approximate controllability for nonlinear degenerate parabolic problems with bilinear control. *Journal of Differential Equations*, 257(9):3382–3422, 2014.
- [36] Mark I. Freidlin and Alexander D. Wentzell. *Random Perturbations of Dynamical Systems*. Springer Berlin Heidelberg, 2012.
- [37] C.T. Fulton and S.A. Pruess. Eigenvalue and eigenfunction asymptotics for regular sturm-liouville problems. *Journal of Mathematical Analysis and Applications*, 188(1):297–340, 1994.
- [38] Pedro Gaspar and Marco AM Guaraco. The allen–cahn equation on closed manifolds. *Calculus of Variations and Partial Differential Equations*, 57:1–42, 2018.
- [39] M. Ghil and S. Childress. *Topics in Geophysical Fluid Dynamics: Atmospheric Dynamics, Dynamo Theory, and Climate Dynamics*. Springer New York, 1987.
- [40] Michael Ghil. Climate stability for a sellers-type model. *Journal of Atmospheric Sciences*, 33(1):3 – 20, 1976.
- [41] Michael Ghil, Mickaël D. Chekroun, and Eric Simonnet. Climate dynamics and fluid mechanics: natural variability and related uncertainties. *Phys. D*, 237(14-17):2111–2126, 2008.
- [42] Michael Ghil and Valerio Lucarini. The physics of climate variability and climate change. *Rev. Mod. Phys.*, 92:035002, Jul 2020.
- [43] Charles E Graves, Wan-Ho Lee, and Gerald R North. New parameterizations and sensitivities for simple climate models. *Journal of Geophysical Research: Atmospheres*, 98(D3):5025–5036, 1993.
- [44] K. Hasselmann. Stochastic climate models part i. theory. *Tellus*, 28(6):473–485, 1976.
- [45] J. T. Houghton, Y. Ding, D. J. Griggs, M. Noguier, P. J. van der Linden, X. Dai, K. Maskell, and C. A. Johnson, editors. *Climate Change 2001: The Scientific Basis*. Contribution of Working Group I to the Third Assessment Report of the Intergovernmental Panel on Climate Change, 2001.
- [46] John Theodore Houghton, YDJG Ding, David J Griggs, Maria Noguier, Paul J van der Linden, Xiaosu Dai, Kathy Maskell, Colin A Johnson,

- et al. *Climate change 2001: the scientific basis*, volume 881. Cambridge university press Cambridge, 2001.
- [47] Yi Huang, Yan Xia, and Xiaoxiao Tan. On the pattern of CO₂ radiative forcing and poleward energy transport. *J. Geophys. Res.*, 122(20):10,578–10,593, October 2017.
- [48] Nobuyuki Ikeda and Shinzo Watanabe. *Stochastic differential equations and diffusion processes*, volume 24 of *North-Holland Mathematical Library*. North-Holland Publishing Co., Amsterdam-New York; Kodansha, Ltd., Tokyo, 1981.
- [49] Peter Imkeller. Energy balance models — viewed from stochastic dynamics. In Peter Imkeller and Jin-Song von Storch, editors, *Stochastic Climate Models*, pages 213–240, Basel, 2001. Birkhäuser Basel.
- [50] Youssef Jabri. *The Mountain Pass Theorem*. Cambridge University Press, September 2003.
- [51] R. Kannan and Carole King Krueger. *Advanced Analysis*. Springer New York, 1996.
- [52] Yuri Kifer. Averaging and climate models. In *Stochastic climate models*, pages 171–188. Springer, 2001.
- [53] Yuri Kifer. L₂ diffusion approximation for slow motion in averaging. *Stochastics and Dynamics*, 03(02):213–246, 2003.
- [54] Christian Kuehn. A mathematical framework for critical transitions: Bifurcations, fast–slow systems and stochastic dynamics. *Physica D: Nonlinear Phenomena*, 240(12):1020–1035, 2011.
- [55] Tony Lelièvre and Gabriel Stoltz. Partial differential equations and stochastic methods in molecular dynamics. *Acta Numerica*, 25:681–880, May 2016.
- [56] T. M. Lenton, V. N. Livina, V. , E. H. van Nes, and M. Scheffer. Early warning of climate tipping points from critical slowing down: comparing methods to improve robustness. *Philosophical Transactions of the Royal Society A: Mathematical, Physical and Engineering Sciences*, 370(1962):1185–1204, 2012.
- [57] Timothy M Lenton, Hermann Held, Elmar Kriegler, Jim W Hall, Wolfgang Lucht, Stefan Rahmstorf, and Hans Joachim Schellnhuber. Tipping elements in the earth’s climate system. *Proceedings of the national Academy of Sciences*, 105(6):1786–1793, 2008.

- [58] RW Lindsay and J Zhang. The thinning of arctic sea ice, 1988–2003: Have we passed a tipping point? *Journal of Climate*, 18(22):4879–4894, 2005.
- [59] Luca Lombroso and Salvatore Quattrocchi. *L’ osservatorio di Modena: 180 anni di misure meteorologiche*. SMS, 2008.
- [60] Gabriel J. Lord, Catherine E. Powell, and Tony Shardlow. *An Introduction to Computational Stochastic PDEs*. Cambridge Texts in Applied Mathematics. Cambridge University Press, 2014.
- [61] Valerio Lucarini and Tamás Bódi. Transitions across melancholia states in a climate model: Reconciling the deterministic and stochastic points of view. *Physical review letters*, 122(15):158701, 2019.
- [62] Valerio Lucarini, Larissa Serdukova, and Georgios Margazoglou. Lévy noise versus gaussian-noise-induced transitions in the ghil–sellers energy balance model. *Nonlinear Processes in Geophysics*, 29(2):183–205, May 2022.
- [63] Peter Imkeller Ludwig Arnold and Yonghui Wu. Reduction of deterministic coupled atmosphere–ocean models to stochastic ocean models: a numerical case study of the lorenz–maas system. *Dynamical Systems*, 18(4):295–350, 2003.
- [64] David I. Armstrong McKay, Arie Staal, Jesse F. Abrams, Ricarda Winkelmann, Boris Sakschewski, Sina Loriani, Ingo Fetzer, Sarah E. Cornell, Johan Rockström, and Timothy M. Lenton. Exceeding 1.5°C global warming could trigger multiple climate tipping points. *Science*, 377(6611):eabn7950, 2022.
- [65] Gunnar Myhre, Eleanor J. Highwood, Keith P. Shine, and Frode Stordal. New estimates of radiative forcing due to well mixed greenhouse gases. *Geophysical Research Letters*, 25(14):2715–2718, July 1998.
- [66] Gunnar Myhre, Arne Myhre, and Frode Stordal. Historical evolution of radiative forcing of climate. *Atmospheric Environment*, 35(13):2361–2373, 2001.
- [67] Gerald R. North. Theory of energy-balance climate models. *Journal of Atmospheric Sciences*, 32(11):2033 – 2043, 1975.
- [68] Gerald R. North. Multiple solutions in energy balance climate models. *Global and Planetary Change*, 2(3):225–235, 1990.
- [69] Gerald R. North and Robert F. Cahalan. Predictability in a Solvable Stochastic Climate Model. *Journal of Atmospheric Sciences*, 38(3):504–513, March 1981.

- [70] Gerald R. North, Robert F. Cahalan, and James A. Coakley. Energy balance climate models. *Reviews of Geophysics*, 19(1):91, 1981.
- [71] Gerald R. North, Louis Howard, David Pollard, and Bruce Wielicki. Variational formulation of budyko-sellers climate models. *Journal of Atmospheric Sciences*, 36(2):255 – 259, 1979.
- [72] Gerald R. North and Kwang-Yul Kim. *Energy Balance Climate Models*. Wiley, August 2017.
- [73] Intergovernmental Panel on Climate Change (IPCC). *Climate Change 2021 – The Physical Science Basis: Working Group I Contribution to the Sixth Assessment Report of the Intergovernmental Panel on Climate Change*. Cambridge University Press, 2023.
- [74] Alfio Quarteroni and Alberto Valli. *Numerical approximation of partial differential equations*, volume 23. Springer Science & Business Media, 2008.
- [75] Ralph Tyrell Rockafellar. *Convex Analysis*, volume 28. Princeton University Press, 1970.
- [76] Marten Scheffer, Jordi Bascompte, William Brock, Victor Brovkin, Stephen Carpenter, Vasilis Dakos, Hermann Held, Egbert Nes, Max Rietkerk, and George Sugihara. Early-warning signals for critical transitions. *Nature*, 461:53–9, 10 2009.
- [77] William D. Sellers. A global climatic model based on the energy balance of the earth-atmosphere system. *Journal of Applied Meteorology and Climatology*, 8(3):392 – 400, 1969.
- [78] Joel Smoller. *Shock waves and reaction—diffusion equations*, volume 258. Springer Science & Business Media, 2012.
- [79] David B Stephenson, HF Diaz, and RJ Murnane. Definition, diagnosis, and origin of extreme weather and climate events. *Climate extremes and society*, 340:11–23, 2008.
- [80] Thomas Stocker, Gian-Kasper Plattner, and Qin Dahe. Ipcc climate change 2013: the physical science basis-findings and lessons learned. In *EGU general assembly conference abstracts*, page 17003, 2014.
- [81] Thomas F Stocker, Lawrence A Mysak, and Daniel G Wright. A zonally averaged, coupled ocean-atmosphere model for paleoclimate studies. *Journal of Climate*, 5(8):773–797, 1992.
- [82] Roger Temam. *Infinite-Dimensional Dynamical Systems in Mechanics and Physics*. Springer New York, 1997.

- [83] James William Thomas. *Numerical partial differential equations: finite difference methods*, volume 22. Springer Science & Business Media, 2013.
- [84] Krystyna Twardowska. Wong-Zakai approximations for stochastic differential equations. *Acta Appl. Math.*, 43(3):317–359, 1996.
- [85] Nicholas W. Watkins, Raphael Calel, Sandra C. Chapman, Aleksei Chechkin, Rainer Klages, and David A. Stainforth. The challenge of non-Markovian energy balance models in climate. *Chaos: An Interdisciplinary Journal of Nonlinear Science*, 34(7):072105, 07 2024.
- [86] Xuezhen Zhang, Xiaxiang Li, Deliang Chen, Huijuan Cui, and Quansheng Ge. Overestimated climate warming and climate variability due to spatially homogeneous co2 in climate modeling over the northern hemisphere since the mid-19th century. *Scientific Reports*, 9(1), November 2019.